NASA Technical Memorandum 83197

Comparison of Thin-Film Resistance Heat-Transfer Gages With Thin-Skin Transient Calorimeter Gages in Conventional Hypersonic Wind Tunnels

Charles G. Miller III
Langley Research Center
Hampton, Virginia

National Aeronautics
and Space Administration

**Scientific and Technical
Information Branch**

1981

SUMMARY

A comparison of thin-film resistance heat-transfer gages, developed for use in supersonic-hypersonic impulse facilities having run times less than 0.01 sec, with thin-skin transient calorimeter gages has been performed in the Langley Continuous-Flow Hypersonic Tunnel (CFHT) and in the Langley Hypersonic CF_4 Tunnel (CF_4 Tunnel). Thin-film gages deposited at the stagnation region of small (8.1-mm-diameter) hemispheres of quartz or of a machinable glass-ceramic provided a test of durability and performance in the high-temperature environment of these two wind tunnels. The performance of these gages at much lower temperatures and heat-transfer rates was examined by installing the gages flush with the surface of a sharp-leading-edge flat plate. Also tested were 8.1-mm-diameter hemispheres utilizing the thin-skin transient calorimetry technique generally employed in conventional hypersonic wind tunnels. Two different methods of construction of these thin-skin hemispheres were tested. One hemisphere was a thin shell of stainless steel with a thermocouple attached to the inner surface at the stagnation region. The other hemisphere was fabricated from a machinable glass-ceramic and had a small stainless-steel insert, with a thermocouple attached to the backside, installed at the stagnation region. Measured values of heat-transfer rate from the different hemispheres were compared with one another and with predicted values.

The present study demonstrated the feasibility of using thin-film resistance heat-transfer gages in conventional hypersonic wind tunnels over a wide range of conditions. These gages offer the following advantages over the transient calorimeter thin-skin gages: (1) The fast response provides a detailed time history of the heat-transfer rates. (2) Their high sensitivity allows the same gage to be used for a wide range of surface heat-transfer rates. (3) Many gages can be deposited in a small area without concern for conduction effects or large corrections to determine the effective skin thickness. (4) Thin-film gages eliminate the need to measure a skin thickness to an accuracy of 0.015 mm, sometimes an impossible feat on a complex model. The primary disadvantages of the thin-film gage are its susceptibility to damage when facing the flow and the large corrections required to account for the variation of substrate thermal properties with temperature. Values of heat-transfer coefficient measured with the thin-film hemisphere and machinable glass-ceramic hemisphere with an insert agreed to within 5 percent of one another and with predicted values.

INTRODUCTION

The continuous thin-skin transient calorimeter technique is widely used in conventional hypersonic wind tunnels to measure heat-transfer rates on configurations of various degrees of complexity. (See for example, refs. 1 to 6.) As the name implies, calorimeter gages attempt to determine the instantaneous heat-transfer rate to the surface of the model by measuring the time rate of change of the thermal energy within an element of the skin. These gages usually take the form of a thermocouple spot-welded to the inside surface of the metallic thin skin. The transient calorimeter effect is achieved by rapidly injecting the thin-skin model, which is generally at a uniform temperature, into the established test flow and retracting it after a few seconds. As with most measurement techniques, the continuous thin-skin transient calorimeter technique has advantages and disadvantages. One of the more

serious disadvantages is lateral-conduction effects due to temperature gradients within the thin skin. In regions of high heat-transfer gradients, such as those generally experienced on very small models and models with large surface curvature, lateral conduction may cause large experimental errors in the inferred heating distribution. Another disadvantage with models having large surface curvature is that large geometric corrections to the measured skin thickness are generally required to determine the effective skin thickness.

The present study investigates alternative methods for measuring heating rates in regions where lateral-conduction effects or miniaturization are important. One method examined, which is not new to conventional hypersonic wind tunnels, was a slug-type calorimeter gage. This gage is similar to the continuous thin-skin calorimeter gage, differing only in that the metallic skin is limited to a small area and mounted in an insulator. The other method examined was the thin-film resistance gage. This gage, which is characterized by a very rapid response time (less than 1 μsec), was developed primarily to measure heat-transfer rates in hypersonic-hypervelocity impulse facilities having short run times, typically 0.1 to 10 msec. (See refs. 7 to 28.) Thin-film heat-transfer gages are constructed at the Langley Research Center to measure heating rates in the Langley Expansion Tube (refs. 29 and 30), a facility that has a run time of only 200 to 300 μsec and uses small (5-cm-diameter, or less) models. Because the thin-film sensors may be made quite small, detailed heating distributions are measured on these small models.

To the author's knowledge, experience with thin-film heat-transfer gages in conventional hypersonic wind tunnels at the Langley Research Center is limited to a single study. (See ref. 31.) In this study, the heating distribution along a slender cone was measured with thin-film gages in the low-heating environment of the Langley Hypersonic Helium Tunnel. However, Edney (ref. 20) tested thin-film gages on blunt models in a conventional supersonic wind tunnel a number of years ago. Small (10-mm-diameter) Pyrex hemispheres with a platinum thin-film gage placed at the stagnation point were tested at a Mach number of 4.6 prior to being tested in a hypersonic gun tunnel. (Pyrex is a trademark of Corning Glass Works.) The purpose of initially testing the gages in a conventional wind tunnel was to examine the performance of these gages and the associated high-response data-acquisition system for flow conditions that were accurately known. The good agreement observed between measured and predicted stagnation-point heating rate led Edney (see ref. 20) to suggest that this technique be used to calibrate thin-film gages prior to their being subjected to the high-enthalpy flow in an impulse wind tunnel.

The purpose of this report is to present the results of a study performed in the Langley Continuous-Flow Hypersonic Tunnel (CFHT) (refs. 4 and 32) and in the Langley Hypersonic CF_4 Tunnel (CF_4 Tunnel) (ref. 33) to evaluate the performance of thin-film resistance heat-transfer gages over a range of flow conditions. Small hemispheres (8.1-mm diameter) fabricated from quartz and MACOR (see ref. 34) were instrumented with a thin-film gage located at the geometric stagnation point. (MACOR, a machinable glass-ceramic, is a trademark of Corning Glass Works.) Stagnation-point heat-transfer rates measured with these thin-film hemispheres are compared with those measured with continuous thin-skin calorimeter hemispheres and with a slug-type calorimeter hemisphere having the same diameter. In order to examine the performance of the thin-film gages under relatively low heating conditions, several gages were mounted flush with the surface of a sharp-leading-edge flat-plate model. Variables in this study include flow conditions (Mach number, test gas, and range of reservoir pressure for a given reservoir temperature), type of heat-transfer sensor (thin-film resistance gages and thin-skin transient calorimeter gages), and model geometry

(hemisphere or flat plate). The use of trade names in this publication does not constitute endorsement, either expressed or implied, by the National Aeronautics and Space Administration.

SYMBOLS

a_1, a_2, a_3	constants used in equation (3)
b	constant used in equation (A4)
C_h	heat-transfer coefficient, $\dot{q}/(T_{aw} - T_w)$, W/m^2-K
c	specific heat, J/kg-K
d	diameter
E	voltage, V
h	enthalpy, J/kg
I	current, A
k	thermal conductivity, W/m-K
ℓ	substrate thickness, m
M	Mach number
N_{Pr}	Prandtl number, $\mu c/k$
N_{Re}	unit Reynolds number per m
p	pressure, Pa
$\dot{q}$	heat-transfer rate, W/m^2
R	resistance, Ω
R_{gas}	univeral gas constant, 8.31434 J/mol-K
r	radius
r_g	radius of outer surface of hemisphere, m
s	slope
T	temperature, K
T_x	temperature at penetration depth x, K
t	time, where t = 0 corresponds to model arrival at plane of nozzle wall during model injection into the flow, sec

t'	time, where $t' = 0$ corresponds to full-scale output of injector switch (see fig. 9), sec
U	velocity
W	molecular weight of undissociated air (28.967 kg/kmol)
x	penetration depth into infinite slab, m
x^*	$\equiv x/(2\sqrt{\alpha t})$
z	distance downstream from leading edge of flat plate, m
α	thermal diffusivity, $k/\rho c$, m^2/sec
α_R	temperature coefficient of resistance per K (see eq. (10))
β	$= \sqrt{\rho c k}$, $W\text{-}sec^{1/2}/m^2\text{-}K$
Γ	stagnation-point velocity gradient (see eq. (17))
γ	ratio of specific heats
δ	thickness of thin film or substrate, m
ε	emissivity
η	coefficient of linear expansion per K
η_r	recovery factor
θ	angle subtended by a circular arc measured from the sphere axis (see fig. 31)
λ	dummy variable of integration (see eq. (6))
μ	coefficient of viscosity, $N\text{-}sec/m^2$
ρ	density, kg/m^3
σ	Stefan-Boltzmann constant, 5.6697×10^{-8} $W/m^2\text{-}K^4$
τ	thickness of thin skin, m
ϕ	$= \int_0^T (k/k_o)\, dT$, K
ω	thin-skin curvature correction factor, τ_{eff}/τ_m

Subscripts:

av	average or mean
aw	adiabatic-wall conditions

B	ballast
b	battery
c	coating or overlayer
eff	effective
f	thin film
i	inner surface
m	thin-skin material
o	ambient or initial (t = 0)
s	substrate or backing material
t,1	reservoir stagnation conditions
t,2	stagnation conditions behind a normal shock
w	wall or outside surface
2	static conditions immediately behind a normal shock
∞	free-stream conditions

A bar over a quantity denotes the mean value.

FACILITIES AND TEST CONDITIONS

The Langley Continuous-Flow Hypersonic Tunnel

The Langley Continuous-Flow Hypersonic Tunnel (CFHT) (refs. 4 and 32) is shown schematically in figure 1. This facility was operated in the blowdown mode for the present study. Dry air to the settling chamber is obtained from a 34.5-MPa bottle field, and the maximum operating reservoir pressure of the tunnel is 15.2 MPa. This air is heated by a 15-MW electric-resistance tube heater, the maximum tube temperature is 1255 K, and maximum reservoir-stagnation temperature is 1060 K. The CFHT uses a water-cooled, three-dimensional contoured nozzle to generate a nominal Mach number of 10. The nozzle throat is 2.54 cm square and the test section is 78.7 cm square. Maximum run time in the blowdown mode, using two 12.2-m-diameter vacuum spheres, is 60 to 80 sec.

The model is positioned in an injection chamber mounted on the right side of the tunnel when looking upstream toward the nozzle throat. (This chamber allows access to the model without opening the test section to atmosphere.) The injection system rapidly (in about 0.5 sec) inserts a model into the flow for heat-transfer tests.

Reservoir stagnation conditions and free-stream flow parameters for the present tests in the CFHT are presented in the following table:

Run	$p_{t,1'}$, MPa	$T_{t,1'}$, K	M_∞	p_∞, Pa	T_∞, K	$N_{Re,\infty}$ per m	$p_{t,2'}$, kPa
1	2.43	973	9.90	59.4	49.1	1.88×10^6	7.77
2	2.40	975	9.89	58.6	49.2	1.84	7.56
3	5.14	986	10.04	115.4	48.6	3.76	15.43
4	11.02	989	10.19	228.1	47.5	7.85	30.14
6	2.40	981	9.89	58.6	49.6	1.82	7.69
7	5.13	998	10.04	115.2	49.1	3.69	15.40
11	2.37	965	9.89	57.9	48.8	1.85	7.58
12	2.49	958	9.90	60.8	48.4	1.97	7.98
13	11.32	980	10.20	233.1	49.0	7.62	28.75
14	2.47	979	9.90	60.3	49.4	1.89	7.67

The Langley Hypersonic CF_4 Tunnel

The Langley Hypersonic CF_4 Tunnel (CF_4 Tunnel) (ref. 33) is a conventional-type, blowdown wind tunnel that uses tetrafluoromethane (CF_4) as the test gas. This facility, which is a conversion of the Langley 20-Inch Hypersonic Arc-Heated Tunnel (ref. 32), is shown schematically in figure 2. The CF_4 from the high-pressure storage field is heated to a maximum temperature of approximately 900 K by two lead-bath heaters in parallel. The high-pressure heated CF_4 is then introduced into the settling chamber and expanded along an axisymmetric, contoured nozzle designed to generate a Mach number of 6 at the nozzle exit. Models are supported at the nozzle exit by a pneumatically driven insert mechanism and are tested in an open jet. After having passed over the test model, the CF_4 test gas is collected by a diffuser and is then cooled and dumped into two vacuum spheres which serve as receivers. When the spheres are evacuated, the exhaust of the vacuum pumps is piped to the CF_4 reclaimer where the CF_4 is liquified and the gaseous impurities are exhausted to atmosphere. A detailed description of the CF_4 Tunnel is presented in reference 33.

Reservoir stagnation conditions and free-stream flow parameters for the present tests in the CF_4 Tunnel are presented in the following table:

$p_{t,1'}$, MPa	$T_{t,1'}$, K	M_∞	p_∞, Pa	T_∞, K	$N_{Re,\infty}$ per m	ρ_2/ρ_∞	$p_{t,2'}$, kPa
7.48	668	6.20	194	177	0.952×10^6	11.84	8.97
11.24	679	6.21	285	181	1.355	11.91	13.15
16.63	684	6.21	420	181	1.989	11.92	19.39

MODELS AND INSTRUMENTATION

Models

This section describes the models and the holder used to place these models into the flow. In the case of the hemisphere models, the model is actually a type of

heat-transfer gage. The types of heat-transfer gages used in this study are discussed in the next section.

Hemispheres.- Models used to measure stagnation-point heat-transfer rates in the two wind tunnels were hemispheres having diameters from 7.87 to 8.13 mm. In the CFHT, five hemispheres were mounted in a vertical survey rake, having a probe spacing of 5.1 cm, that was injected horizontally into the flow; that is, all five hemispheres were exposed to the flow at the same time. The survey rake came to rest 5.1 cm from the nozzle center line. This same rake was used in the CF_4 Tunnel to inject four hemispheres into the flow. For this facility, the rake was horizontal and injected vertically such that the probes were positioned 7.62 cm below the nozzle center line. (The probes were tested off center line to avoid disturbances focused along the center of the nozzle when the tunnel is operated at reservoir conditions other than those for which the nozzle was designed (ref. 33).)

The radius of all hemispheres tested was measured by placing the hemispheres in an optical comparator and enlarging the image to 20 times the actual size. Representative photographs of the shape for a continuous thin-skin model, a MACOR (ref. 34) model with a stainless-steel insert, and a thin-film MACOR model are shown in figure 3. (These types of heat-transfer gages are discussed in the next section.) The optical comparator showed that the thin-film models and MACOR model with a stainless-steel insert had true nose radii, whereas the continuous thin-skin models had somewhat flattened noses (nose flattened approximately 0.18 mm for both models).

Flat Plate.- To generate a region of relatively low heat-transfer rate, a sharp-leading-edge flat-plate model was tested at zero incidence. This stainless-steel plate, which is shown in figure 4, is 7.62 cm wide, 16.05 cm long, and has a leading-edge angle of 20°. A single quartz substrate is mounted flush with the surface, with the axis of the substrate coincident with the plate center line in the stream direction. This substrate has 13 thin-film sensors deposited 3.2 mm apart along its length (fig. 4(b)).

Disks.- To determine the thin-film-gage substrate thickness required for the substrate to behave as a semi-infinite slab for a given time interval, MACOR disks having diameters of 1.27 cm and thicknesses of 1.27, 2.54, 3.81, 5.08, and 6.35 mm were tested in the CF_4 Tunnel. These disks contained a thin-film sensor at the center of both the front and rear surfaces and were mounted on the holders used for the hemispheres. (See fig. 5.) The thin-film sensor on the rear of the disk was within the interior of the holder and, thus, was not exposed to the flow. The five disks were mounted in the same rake as that used for the hemispheres and were injected into the flow, coming to rest 7.62 cm below the nozzle center line; hence, the probes were exposed to the flow at essentially the same time.

Heat-Transfer Gages

Thin-skin transient calorimeter.- In the conventional thin-skin transient calorimetry technique (refs. 1 to 6), the rate of heat storage in the model skin is inferred from a thermocouple generally attached to the inside surface of the skin. Two different fabrication procedures were used in the present study for the calorimetry technique. One procedure involved the fabrication of a hemisphere from type 347 stainless steel. The temperature of the inside surface at the stagnation point was measured by using a chromel-alumel thermocouple; this thermocouple junction was formed by spot-welding the No. 36 (0.127-mm-diameter) chromel wire and the No. 36

alumel wire to the inner surface. Two such continuous thin-skin hemispheres were constructed with skin thicknesses at the geometric stagnation point of 1.135 mm and 1.034 mm.

The second fabrication procedure also involved a thin-skin calorimeter of type 347 stainless steel. However, for this sensor, a small (1.123-mm-diameter, 1.067-mm-thick) stainless-steel insert was mounted flush with the surface of a MACOR hemisphere. The primary purpose of this technique was to reduce conduction losses from the nose region of the hemisphere by using an insulator as the model material. As a check of the measured dimensions of this insert, the insert was weighed, and the density was computed and compared with the handbook value for type 347 stainless steel (8027 kg/m^3). The inferred density was within 5.7 percent of the handbook value. As with the continuous thin-skin hemispheres, the temperature of the inside surface of the stainless-steel insert was measured by using a chromel-alumel thermocouple (No. 36 wire) welded to the inner surface.

Thin-film resistance.- The second type of heat-transfer sensor was a thin-film resistance gage deposited at the stagnation region of hemispheres (hereinafter referred to as thin-film hemispheres) fabricated from quartz (fig. 6) or MACOR. Quartz was selected as a substrate material because its thermal properties are well documented and the variation of these properties with temperature is less than the other commonly used substrate material, Pyrex (ref. 2). MACOR (ref. 34), a machinable glass-ceramic, was selected because the variation of thermal properties with temperature for most ceramics is quite small and MACOR may be machined with metal-working tools; hence, the fabrication of substrates from MACOR is less expensive.

The quartz hemispheres were obtained from a solid quartz rod having a nominal diameter of 8.13 mm. The rod was placed in a lathe and the end of the rod was heated to the melting point. A high-density graphite tool machined to the desired radius for the rod was placed on the heated rod as it rotated, providing the spherical tip. The rod was then optically polished, and the residue from the polishing compound was baked off by placing the rod in an oven. MACOR hemispheres were machined by using conventional machining techniques for metals (ref. 34); they were polished first with No. 600 metallurgical paper, then with No. 1000 paper, and finally with No. 2000 paper.

As observed from figure 6, a serpentine thin-film sensing element was deposited at the stagnation region of these quartz and MACOR hemispheres by using a photolithographic technique. This element measures 1.27 mm long and 1.02 mm wide on a flat surface. The serpentine pattern was designed to provide a gage resistance of 100 to 125 Ω on a quartz substrate and yet give an approximate point measurement. (The element was contained within 8° of the stagnation point, as described by an arc from the axis of symmetry with the apex originating at the center of the sphere.)

For both the quartz and MACOR hemisphere substrates, the first step in the gage fabrication was to deposit a very thin layer of chromium on the surface. The purpose of this chromium underlayer is to improve the adherence of the palladium sensing element to the highly polished substrate surface. (See refs. 2, 26, and 28.) Palladium was sputtered over the chromium, which completed the metal deposition. The resulting film thickness δ_f was 1500 to 1800 Å. A photomask (positive photoimage for positive resist) of the serpentine pattern and leads was placed into position at the nose of the hemisphere, and the hemisphere was exposed to ultraviolet light for a prescribed period. The hemisphere was then placed into a developer, which removed the photoresist (the area masked off from the light) in the areas exposed to light,

leaving the serpentine and conductor pattern on the model surface. This resist image on the model was then baked (413 K for one-half hour) onto the surface and palladium etch was applied. This etch (aqua regia) will not penetrate the photoresist. The model was rinsed, a chrome etch was applied to remove the chrome deposit, and the model was rinsed again.

Thick-film leads of silver were screened on the hemisphere so as to overlap the palladium leads (fig. 6) and were fired on in a kiln. The model was then placed in a sputtering system and an insulation coat was applied. For the quartz models a deposit of silicon dioxide (SiO_2) was applied over the model surface, whereas a deposit of aluminum oxide (Al_2O_3) was applied over the MACOR models. The wire leads were soldered onto the silver thick-film conductor.

These thin-film hemispheres were fabricated and calibrated for testing in the Langley Expansion Tube (refs. 29 and 30), a hypersonic-hypervelocity impulse facility with a run time of only 0.0002 sec; no special preparation was made for their being tested in conventional wind tunnels. The SiO_2 and Al_2O_3 overlayers, which were relatively thin (less than approximately 5000 Å), are required for high-enthalpy facility use where ionization is present; but presumably the overlayers would not have been needed for the present tests.

Recording System

For tests in the CFHT, output signals from the heat-transfer gages were recorded on magnetic tape by a Beckman 210 analog-to-digital data recording system interfaced to a Control Data series 6000 computer system. The maximum sampling rate of this system was used (40 per sec). Thin-skin hemisphere temperature prior to injection into the flow from the sheltered position was also recorded by the Beckman system. The ambient temperature of the enclosed injection system was manually recorded by using a digital readout. For tests in the CF_4 Tunnel, output signals were fed into a 64-channel, analog-to-digital, differential amplifier interfaced to a Hewlett-Packard 9845T computer. The sampling rate used with this data-acquisition system for the present tests was 50 samples per sec.

The electrical circuit used to measure the change in resistance of the thin-film gage during a run is shown in figure 7. The ballast resistance R_B was 10.2 kΩ. For tests in the CFHT, the excitation voltage was supplied by a wet-cell battery, the battery voltage being 1.29 V for tests with the hemispheres and 6.06 V for tests with the flat plate. The output from this circuit was fed first to a differential amplifier and then into the Beckman recording system, which has an upper limit of 100 mV. The differential amplifier was dc coupled and had an upper bandwidth setting of 10 kHz and a lower frequency setting of dc. The amplifier gain setting was 1 for tests with the hemispheres and was 20 or 100 for the flat-plate model. The excitation voltage for tests in the CF_4 Tunnel was 5.85 V. The output from the electrical circuit for the thin-film hemispheres was fed directly into the 64-channel analog-to-digital, differential amplifier system; the smaller output for the flat-plate model and thin-film gages on the rear surface of the disks was first fed into an individual differential amplifier having a gain of 100 and then to the analog-to-digital multichannel system.

Pitot pressure in the CFHT was monitored for each test by using a flat-faced tube having an inside diameter of 2.29 mm and an outside diameter of 3.175 mm. The tip of the pitot probe was at the same nozzle axial station as the five hemisphere heat-transfer gages and was approximately 5 cm to the left of the center heat-transfer gage as viewed by the flow. This pressure was measured by using a

variable-capacitance diaphragm transducer having seven ranges of pressure, the maximum being 133 kPa. The signal from the transducer was also recorded on a magnetic tape by the Beckman recording system at 40 samples per sec. The pitot pressure for tests in the CF_4 Tunnel was inferred from unpublished pitot-pressure distributions measured at the nozzle exit for the reservoir conditions of this study.

DATA-REDUCTION PROCEDURE FOR HEAT-TRANSFER GAGES

Thin-Skin Transient Calorimeter Gages

For the continuous thin-skin hemispheres and the MACOR hemisphere with a stainless-steel insert, the model-surface heat-transfer rate was inferred from the heat balance equation

$$\dot{q}_{aerodynamic} = \dot{q}_{stored} + \dot{q}_{conduction} + \dot{q}_{radiation} \tag{1}$$

By assuming that conduction and radiation (from model to test-section walls or from walls to model) contributions are negligible and the skin thickness, density, and specific heat are constant, the following calorimeter equation is obtained:

$$\dot{q} = \rho_m c_m \tau_m \frac{dT_1}{dt} \omega \tag{2}$$

The temperature time history from the thermocouple welded to the inner surface was used to determine dT_i/dt. Second-order least-squares curve fits were applied to this temperature time data and differentiated to obtain dT_1/dt. Thus,

$$\left.\begin{aligned} T_1 &= a_1 + a_2 t + a_3 t^2 \\ \frac{dT_1}{dt} &= a_2 + 2a_3 t \end{aligned}\right\} \tag{3}$$

A second-order curve fit is used because the variation of T_1 with t is not linear, as will be illustrated subsequently in the section "Results and Discussion." The method used to determine the time interval for which dT_1/dt is evaluated is also discussed in "Results and Discussion." Thin-skin thickness τ_m, density ρ_m, and specific heat c_m vary with temperature, and, thus, there is a limit to the maximum allowable temperature before significant errors are introduced by assuming that these quantities are constant. For the conditions of this study, the skin thickness and density may, with good accuracy, be assumed constant. The skin thickness was measured by using a micrometer and is given in a previous section ("Heat-Transfer Gages") for the two continuous thin-skin stainless-steel hemispheres and the MACOR hemisphere with a stainless-steel insert. The density used for type 347

stainless steel was 8027.17 kg/m^3, and the variation in specific heat for type 347 stainless steel with temperature was accounted for by using the equation

$$c_m = 370.799 + 0.3033T_i \tag{4}$$

where c_m is given in J/kg-K and T_i is given in K.

The tunnel-wall temperature was less than 350 K, and, thus, the radiative heat transfer, $\varepsilon\sigma T^4$, from the tunnel wall to the hemispheres was insignificant. The radiative heat transfer from the hemisphere, assuming a maximum surface temperature of about 400 K, to the tunnel walls is less than 1 percent of the aerodynamic heating and is also considered insignificant.

The curvature correction factor ω represents a geometric correction accounting for the difference in surface area between the inner and outer surfaces of the thin-skin element. (See refs. 35 and 36.) The product $\tau_m\omega$ is referred to as the effective skin thickness τ_{eff} and is defined as the ratio of the volume of the skin element to the area of the skin element subjected to aerodynamic heating. For a sphere having an outer surface radius r_g and inner surface radius $r_g - \tau_m$,

$$\tau_{eff} = \tau_m\left(1 - \frac{\tau_m}{r_g} + \frac{\tau_m^2}{3r_g^2}\right) \tag{5a}$$

Thus, for the continuous thin-skin hemispheres, τ_{eff}/τ_m is equal to 0.75 for the hemisphere having $\tau_m = 1.135$ mm and is equal to 0.76 for the other hemisphere.

Dimensions of the insert for the MACOR hemisphere are shown in the following sketch:

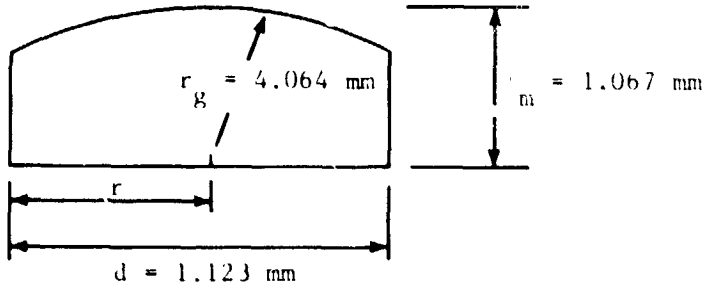

The effective skin thickness in terms of r_g, r, and τ_m is given by the equation

$$\tau_{eff} = \frac{r_g}{6}\left(1 - \sqrt{1 - \left(\frac{r}{r_g}\right)^2}\right) + \frac{r^2}{r_g}\left[\frac{\tau_m}{2\,r_g\left(1 + \sqrt{1 - \left(\frac{r}{r_g}\right)^2}\right)} - \frac{1}{3}\right] \tag{5b}$$

The value of τ_{eff} calculated from this equation for the stainless-steel insert is 1.043 mm, or $\tau_{eff}/\tau_m = 0.977$. By using the measured volume of the insert obtained from the weighing (see the previous section entitled "Thin-Skin Transient Calorimeter"), $\tau_{eff} = 0.995$ mm, or $\tau_{eff}/\tau_m = 0.933$. This latter value of τ_{eff} was used to compute the heat-transfer rate.

One of the more important contributors to uncertainties in heating rates inferred from thin-skin calorimeter gages is conduction effects. These effects take three basic forms: (1) normal conduction, whereby heat is lost from the rear of the thin skin to the backing material, (2) lateral conduction due to temperature gradients within the skin, and (3) conduction of heat along the thermocouple wires. Lateral-conduction effects are discussed in a subsequent section and the other two effects are discussed briefly at this point.

For any calorimeter gage, heat will be lost to the backing material and this loss can result in an erroneous value of the heat-transfer rate. The heat loss due to normal conduction to the rear surface increases with increasing β_s/β_m (ref. 2), where

$$\frac{\beta_s}{\beta_m} \equiv \sqrt{\frac{\rho_s c_s k_s}{\rho_m c_m k_m}}$$

For the stainless-steel continuous thin-skin hemispheres, the backing material was air under vacuum; thus, $\beta_s/\beta_m \approx 0.0007$. The error in the time rate of change of the temperature of the rear surface dT_1/dt for this small value of β_s/β_m is negligible. For the MACOR hemisphere with a stainless-steel thin-skin insert, the insert was held in place by a thin layer of RTV (room-temperature vulcanizing rubber) around its perimeter; hence, a relatively small portion of the insert was backed with RTV. The ratio β_s/β_m for the stainless-steel thin skin and with RTV backing material is approximately 0.09. If one-third of the rear surface area of the insert is assumed to be backed by RTV, then the slope dT_i/dt will be in error by about 3 percent. (See ref. 2.) Because the backing material in the vicinity of the thermocouple was air and a worst case represented an error less than 3 percent, no correction for this effect was applied to the present results for the MACOR hemisphere with a thin-skin insert.

Conduction effects due to the presence of thermocouple wires attached to the inside surface of the thin skin are discussed in reference 2. For the present ratio of wire diameter to skin thickness of 0.12 and for times greater than 0.3 sec, the maximum error in inferred heat-transfer rate due to heat conduction in a single thermocouple lead should be less than 3 percent. (See ref. 2.) A single wire with the same cross-sectional area as two No. 36 wires yields a ratio of equivalent wire diameter to skin thickness of 0.17, corresponding to errors in inferred heating rate of about 5 percent. No attempt was made in the present study to correct the thin-skin calorimeter data for heat losses along the thermocouple wires.

Thin-Film Resistance Gages

A sketch of a thin-film resistance gage and associated electrical circuit is shown in figure 7. A thin metallic film of thickness δ_f is deposited on the

surface of an electrical insulating material. This thin film serves as an active element in a constant-current circuit; that is, the metallic film serves as a resistance thermometer which is assumed to be of negligible heat capacity. (The temperature of the lower surface of the film is assumed to equal the temperature of the upper surface instantaneously; hence, the film does not affect the temperature history of the substrate.) The thickness of the substrate is assumed to be sufficient for the substrate to behave as a semi-infinite medium. A coating of thickness δ_c of a dielectric is deposited over the film to eliminate possible electrical shorting of the gage in an ionized flow; also, this deposit tends to enhance the durability of the gage.

The basic equation for determining the heat-transfer rate for the thin-film gage previously described is (refs. 2 and 7)

$$\dot{q}(t) = \frac{\sqrt{\pi}\beta_{s,o}}{2}\left[\frac{\Delta T(t)}{\sqrt{t}} + \frac{1}{\pi\sqrt{t}}\int_0^t \frac{\sqrt{\lambda}\,\Delta T(t) - \sqrt{t}\,\Delta T(\lambda)}{(t-\lambda)^{3/2}}\,d\lambda\right] \tag{6}$$

where the substrate thermal properties ($\beta_s = \sqrt{\rho_s c_s k_s}$) are assumed to be constant during the run, $\Delta T(t)$ is an arbitrary surface-temperature time history ($\Delta T(0) = 0$), λ is a dummy variable, and the presence of the thin-film sensor is neglected. Equation (6) is integrated numerically to obtain the heating rate. A difficulty arises in the numerical integration due to the singularity in the integrand evaluated at the upper limit $t = \lambda$. To avoid this singularity, which will give rise to errors in the deduced value of heating rate, Cook (refs. 22 and 23) developed the following equation

$$\dot{q}(t) = \frac{2\beta_{s,o}}{\sqrt{\pi}} \sum_{i=1}^{n} \frac{\phi(t_i) - \phi(t_{i-1})}{\sqrt{t_n - t_i} + \sqrt{t_n - t_{i-1}}} \tag{7}$$

where $\phi = \int_0^T (k/k_o)\,dT$ and n is the number of steps (time intervals); for constant thermal conductivity, k, $\phi(t) = \Delta T(t)$. Equation (7) provides a simple method for determining the heating rate and is highly accurate, provided a sufficient number of steps have been used. (See refs. 21 to 23.) To illustrate this point, the heating rate was assumed constant so that equation (6) becomes

$$\dot{q}(t) = \frac{\sqrt{\pi}\beta_{s,o}}{\sqrt{t}}\,\frac{\Delta T(t)}{2} \tag{8}$$

A value of $\dot{q}(t)$ representative of that expected on a small hemisphere in the CFHT was chosen for a given value of $\beta_{s,o}$. The temperature change $\Delta T(t)$ was computed as a function of time t from equation (8) and the data were introduced into equation (7). The results obtained are shown in the following table:

Number of steps, n	Error in $\dot{q}(t)$, percent
6	1
9	.5
14	.25
25	.1

Thus, for a data-acquisition rate of 40 samples per sec, the uncertainty in the heating rate introduced by the use of equation (7) will be less than 1 percent for times greater than 0.175 sec.

The assumption of constant substrate thermal properties made in the derivation of equation (6) is appropriate when the substrate temperature change is small, such as in the case for a flat plate. However, this assumption will not be valid for the small hemispheres. Methods of correcting for the effect of variable substrate thermal properties are presented in reference 11 for Corning Code 7740 Pyrex and quartz and in references 22 and 23 for Code 7740 Pyrex (hereinafter referred to as Pyrex 7740). These methods are discussed in appendix A along with the correction factors applied herein to the heating rates computed by using equation (7).

Because the test time of the CFHT and the CF_4 Tunnels is several orders of magnitude longer than that of impulse facilities, the assumption of the substrate behaving as an infinite slab during the test period is subject to question. An analysis for a surface subjected to a step function of temperature is presented in reference 2. In this analysis, a dimensionless penetration depth $x^* \equiv x/(2\sqrt{\alpha t})$ is introduced. For the temperature at a given depth to be less than 1 percent of the surface temperature, x^* must exceed 1.58; similarly, for the heat-transfer rate at a given depth to be less than 1 percent of the surface value, x^* must exceed 1.87. The analysis of reference 2 shows that the substrate thickness, for a total test time of 1 sec, must exceed 0.35 cm for both quartz and MACOR to insure the validity of a one-dimensional substrate. This condition was examined experimentally in the present study by using MACOR disks having thin-film gages on the front and rear surfaces. (See previous section entitled "Models.")

The change in surface temperature of the substrate is inferred from the voltage change measured with the circuit shown in figure 7. (This circuit was borrowed for this study and has since been replaced by a circuit containing a constant-current diode.) If the current is assumed constant in this circuit, the change in voltage corresponding to the change in resistance of the thin film during a test is given by the relation

$$\Delta E_f(t) = I_{f,o}\,\Delta R_f(t) = E_{f,o}\,\frac{\Delta R_f(t)}{R_{f,o}} \tag{9}$$

Each thin-film gage is calibrated by immersion in a well-stirred oil bath. The oil is heated to various temperatures and the gage resistance is measured for a specified current through the gage (generally 1 mA). Because of the near-linear variation of

the film resistance with temperature, the usual procedure (ref. 2) is to introduce the temperature coefficient of resistance α_R, defined as

$$\alpha_R \equiv \frac{1}{R_{f,o}} \frac{\Delta R_f}{\Delta T} \tag{10}$$

which is determined from the calibration. The temperature range of the calibration should span the range of surface temperature expected during a test, since α_R is generally not constant. (See refs. 2 and 16.) For the present study, $R_{f,o}$ in equation (10) corresponds to the resistance measured at a temperature of 297.2 K during the calibration, and $\Delta R_f/\Delta T$ was inferred from the calibration data of resistance as a function of temperature. Calibration results for the thin-film hemispheres obtained before, during, and after the present test series are discussed in detail in appendix B. Also discussed in this appendix is the effect of gage current on the variation of resistance with temperature.

From equations (9) and (10), the change in substrate temperature is given by the equation

$$\Delta T(t) = \frac{\Delta E_f(t)}{\alpha_R E_{f,o}} \tag{11}$$

where $\Delta E_f(t)$ is measured during the test at given times and the initial voltage $E_{f,o}$ is measured just prior to the test.

If the gage resistance is not negligible in comparison to the ballast resistance, the current variation must be considered. For this case, the temperature change is found by using the equation (eq. (7c) in ref. 28)

$$\Delta T(t) = \left[\frac{1 + \frac{R_{f,o}}{R_B}}{1 - \frac{R_{f,o}}{R_B} \frac{\Delta E_f(t)}{E_{f,o}}} \right] \frac{\Delta E_f(t)}{\alpha_R E_{f,o}} = \left[\frac{1 + \frac{E_{f,o}}{E_b - E_{f,o}}}{1 - \frac{\Delta E_f(t)}{E_b - E_{f,o}}} \right] \frac{\Delta E_f(t)}{\alpha_R E_{f,o}} \tag{12}$$

Different zero times are used herein for the thin-skin and the thin-film models. Zero time for the thin-film hemispheres corresponds to the time at which these fast-response gage first experience an increase in the surface temperature as the model is injected into the flow. This time scale is denoted as t. For the thin-skin hemispheres in the CFHT, zero time is selected as the time at which the two-way switch on the injection system reaches full-scale output. At this zero time, the hemisphere models will have been at rest, 5.1 cm from the nozzle center line, for approximately 0.1 sec. In the CF_4 Tunnel, zero time for the thin-skin hemispheres corresponds to arrival of the hemispheres 7.62 cm below the nozzle center line, as determined from a slide wire. This time scale is denoted as t' in the text and plots.

PREDICTION OF FLOW CONDITIONS AND STAGNATION-POINT HEAT-TRANSFER RATE

Flow Conditions

Free-stream and post-normal shock flow conditions for the CFHT were determined by using the measured reservoir pressure, reservoir temperature, and pitot pressure. The ideal-air value of $p_{t,2}/p_{t,1}$, corresponding to the measured value of $p_{t,2}/p_{t,1}$, was determined from the imperfect-air calculations of reference 37. (The results of ref. 37 account for intermolecular force effects that occur at the present reservoir stagnation conditions.) Ideal-air flow quantities corresponding to this ideal-air value of $p_{t,2}/p_{t,1}$ were obtained from the tables of reference 38 and were corrected for imperfect-air effects by using reference 37.

Free-stream and post-normal shock flow conditions for the CF_4 Tunnel were computed from the measured reservoir pressure and temperature, pitot pressure, and imperfect CF_4 relations of reference 39. Imperfect CF_4 values of reservoir density, enthalpy, and entropy, were computed from the measured reservoir pressure and temperature. An isentropic expansion was performed from the reservoir, through the nozzle throat, and to an estimated value of free-stream static temperature at the test section. A normal shock crossing is performed and the resulting stagnation pressure behind the shock is compared with the measured pitot pressure. The free-stream static temperature is varied until the measured and computed pitot pressures agree to within a given tolerance, usually 0.05 percent.

Stagnation-Point Heat-Transfer Rate

Predicted values of the stagnation-point heat-transfer rate to a sphere in airflow were obtained by using the method of reference 40. The correlation of numerical results performed by Fay and Riddell (ref. 40) for undissociated airflow resulted in the following equation for the heat-transfer rate

$$\dot{q}_{t,2} = \frac{0.76}{N_{Pr,w}^{0.6}}(\rho_{t,2}\mu_{t,2})^{0.4}(\rho_w\mu_w)^{0.1}(h_{t,2} - h_w)\Gamma^{0.5} \tag{13}$$

The post-normal shock flow region in the CFHT is thermally perfect (the compressibility factor is equal to unity) but calorically imperfect ($\gamma_{t,2} \neq \gamma_\infty$). Hence,

$$\rho_w = \frac{p_{t,2}W}{R_{gas}T_w} \tag{14}$$

and

$$\rho_{t,2} = \frac{I_{t,2}W}{R_{gas}T_{t,2}} \tag{15}$$

The viscosity corresponding to T_w and $T_{t,2}$ is determined from Sutherland's formula (ref. 38)

$$\mu = 1.462 \times 10^{-6}\left(\frac{T^{1.5}}{T + 112}\right) \tag{16}$$

where T is given in K and μ is given in N-sec/m^2; and the velocity gradient Γ is determined from the modified Newtonian relation for axisymmetric bodies (ref. 40)

$$\Gamma = \frac{1}{r_g}\sqrt{\frac{2(p_{t,2} - p_\infty)}{\rho_{t,2}}} \tag{17}$$

The value of free-stream static pressure p_∞ is determined from the relation (ref. 38)

$$p_\infty = 0.995 p_{t,2} \Bigg/ \left\{\left[\frac{(\gamma_\infty + 1)M_\infty^2}{2}\right]^{\frac{\gamma_\infty}{\gamma_\infty - 1}}\left[\frac{\gamma_\infty - 1}{2\gamma_\infty M_\infty^2 - (\gamma_\infty - 1)}\right]^{\frac{1}{\gamma_\infty - 1}}\right\} \tag{18}$$

where the quantity 0.995 represents a correction for imperfect-air effects. Although γ_∞ is equal to 1.4 (ideal-air value) in the CFHT, the ratio of specific heats in the post-normal shock region $\gamma_{t,2}$ is less than that in the free stream ($\gamma_{t,2} \approx 1.34$). Thus, the enthalpy at the stagnation point $h_{t,2}$ must be determined from imperfect-air results (ref. 41). For $200\ K < T < 1200\ K$, the imperfect-air enthalpy h is given to within 0.1 percent by the equation

$$\frac{hW}{R_{gas}T} = 3.51715 - 2.5041 \times 10^{-4}T + 5.5079 \times 10^{-7}T^2 - 1.7197 \times 10^{-10}T^3 \tag{19}$$

Values of $h_{t,2}$ and h_w were obtained by using equation (19).

The Prandtl number at the wall $N_{Pr,w}$ was assumed equal to 0.71. Because $p_\infty << p_{t,2}$ at a Mach number of 10, the heat-transfer rate determined from equation (13) is a function of the measured quantities T_w, $T_{t,2}$ (which is nearly equal to $T_{t,1}$ (ref. 37)), $p_{t,2}$, and r_g.

Measured values of the heating rate are presented in terms of the heat-transfer coefficient as defined in the equation

$$C_h \equiv \frac{\dot{q}}{T_{aw} - T_w} \tag{20}$$

For a hemisphere in hypersonic flow, the adiabatic-wall temperature T_{aw} at the stagnation point is equa' to the stagnation temperature $T_{t,2}$ (ref. 42). Because γ_{aw} is not equal to γ_∞ for the CFHT flow conditions, the adiabatic-wall temperature for the flat plate was obtained from the relation

$$h_{aw} = h_\infty + \frac{\eta_r U_\infty^2}{2} = \frac{\gamma_\infty}{\gamma_\infty - 1} \frac{R_{gas}}{W} T_\infty \left(1 + \frac{\gamma_\infty - 1}{2} \eta_r M_\infty^2\right) \tag{21}$$

To obtain an imperfect-air expression for T_{aw} as a function of h_{aw}, a first-order least-squares fit was applied to the imperfect-air data of reference 41 for $200\ K < T_{aw} < 1200\ K$. The resulting equation is

$$\frac{h_{aw} W}{R_{gas} T_{aw}} = 3.4056 + 2.3729 \times 10^{-4} T_{aw} \tag{22}$$

and is accurate to within 1 percent. The nominal value of free-stream Mach number for the present tests in the CFHT is 10.05, and the corresponding value of T_∞ corrected for imperfect-air effects is given to within 3 percent by the relation

$$T_\infty = 0.0492 T_{t,2} \tag{23}$$

By combining equations (21) to (23), setting γ_∞ equal to 1.4, and setting M_∞ equal to 10.05, the adiabatic-wall temperature is given by the relation

$$T_{aw} = 7176\left(\sqrt{1 + (1.409 \times 10^{-5}) T_{t,2}(1 + 20.2\eta_r)} - 1\right) \tag{24}$$

For a blunt body, where $\eta_r = 1$ and $T_{aw} = T_{t,2}$, this expression is accurate to within 3 percent for $600\ K < T_{t,2} < 1000\ K$.

The flow over the flat plate is expected to be laminar; hence, from reference 42, the recovery factor is given by the relation

$$\eta_r = \sqrt{N_{Pr,w}} \tag{25}$$

The reservoir temperature $T_{t,1}$ for the test on the flat plate (run 14) was equal to 979 K. By setting $N_{Pr,w}$ equal to 0.71 in equation (25), the value of T_{aw} from equation (24) is equal to 842.5 K.

RESULTS AND DISCUSSION

Durability of Thin-Film Gages

From consideration of the method of construction, it is obvious that thin-skin calorimeter models are more substantial, and thus less likely to be damaged by the

flow, than thin-film models. Hence, a primary concern with the usage of thin-film gages that face into the flow of conventional hypersonic wind tunnels is durability. Another concern is performance. As noted previously, thin-film gages were developed for use in impulse facilities. When used in a conventional wind tunnel, the gage is subjected to flow for a period of time roughly 1000 times longer than that in an impulse facility. Thus, the ability of the thin-film gage to survive the high-temperature environment of the CFHT over a relatively long period of time without being destroyed or suffering an appreciable change in physical characteristics was uncertain.

Four thin-film gages with quartz hemisphere substrates and two with MACOR hemisphere substrates were tested in the CFHT. Only one of the four quartz hemispheres survived a test, whereas MACOR hemisphere no. 1 survived the six tests it was subjected to and MACOR hemisphere no. 2 survived all nine tests. Post-test examination of the quartz hemispheres revealed the substrate experienced very little sandblasting by the flow. The palladium leads between the serpentine pattern and silver leads were wiped from the surface during the test period. (See fig. 8(a)). The output of the first two quartz hemisphere gages tested indicated that the circuit opened between 0.675 and 0.875 sec after the gage was injected into the flow.

Adhesive properties of sputtered thin films do not equal those of painted and fired films (ref. 2). Thin-film gages fabricated previously without a chromium sublayer exhibited very poor adhesion (could be wiped off the surface of the substrate with a soft cloth). Application of the chromium sublayer improved adhesion significantly, although a large variation in adhesive properties was observed between various batches. This variation was determined by covering the gage with tape and observing whether the gage remained fixed to the surface upon removal of the tape. No such adhesion test was performed for the present thin-film hemispheres. The only difference in the fabrication procedure between the quartz and MACOR hemispheres was the material used as an overlayer on the thin-film gage. The quartz hemispheres received a SiO_2 overlayer, whereas the MACOR hemispheres received an Al_2O_3 overlayer. (See the previous section entitled "Heat-Transfer Gages.") However, the contribution of the overlayer to the difference in survivability between the MACOR and quartz hemispheres is believed to be small. The fact that the initial gage resistance for the MACOR hemispheres was 50 to 70 percent greater than that for the quartz hemispheres (appendix B) implies a rougher surface for the MACOR. This is as expected from consideration of the composition of MACOR and the method used to fabricate the hemispheres. The survivability of the MACOR hemispheres is attributed primarily to the improved adhesion provided by the greater surface roughness.

Although the survival of the MACOR thin-film hemispheres under the hostile temperature environment generated in the CFHT is encouraging, it should be noted that models tested before and after the present study were sandblasted by solid contaminants carried in the flow. Such sandblasting is common to most hypersonic wind tunnels and varies between facilities, depending on the condition of filters, cleanliness of the supply gas, and level of reservoir stagnation pressure and temperature. New in-line filters ahead of the reservoir were installed in the CFHT immediately prior to the present tests and are credited, in part, to the survival of the MACOR gages.

Following the tests made in the CFHT, the two MACOR hemispheres were tested in the CF_4 Tunnel. These tests in the CF_4 Tunnel were performed for three primary reasons: (1) to determine if the high-temperature tetrafluoromethane would have any effect, such as corrosion, on the thin-film gages, (2) to subject the thin-film gages to a somewhat higher flow-contamination level than that usually experienced in the

CFHT, and (3) to obtain values of stagnation-point heat-transfer rate and time histories of the heat-transfer coefficient to supply information concerning the flow characteristics of the CF_4 Tunnel.

Models tested in the CF_4 Tunnel previous to the present study had been severely sandblasted by solid contaminants carried by the flow. The primary source of these contaminants is rust-like particles. These particles form on the inner surface of the stainless-steel heater tubing and are a result of the Freon gas reacting with the tubing at elevated temperatures (ref. 33). (Freon is a trademark of E. I. du Pont de Nemours & Co., Inc.) A rotating disk serving as a particle collector revealed that most of the contaminants arrived at the test section during the nozzle starting process, which requires about 3 sec. In an effort to reduce the level of contamination during the present tests, several changes were made in the operating procedure of the CF_4 Tunnel. The facility was operated at a lower heater, hence reservoir, temperature than in previous tests. The heater tubing was evacuated and filled with an inert gas (argon) between runs. One or two short, high-pressure runs were made prior to actual testing to help clean the tubing out. The thin-film hemispheres were injected into the flow approximately 5 sec after tunnel start. With these procedures, the gages survived all three tests. The MACOR hemispheres (fig. 8(b)) were somewhat discolored from the tests in the CF_4 Tunnel, but they did not suffer any appreciable change in properties. It should also be noted that all five MACOR disks survived both the runs they were subjected to.

Calibration of Thin-Film Gages

Calibrations of two MACOR thin-film hemispheres before, during, and after the test series in the CFHT showed that large variations in $\Delta R/\Delta T$ occurred during the tests. (See appendix B.) For example, MACOR hemisphere no. 1 experienced a 45-percent decrease in $\Delta R/\Delta T$ after four runs, and MACOR hemisphere no. 2 experienced a 28-percent decrease after six runs. The corresponding decreases in the temperature coefficient of resistance α_R were 6 and 3.3 percent, respectively. The measured values of gage resistance prior to a run R_o showed that the decrease in R_o with number of runs was accelerated by an increase in reservoir pressure, hence maximum surface temperature. This variation in thin-film properties is attributed to the fact that the films were not annealed prior to testing. The initial calibration of the MACOR hemispheres was for temperatures from 297 K to only 353 K. This upper temperature was established from previous studies to avoid decomposition of adhesives used on various models. Thus, the thin-films deposited on the MACOR hemispheres were not subjected to the high temperatures (in excess of 525 K (ref. 2)) required for stabilization of the thin film prior to being tested in the CFHT.

The quartz thin-film hemispheres were initially calibrated between 297 K and 505 K. (See appendix B.) These calibrations revealed a discrepancy between the gage resistance at a given temperature for ascending and descending temperature, indicative of an annealing of the thin film. The contribution of the uncertainty in α_R to the inferred value of $\dot{q}_{t,2}$ for the quartz hemispheres is believed to be small, since these gages were calibrated prior to being tested. For the MACOR thin-film data presented herein (last three runs in the CFHT), the MACOR gages had become relatively stable and before-and-after calibrations showed a variation in α_R less than 3.2 percent.

After completion of the present tests in the CFHT, MACOR hemispheres nos. 1 and 2 were examined for ohmic (I^2R) heating effects. (See appendix B.) Although the

resistance at a given temperature increased for values of the current greater than 10 mA, corresponding values of α_R varied less than 1.3 percent over the range of I_o from 1 to 20 mA for both hemispheres. Values of stagnation-point heat-transfer rate inferred from the thin-film hemispheres correspond to excitation currents less than 0.2 mA for tests in the CFHT and less than 0.8 mA for tests in the CF_4 Tunnel; the current used during tests with the flat-plate model was less than 0.8 mA. For such low levels of current, ohmic heating effects were negligible.

Time Histories of Measured Outputs

Time histories of the pitot pressure, temperature inferred from the output of the thermocouple attached to the inside surface of a stainless-steel insert in a MACOR hemisphere, millivolt output of MACOR thin-film hemisphere no. 2, and the output from a switch mounted on the injection mechanism are shown in figure 9 for CFHT run 11 ($p_{t,1}$ = 2.4 MPa) and in figure 10 for CFHT run 13 ($p_{t,1}$ = 11.3 MPa). Zero time corresponds to the instant that the output from the thin-film gage(s) increases from the base-line value, indicating initial exposure to the flow. (That is, $t = 0$ denotes arrival at the plane of the nozzle wall during injection into the flow.) The thermocouple output of the MACOR hemisphere with the insert (fig. 9) begins to increase approximately 0.05 sec after the output of the thin-film gage begins to increase. According to the injection-switch output, the time required for the five-probe rake to travel from the plane of the nozzle wall to a position within 5.1 cm of the nozzle center line is about 0.4 sec. The time at which the full-scale output of the injector switch is obtained is designated as $t' = 0$. The pitot-pressure probe is subjected to the flow at a later time than the heat-transfer gages since it was mounted to the left of these gages as viewed by the flow. Because the pressure transducer for the pitot pressure is mounted external to the tunnel, a pressure lag will exist. For the low-pressure run (fig. 9), the transducer first experiences an increase in pressure at a time of about 0.225 sec, and the pressure time history is characterized by an increase to a peak value, followed by a decrease then increase to a near-constant (within 1 percent) value. This peak is believed to be due to the dynamics of the transducer as the diaphragm is pulsed and is not indicative of the true pressure history. The pitot-pressure ratio $p_{t,2}/p_{t,1}$ was essentially constant for times greater than 0.7 sec and the pressure ratio between the time the hemispheres entered the test core and 0.7 sec is assumed equal to this constant value of $p_{t,2}/p_{t,1}$. As expected, the lag in pitot pressure at the highest reservoir pressure (fig. 10) is less than that at the lowest reservoir pressure, and $p_{t,2}$ becomes constant at about the time that the five-probe rake comes to rest.

Time Histories of Substrate Surface Temperature and Heat-Transfer Rate for Thin-Film Hemispheres

The variation in substrate surface temperature with time is shown in figure 11(a) for a low-reservoir-pressure test in the CFHT and in figure 11(b) for a high-pressure test. Prior to the low-pressure test (run 11), MACOR hemisphere no. 2 had experienced six tests, quartz hemisphere no. 4 had experienced two previous tests but had been damaged, and quartz hemisphere no. 2 was being tested for the first time. At a time of 1 sec for the low-pressure run (fig. 11(a)), the change in surface temperature of the substrate is about 150 K. This surface-temperature change exceeds the calibration temperature range for MACOR hemisphere no. 2 at the time of the test. The surface-temperature change at a time of 1 sec for the high-pressure run (fig. 11(b)) is 210 K to 220 K.

Calibrations performed immediately after the high-pressure run (run 13) revealed that the resistance of MACOR hemisphere no. 2 varied linearly with temperature for ΔT equal to 210 K; however, the initial high-temperature calibration of MACOR hemisphere no. 1 after run 13 showed that the variation of R with T became nonlinear for $\Delta T > 125$ K. That is, annealing was occurring during the rather long calibration of the gage. Thus, the surface-temperature change inferred for MACOR hemisphere no. 1 is expected to contain a larger uncertainty (approximately 4 percent) than that for MACOR hemisphere no. 2 for times in excess of approximately 0.4 sec at the highest reservoir pressure.

The surface-temperature change with time for MACOR hemisphere no. 1 in the CF_4 Tunnel is shown in figure 12 for reservoir pressures of 7.5 and 16.6 MPa. As observed in the CFHT, ΔT_w increases monotonically with t and is free of any inflections over the time interval $0.1 < t < 2$ sec. For a given time, the value of ΔT_w at the highest reservoir pressure in the CF_4 Tunnel is less than that experienced at the lowest reservoir pressure in the CFHT. Even at a time of 2 sec, ΔT_w in the CF_4 Tunnel is still within the linear range of the thin-film calibrations.

Time histories of stagnation-point heat transfer for runs 11 and 13 in the CFHT are shown in figures 13(a) and 13(b), respectively. The stagnation-point heat-transfer rate inferred from the thin-film gages is observed to increase rapidly as the hemispheres traverse the nozzle-wall boundary layer, reach a maximum value at a time t of approximately 0.3 sec, and decrease monotonically thereafter. These results (fig. 13) show that approximately 0.3 sec is required for the 5-probe survey rake to travel through the nozzle-wall boundary layer; thus, the hemispheres experience inviscid test flow for about 0.15 sec prior to coming to rest within 5.1 cm of the nozzle center line. The decrease in heat-transfer rate for $t > 0.3$ sec is due to the corresponding increase of the hemisphere surface temperature with time and is, naturally, more pronounced at the higher reservoir pressure because of the larger change in surface temperature.

The stagnation-point heat-transfer rate predicted by using the method of reference 40 is compared with measurement in figure 13. The open symbols for the MACOR hemispheres in figure 13 correspond to the substrate thermal conductivity k_s being assumed constant and to the correction factor accounting for the variation in substrate thermal properties being near unity. The closed symbols denote $k_s = k_s(T)$ and a revised method for obtaining correction factors. (See appendix A.) The trend of decreasing heat-transfer rate with time for the lowest reservoir pressure (fig. 13(a)) is predicted quite well by the method of reference 40. Over the time interval from 0.5 to 1.0 sec, the prediction is 2 to 3 percent greater than that measured for the MACOR hemisphere no. 2 assuming k_s constant; for $k_s = k_s(T)$, measured heat-transfer rate exceeds prediction by 4 to 7 percent. At the highest reservoir pressure (fig. 13(b)), the discrepancy between predicted heat-transfer rate and that measured by MACOR hemisphere no. 2, assuming k_s = Constant, increases with time. (This discrepancy is 13 percent at 0.5 sec and 19 percent at 1.0 sec.) A significant improvement in the agreement between measurement and prediction occurs for the case $k_s = k_s(T)$.

From figure 13(a), the values of stagnation-point heat-transfer rate measured with the two quartz hemispheres agree to within 10 percent; and the heat-transfer rate obtained from MACOR hemisphere no. 2, $k_s = k_s(T)$, agrees quite well with the values of quartz hemisphere no. 2. Quartz hemisphere no. 2 was being tested for the first time in run 11, whereas quartz hemisphere no. 4 had been damaged in previous runs and is believed to be less accurate than quartz hemisphere no. 2. (See appendix C.) Unfortunately, CFHT run 11 (fig. 13(a)) provided the only opportunity to

compare values of heat-transfer rate obtained from the MACOR hemispheres and quartz hemispheres. In such a comparison, it is of interest to examine the magnitude of the correction required to account for variation in substrate thermal properties. For a surface-temperature change ΔT_w of 140 K (fig. 11(a)), β_s is 1.30 times the value at ambient temperature $\beta_{s,o}$ for a quartz substrate (appendix A); for a MACOR substrate, the ratio $\beta_s/\beta_{s,o}$ is approximately 1.13. The corresponding ratio of heat-transfer rate for variable β_s to heat-transfer rate for constant β_s (that is, $(\dot{q})_{\beta_s(T)}(t) \Big/ (\dot{q})_{\beta_{s,o}}(t)$) is 1.17 for quartz and 1.08 for MACOR. The magnitude of the correction factor $(\dot{q})_{\beta_s(T)} \Big/ (\dot{q})_{\beta_{s,o}}$ will be discussed in more detail subsequently.

Time Histories of Heat-Transfer Coefficient for Thin-Film Hemispheres

Although the heat-transfer rate varies with time, the stagnation-point heat-transfer coefficient $C_h = \dot{q}_{t,2} \Big/ (T_{aw} - T_w)$, where $T_{aw} = T_{t,2} = T_{t,1}$, is expected to be nearly constant with time. (Examination of eq. (13) shows C_h varies less than 0.1 percent for $\Delta T_w = 200$ K.) The heat-transfer coefficient for MACOR hemisphere no. 2 is shown as a function of time for CFHT runs 11 and 13 in figure 14. Also shown in figure 14 are predicted values (ref. 40) of the heat-transfer coefficient. The results for the low-reservoir pressure test (run 11) show that the heat-transfer coefficient is nearly constant (varies less than 1 percent) over the time interval of 0.5 to 1.0 sec. In fact, the heat-transfer coefficient remained essentially constant up to the last time that data were obtained (t = 1.625 sec), corresponding to $\Delta T_w = 181$ K. For the high-reservoir pressure test (run 13), the measured heat-transfer coefficient decreases 5 percent between 0.5 and 1.0 sec, and this decrease is nearly linear for $0.3 \text{ sec} < t < 1.75 \text{ sec}$. This decrease in heat-transfer coefficient may be due, in part, to accounting incorrectly for the variation of substrate thermal properties with temperature for MACOR.

The value initially used for the thermal conductivity of MACOR (appendix A) was determined by Dynatech R/D Company, Cambridge, Massachusetts, and was limited to a range in temperature from 300 K to 400 K; thus, the value of k_s at the high surface temperatures experienced during runs 11 and 13 was unknown. The results of figure 14 suggest that a more accurate determination of k_s for MACOR may be realized by superimposing the trend of k with T (see appendix A) measured by Wyle Laboratories, Hampton, Virginia, onto the value of k deduced for a temperature of 300 K. The resulting equation is

$$k = 0.013699 + 8.27529 \times 10^{-6} T \tag{26}$$

where k is given in W/cm-K and T is given in K.

The correction factor for MACOR was also modified, as discussed in appendix A and represented by equation (A9). The effect of these modifications to the expressions used to infer heating rates for MACOR substrates is shown in figures 13 and 14 by the solid symbols. From figure 13, modified heating rates were observed to exceed prediction (ref. 40) by 4 to 7 percent for a range in time from 0.5 to 1.0 sec at the lowest value of $p_{t,1}$ (fig. 13(a)), whereas prediction exceeds the modified values by about 3 to 6 percent at the highest value of $p_{t,1}$ (fig. 13(b)). Turning to figure 14, the modified heat-transfer coefficient was observed to be constant to within

4 percent for both reservoir pressures and for a range in time from 0.5 to 1.0 sec. These facts imply that equations (26), (A3b), (A3c), and (A9) provide a reasonably accurate value of the heat-transfer rate over a wide range of ΔT_w for MACOR substrates. However, it must be emphasized that the method used to correct for the variation in substrate thermal properties is quite crude, and additional study is required in this area.

Time histories of the stagnation-point heat-transfer coefficient for MACOR thin-film hemisphere no. 1 in the CF_4 Tunnel are shown in figure 15 for three reservoir pressures. Values of the heat-transfer rate used to compute the heat-transfer coefficient were obtained by using equation (A9). From figure 15, MACOR hemisphere no. 1 reaches the inviscid test core in about 0.2 sec, although the rake does not reach a position 7.62 cm below the nozzle center line until $t = 1.36$ sec, corresponding to $t' = 0$. The heat-transfer coefficient is relatively constant over the time interval $0.5 \text{ sec} < t < 1.0 \text{ sec}$, increasing 4 to 5 percent for the three values of reservoir pressure tested.

Tests With Thin-Film MACOR Disks of Various Thicknesses

Another possible explanation, in part, for the measured variation of heat-transfer coefficient with time is the assumption that the substrate behaves as an infinite slab. This assumption may not be valid for the relatively long test times of the present study. To examine the validity of the infinite-slab assumption experimentally, MACOR disks of various thicknesses were tested. Each of the five disks had a thin-film gage at the center of the front surface confronting the flow and a gage at the center of the rear surface, which was shielded from the flow. These disks were injected into the flow simultaneously. The measured change in surface temperature at the stagnation region is shown in figure 16 as a function of disk thickness ℓ for various times and two reservoir pressures. These data show that ΔT_w is approximately constant with thickness for times less than 1 sec for both reservoir pressures. For $t < 1$ sec, the value of ΔT_w for the thinnest disk ($\ell = 1.27$ mm) at a given time exceeds that of the other disks. The effect of this increase in ΔT_w on the heat-transfer rate calculated by assuming a semi-infinite slab (eq. (7)) is shown in figure 17. For $\ell > 2.54$ mm, the heat-transfer rate is nearly constant over the time interval from 0.5 to 4 sec (within 3 percent of 4.6×10^4 W/m^2); whereas for $\ell = 1.27$ mm, the heat-transfer rate increases with time. Thus, the measured values of ΔT_w and heating rates on the front of the disks imply that the assumption of an infinite slab is questionable for the thinnest disk.

The ratio of the temperature change on the rear surface to that on the front surface is plotted as a function of $\ell/2\sqrt{\alpha t}$ in figure 18 for several thicknesses. The heat-transfer rate measured on the rear surface is shown in figure 19 as a function of time for several thicknesses. The results of figures 18 and 19 show that the infinite-slab assumption is valid for substrate thicknesses greater than 3.81 mm for the conditions of the present study. This thickness is close to the radius of curvature of the thin-film hemispheres. Although the substrate thickness normal to the thin-film gage on the hemispheres exceeds 3.81 mm, lateral flow of heat may invalidate the assumption of semi-infinite-slab behavior, causing C_h to increase with time. The results of figures 14 and 17 tend to imply that the variation of C_h with time for the thin-film hemispheres is due primarily to the uncertainty in the method used to correct for the variation in substrate thermal properties for MACOR; the hemispherical substrate is believed to behave as a semi-infinite slab at the geometric stagnation point.

Flat Plate With Thin-Film Gages

In order to examine the performance of the thin-film gages in a low-heating environment, the thin-film gages were tested on a sharp-leading-edge flat plate in the CFHT. The heat-transfer coefficient measured at the surface of the plate with 2 (z = 6.55 and 9.40 cm) of the 13 thin-film gages or the quartz substrate are shown in figure 20 as a function of time. The change in substrate surface temperature was less than 2.8 K for a time interval of 1 sec for both gages. The heat-transfer coefficient was constant (within 1.7 percent of mean value) for a range in time t from 0.3 to 2 sec. For tests involving very small changes in surface temperature, the high sensitivity (signal-to-noise ratio) of the thin-film gages enjoys a distinct advantage over the thin-skin calorimeter gages and, accordingly, are expected to provide a more accurate value of measured heat-transfer rate.

Thin-Skin Calorimeter Heat-Transfer Gages

The time variation of the inner surface temperature of the two continuous thin-skin hemispheres and the MACOR hemisphere with an insert is shown in figure 21. These CFHT data correspond to a reservoir stagnation pressure of 11 MPa and are plotted as a function of time t. Zero time was determined from the output of the fast-response thin-film hemispheres and represents the initial exposure of the hemispheres to the nozzle boundary-layer flow during the insertion process. Also illustrated in figure 21 is the time at which the thin-film hemispheres show that the heat-transfer coefficient becomes constant (t > 0.325 sec). From figure 21, the inner surface temperature of the insert in the MACOR hemisphere increases from 301 K to 395 K over the period of time from 0 to 0.9 sec. The surface-temperature change is somewhat less for the continuous thin-skin hemispheres over this same period, although the data of the MACOR hemisphere and of the thin-skin hemisphere with a shell thickness of 1.034 mm are in close agreement from 0 to 0.6 sec. The surface-temperature time history repeats quite well between runs 4 and 13 for the continuous thin-skin hemisphere having a shell thickness of 1.135 mm.

Consider equations (2) and (20) in the form

$$C_h = \rho_m c_m \tau_{eff} \frac{dT_1/dt}{T_{t,2} - T_w} \tag{27a}$$

or assuming that $T_w = T_1$,

$$\frac{C_h}{\rho_m c_m \tau_{eff}}\, dt = \frac{dT_1}{T_{t,2} - T_1} \tag{27b}$$

For small time intervals (Δt < 0.25 sec), the maximum change in T_1 for the thin-skin hemispheres is approximately 40 K. From equation (4), the variation in c_m for

this change in T_i is less than 2.6 percent. If it is assumed that c_m, ρ_m, τ_{eff}, and C_h are constant, then integration gives

$$\frac{C_h}{\rho_m c_m \tau_{eff}}(t - t_o) = \ln\left(\frac{T_{t,2} - T_{i,o}}{T_{t,2} - T_i}\right) \tag{28}$$

Thus, in the absence of conduction effects, the quantity $\ln[(T_{t,2} - T_{i,o})/(T_{t,2} - T_i)]$ will vary linearly with time. As discussed in reference 5, data falling below the linear fit indicate conduction of heat away from the area of the thermocouple, and data lying above the fit indicate a flow of heat into the thermocouple area. Equation (28) also shows that the ideal variation of the inner surface temperature with time is

$$T_i = T_{t,2} - (T_{t,2} - T_{i,o})e^{-\frac{C_h}{\rho_m c_m \tau_{eff}}(t-t_o)} \tag{29}$$

where $T_{t,2}$, $T_{i,o}$, C_h, ρ_m, c_m, and τ_{eff} are assumed to be constant.

Returning to figure 21, the ideal variation of inner surface temperature with time for the continuous thin-skin hemisphere with $\tau_m = 1.135$ mm and run 13 is shown for $\tau_{eff} = 0.75\tau_m$ and $\tau_{eff} = \tau_m$. The value of t_o was selected as 0.35 sec and $C_h = 900$ W/m^2-K. These predicted ideal variations are essentially linear for a range of time from 0.35 to 0.65 sec, and the measured T_i diverges from these predictions with time. This divergence is indicative of conduction effects. It is interesting to note that using the value of C_h measured with a thin-film hemisphere in equation (29), assuming $\tau_{eff} = \tau_m$, provides a much more accurate description of the measured T_i with time than does $\tau_{eff} = 0.75\tau_m$. To establish the time at which conduction effects become significant, the wall-temperature—time histories for the thin-skin hemisphere with $\tau_m = 1.135$ mm and for the MACOR hemisphere with an insert are plotted in figure 22 in terms of $\ln[(T_{t,2} - T_{i,o})/(T_{t,2} - T_i)]$ against time t' for run 4 ($p_{t,1} = 11$ MPa). The time t at which time t' was set equal to zero was obtained from the injector-switch output. (For example, $t' = t - 0.55$ sec for run 4.) Conduction effects become measurable for time t' greater than 0.1 sec for both thin-skin gages, and the conduction of heat is, naturally, away from the region of the thermocouple. This detectable loss of heat from the region of the thermocouple at time t' in excess of 0.1 sec is less for the MACOR hemisphere than for the stainless-steel hemisphere. Based on the results of figure 22, values of stagnation-point heat-transfer rate inferred from thin-skin gages and presented herein correspond to slopes dT_i/dt obtained for a range of t' from -0.125 to 0 sec and are believed to be relatively free of conduction effects.

Results similar to those presented in figure 22 are presented in figure 23 for CFHT run 1, corresponding to $p_{t,1} = 2.4$ MPa. The results of figure 23 show that the MACOR hemisphere does not appear to experience significant conduction effects for

times t' up to approximately 0.3 sec. However, conduction effects are evident for the thin-skin hemisphere for times t' greater than 0.1 sec, as was also observed at higher reservoir pressure.

Comparison of Stagnation-Point Heat-Transfer Rates From Thin-Film and Thin-Skin Hemispheres

Values of the stagnation-point heat-transfer coefficient $\dot{q}_{t,2}/(T_{t,2} - T_w)$ measured with the thin-film hemispheres and the thin-skin hemispheres in both wind tunnels are shown in figure 24 as a function of $\sqrt{p_{t,2}/r_g}$. For the CFHT data, the stagnation-point heat-transfer rate $\dot{q}_{t,2}$ and surface temperature T_w for the thin-film hemispheres correspond to a time t' equal to -0.125 sec; values of $\dot{q}_{t,2}$ for the thin-skin hemispheres correspond to the slope dT_i/dt obtained over the time interval t' from -0.125 to 0 sec. The surface temperature T_w for the thin-skin hemispheres corresponds to the thermocouple readout at $t' = 0$. For the CF_4 Tunnel data, the heat-transfer coefficient for the thin-film hemispheres was evaluated at a time t of 0.4 sec; the slope dT_i/dt for the thin-skin hemisphere was obtained from a second-order fit over a 0.4-sec time interval. The minimum time for this interval corresponds to the time at which the thin-film hemispheres show that the hemispheres have passed through the nozzle boundary layer and are traveling within the inviscid test core. The effective skin thickness $\omega\tau_m$ was used in equation (2) to compute the heat-transfer rate for the thin-skin hemispheres. Heat-transfer rates for the MACOR thin-film hemispheres correspond to equations (A3b), (A3c), and (26) for β_s and to equation (A9) for the correction for variation in substrate properties.

Also shown in figure 24 are values of the stagnation-point heat-transfer coefficient measured on a 10.16-cm-diameter, continuous thin-skin sphere model. This model was tested in the Langley 20-Inch Mach 6 Tunnel (ref. 32) over a wide range of reservoir pressure as part of another study (unpublished) and also in the CF_4 Tunnel. Results from this 10.16-cm-diameter sphere are presented in figure 24 for comparison purposes, and are summarized in the following table for the tests performed in the 20-Inch Mach 6 Tunnel:

$p_{t,2}$, kPa	$\sqrt{\frac{p_{t,2}}{r_g}}, \left(\frac{Pa}{m}\right)^{\frac{1}{2}}$	T_w, K	$T_{t,2}$, K	C_h, $W/m^2\text{-}K$	C_h of ref. 40, $W/m^2\text{-}K$
6.13	347.4	301.5	504.3	105.5	105.1
11.51	477.5	300.4	492.6	143.0	143.5
53.78	1028.9	305.4	490.7	306.7	309.8
98.08	1389.5	315.9	504.0	427.8	420.2

This table shows that measured values of C_h at the stagnation point of this large sphere are predicted to within 2 percent by the method of reference 40 for the ideal-air flow of the 20-Inch Mach 6 Tunnel.

The results obtained in the CFHT are compared with prediction (ref. 40) in figure 24. This prediction corresponds to $r_g = 4.064$ mm, $M_\infty = 10$, $T_w = 400$ K, and $T_{t,2} = 980$ K. The value of T_w represents a mean value, and it should be noted that increasing T_w from 300 K to 500 K changes the predicted value of C_h only 0.5 percent. In view of the uncertainties associated with the present measurements (appendix C), the agreement between the values of heat-transfer coefficient obtained with the thin-film hemispheres and MACOR hemisphere with an insert is quite good (within approximately 5 percent). The values of C_h from these hemispheres also agree to within 5 percent of prediction (ref. 40) for the present range of $\sqrt{p_{t,2}/r_g}$. Relatively poor agreement exists between the continuous thin-skin hemisphere and the other hemispheres. Values of C_h inferred from the continuous thin-skin hemisphere are approximately 30 percent less than predicted values. Because the thin-film and thin-skin hemispheres have essentially the same diameter, any effects due to vibrational nonequilibrium (ref. 43) or to viscosity (Reynolds number) should be of about the same magnitude for both types of gages. Thus, nonequilibrium and viscous effects are not expected to contribute to the discrepancy observed in figure 24 between the continuous thin-skin hemisphere and the other hemispheres.

The primary reason for the large difference between predicted C_h and measured C_h with the continuous thin-skin hemisphere and C_h measured with the other hemispheres is attributed to the nose geometry of the continuous thin-skin hemisphere. Measurements of the outer surface contour on an optical comparator (fig. 3) revealed that the nose region of the continuous thin-skin hemisphere was flattened. This may also be the case for the inner surface; that is, the shell is not spherical in the stagnation region. For the case of a flattened nose, the geometric curvature correction factor ω for the element of the shell in the vicinity of the thermocouple will approach the value for a disk, which is unity. Hence, the true value of τ_{eff} is expected to be larger than that computed, assuming a spherical nose (eq. 5(a)). thus yielding a higher value of the heat-transfer coefficient. This effect, coupled with the decrease in the stagnation-region velocity gradient due to the flattened nose, is believed to cause the heat-transfer coefficient to be too small for the continuous thin-skin hemisphere.

The CF_4 data provide an opportunity to compare the results for the small hemispheres with those for the large sphere for the same flow conditions (free-stream quantities, free-stream turbulence level, and flow-contamination level). For the sake of comparison, values of C_h predicted by using the method of reference 40 are shown in figure 24, where the inputs represent the present CF_4 flow conditions. The values of C_h measured on the large sphere agree to within 10 percent of this quasi CF_4 prediction (the correlations of ref. 40 are based on air properties), whereas values of C_h measured with the MACOR thin-film hemispheres are 15 to 20 percent lower than this prediction. This larger discrepancy with the hemispheres may be due to vibrational nonequilibrium effects. For vibrational equilibrium flow to exist in the shock layer, the relaxation distance must be less than the snock-detachment distance. This implies that the vibrational relaxation time must be less than 3.5×10^{-6} sec to provide equilibrium flow in the post-normal shock region of the small hemispheres for the present CF_4 test conditions. This relaxation time is close to the value given in reference 44 for CF_4 flow at a Mach number of 6. Thus, there is a high probability that vibrational nonequilibrium flow existed within the shock layer of the small hemispheres, which would tend to decrease the value of stagnation-point heat-transfer rate.

CONCLUDING REMARKS

A comparison of thin-film resistance heat-transfer gages, developed for use in supersonic-hypersonic impulse facilities having run times less than 0.01 sec, with thin-skin transient calorimeter gages has been performed in the Langley Continuous-Flow Hypersonic Tunnel (CFHT) and in the Langley Hypersonic CF_4 Tunnel (CF_4 Tunnel). Thin-film gages deposited at the stagnation region of small (8.1-mm-diameter) hemispheres of quartz or of a machinable glass-ceramic provided a test of durability and performance in the high-temperature environment of these two wind tunnels. The performance of these gages at much lower temperatures and heat-transfer rates was examined by installing the gages flush with the surface of a sharp-leading-edge flat plate. Also tested were 8.1-mm-diameter hemispheres utilizing the thin-skin transient calorimetry technique generally employed in conventional hypersonic wind tunnels. Two different methods of construction of these thin-skin hemispheres were tested. One hemisphere was a thin shell of stainless steel with a thermocouple attached to the inner surface at the stagnation region. The other hemisphere was fabricated from a machinable-glass-ceramic and had a small stainless-steel insert, with a thermocouple attached to the backside, installed at the stagnation region. The thin-film and thin-skin heat-transfer gages were tested at a nominal free-stream Mach number of 10, a range of reservoir pressure from 2.4 to 11 MPa, and a reservoir temperature of 990 K in the CFHT; and at a Mach number of 6.2, they were tested in the CF_4 Tunnel for a range of reservoir pressure of 7 to 17 MPa and a reservoir temperature of 680 K. Five hemispheres were installed in a survey rake and injected into the tunnels so that all five experienced the flow simultaneously. Measured values of heat-transfer rate from the different hemispheres were compared with one another and with predicted values.

The present study demonstrated the feasibility of using thin-film resistance heat-transfer gages in conventional hypersonic wind tunnels over a wide range of conditions. These gages offer the following advantages over the transient calorimeter continuous thin-skin gages: (1) The fast response provides a detailed time history of the heat-transfer rate. This time history allows the passage of the model through the nozzle boundary layer to be monitored during the insertion process, and it provides information on the flow establishment over the model and the steadiness of the flow. (2) Their high sensitivity allows the same gage to be used for a wide range of surface heat-transfer rates. (3) Many gages can be deposited in a small area without concern for conduction effects or large corrections to determine the effective skin thickness. (4) Since the gages are deposited on the outer surface, their location can be accurately determined. (5) Thin-film gages eliminate the need to measure a skin thickness to an accuracy of 0.015 mm, sometimes an impossible feat on a complex model. The primary disadvantages of the thin-film gage are its susceptibility to damage when facing the flow and the large corrections required to account for the variation of substrate thermal properties with temperature. Using a thin-skin insert in an insulator also provides advantages over the continuous thin-skin gage. For example, it reduces conduction effects, decreases correction for the effective skin thickness, allows for more accurate measurement of skin thickness regardless of model complexity, permits more accurate location of the gage on the model surface, simplifies model fabrication and thermocouple installation, and allows variation of the thin-skin thickness over the model according to expected heating rates, thereby optimizing output. The thin-skin insert does not furnish a detailed time history or have the sensitivity of a thin-film gage, and it has the disadvantage

of producing a discontinuity in the surface finish and the surface temperature. Values of heat-transfer coefficient measured with the thin-film hemisphere and machinable-glass-ceramic hemisphere with an insert agreed to within 5 percent of one another and with predicted values.

Langley Research Center
National Aeronautics and Space Administration
Hampton, VA 23665
October 9, 1981

APPENDIX A

EFFECT OF THE VARIATION IN SUBSTRATE THERMAL PROPEPTIES OF THIN-FILM RESISTANCE GAGES ON INFERRED HEAT-TRANSFER RATE

In the derivation of the basic equation used to deduce the heat-transfer rate from a change in surface temperature measured with a thin-film resistance gage (eq. (6)), substrate thermal properties were assumed constant. For the high surface temperatures experienced by the thin-film hemispheres tested in the CFHT and CF_4 Tunnels, this assumption is not valid. From equation (6), it is seen that the product $\sqrt{\rho_s c_s k_s}$ is important, rather than the separate quantities ρ_s, c_s, and k_s; thus, the variation of β_s (defined as $\sqrt{\rho_s c_s k_s}$) with temperature must be accurately known to minimize the uncertainty in deduced heating rate at high surface temperatures. Unfortunately, the problem goes beyond knowing the variation of β_s with temperature since the heating rate determined from equation (6) or (7) cannot be corrected accurately for variation in substrate thermal properties by simply multiplying by $\beta_s(T)/\beta_{s,o}$. In this appendix, methods for correcting the heat-transfer rate for variable substrate properties will be discussed, along with the procedure used to determine the quantity β_s as a function of temperature.

Thermal Properties of Substrate Materials

The temperature dependence of density ρ, specific heat c, and thermal conductivity k for Pyrex 7740, quartz, and MACOR are discussed in this section. Although Pyrex was not used as a substrate in the present study, it is probably the most commonly used substrate material. Accordingly, several methods for correcting equation (6) for the variation of substrate properties used Pyrex to obtain correction factors. (See refs. 11 and 22.) For this reason, Pyrex 7740 is considered along with quartz and MACOR.

Equations for k, c, and ρ as a function of temperature were obtained for Pyrex 7740 and quartz by applying curve fits to the data of references 11 and 45. These equations are given as follows with $297\ K < T < 600\ K$:

Pyrex 7740:

$$k = 1.51458 \times 10^{-2} - 5.90677 \times 10^{-5} T + 1.81645 \times 10^{-7} T^2 \ W/cm\text{-}K \qquad (A1a)$$

$$c = -8.54140 \times 10^{-2} + 4.28391 \times 10^{-3} T - 5.74819 \times 10^{-6} T^2 + 3.10468 \times 10^{-9} T^3 \ W\text{-}sec/g\text{-}K \qquad (A1b)$$

$$\rho = 2.227 \ g/cm^3 \qquad (A1c)$$

Quartz:

$$k = 3.08379 \times 10^{-2} - 1.16501 \times 10^{-4} T + 2.06385 \times 10^{-7} T^2 \ W/cm\text{-}K \qquad (A2a)$$

$$c = -7.94345 \times 10^{-2} + 3.92507 \times 10^{-3}T - 4.50433 \times 10^{-6}T^2 + 1.89858 \times 10^{-9}T^3 \text{ W-sec/g-K} \quad \text{(A2b)}$$

$$\rho = 2.1925 \text{ g/cm}^3 \quad \text{(A2c)}$$

The equations for specific heat c for Pyrex and quartz (eqs. (A1b) and (A2b), respectively) represent curve fits to the data of references 11 and 45; equations for thermal conductivity k for Pyrex and quartz (eqs. (A1a) and (A2a), respectively) represent curve fits to the data of reference 11 only. The data of reference 11 were obtained by subjecting platinum films painted on Pyrex and quartz substrates to a square-current pulse. This technique yielded the product ρck, and the values of k were determined by using available specific-heat data and the density ρ. The electrical-discharge technique is commonly used to determine β, since diffusion of film material into the substrate during the film deposition and firing process may significantly change the thermal properties of the substrate (ref. 11); that is, the bulk values of c and k are not applicable. The data of reference 45 represent an assembly of thermal properties from a number of sources and are bulk values. The equation for specific heat c for Pyrex (eq. (A1b)) agrees to within 1.7 percent of the data of references 11 and 45, and equation (A2b) for quartz agrees to within 1.5 percent for $295 \text{ K} < T < 600 \text{ K}$. The data of reference 11 were obtained for $297 \text{ K} < T < 447 \text{ K}$; hence, the expressions for k correspond to this temperature range. However, values of k from these expressions corresponding to $T > 447$ K fall within the data scatter of reference 45 for temperatures up to 600 K; thus, equations (A1a) and (A2a) are believed to be valid for $295 \text{ K} < T < 600 \text{ K}$.

Although actual values of β may be quite different from bulk values for Pyrex, the actual values of β for bulk properties of quartz are in close agreement with the value obtained by using the discharge technique (refs. 2 and 11). In general, the value of β for quartz at a temperature of 295 K ranges from 1510 to 1535 W-sec$^{1/2}$/m^2-K in the literature. For this temperature of 295 K, equations (A2) yield a value of β equal to 1525 W-sec$^{1/2}$/m^2-K, which is within 0.2 percent of the mean value inferred from the literature. Hence, the uncertainty in the inferred heat-transfer rate due to the uncertainty in $\beta_{s,o}$ at low temperatures is believed to be less than 1 percent for quartz.

The possible loss of accuracy associated with the variation of substrate thermal properties during a test makes the use of alternate substrates, such as ceramics, worthy of investigation. For example, the variation of β for beryllia is less than 1 percent for a temperature change of 160 K (ref. 2). In the present study, MACOR, a glass-ceramic that may be safely machined with conventional metal-working tools and techniques (ref. 34), was used as a substrate. MACOR consists of a highly interlocked array of plate-like mica crystals dispersed throughout a glassy matrix and is referred to as Code 9658.

The thermal product β for MACOR was determined initially from the following equations:

For $300 \text{ K} < T < 400 \text{ K}$,

$$k = 0.01614 \text{ W/cm-K} \quad \text{(A3a)}$$

For 295 K < T < 673 K,

$$c = 0.19353 + 3.34813 \times 10^{-3}T - 1.00161 \times 10^{-5}T^2 + 2.81125 \times 10^{-8}T^3 - 4.24805 \times 10^{-4}T^4 + 2.33433 \times 10^{-14}T^5 \text{ W-sec/g-K} \quad \text{(A3b)}$$

For 298 K < T < 773 K,

$$\rho = 2.54384 - 8.0 \times 10^{-5}T \text{ g/cm}^3 \quad \text{(A3c)}$$

The variation of $\sqrt{\rho_s c_s k_s}/\sqrt{\rho_{s,o} c_{s,o} k_{s,o}}$ with temperature is shown in figure 25 for MACOR, as well as for Pyrex and quartz.

Unlike the value of β for quartz (eqs. (A2)), the value of β for MACOR (eqs. (A3)) represents bulk properties only. The expressions for density and specific heat for MACOR represent curve fits to data obtained from private communication with the author of reference 34 and from analysis of samples sent to Dynatech R/D Company (unpublished data). The values of specific heat from these two sources agree to within 1 percent for a range of temperature from 295 to 420 K. The value of thermal conductivity k of MACOR at ambient temperature ($T \approx 300$ K) represents an average of the value presented in reference 34 (0.168 W/cm-K) and that measured at Dynatech R/D Company by using the comparative method (0.155 W/cm-K). This comparative method revealed that the thermal conductivity of MACOR is essentially constant between 295 K and 420 K. However, tests performed by Wyle Laboratories on the same MACOR sample and using the comparative method showed a 6.2-percent increase in thermal conductivity with increase in temperature from 316 K to 453 K.

A fourth source of thermal properties for MACOR was provided by Theodore R. Creel, Jr., of the Langley Research Center. The thermal product β was inferred for quartz and MACOR samples by using the step-input heat-rate method described in reference 46. The results of these measurements are presented in figure 26, where β is plotted as a function of temperature. The measurements are represented by first-order and second-order curve fits to the data; also shown in figure 26 are values of β for quartz predicted from equation (A2) and values for MACOR predicted from equations (A3b), (A3c), and (26). Measured values of β using the method of reference 46 are approximately 2.5 to 7 percent less than predicted values for quartz and are 4 to 7 percent less than those predicted for MACOR. Because the same procedure was used to infer β for quartz and MACOR and the values predicted for quartz are believed to be quite accurate, the results of figure 26 imply that equations (A3b), (A3c), and (26) provide a reasonably accurate value of β for bulk MACOR.

It should be noted that the thermal product β for MACOR has been determined experimentally at Calspan Advanced Technology Center, Buffalo, New York, by using electrical pulses through platinum films painted on MACOR buttons. (The unpublished results of this study performed at Calspan were furnished to the author by Charles E. Wittliff of Calspan.) In order to obtain information on the quality control of the glass-ceramic material, the buttons were fabricated from different manufacturing batches. These tests yielded a mean value of β equal to 2008 W-sec$^{1/2}$/m^2-K with a standard deviation of 5 percent. For a temperature of 298 K, the value of β from

equations (A3) is 1765 W·sec$^{1/2}$/m^2-K; hence, a discrepancy of 14 percent exists between equations (A3) and the Calspan data for the value of β for MACOR at room temperature.

The value of β obtained from equations (A3) for MACOR represents a bulk property, whereas the value from the Calspan study accounts for any variation in substrate thermal properties that may occur during the curing process. These changes are attributed to a diffusion of the metallic thin film, painted on the surface of the substrate, into the substrate material when the gage is cured at temperatures up to 950 K. This curing is performed to provide a bond of the film to the substrate. The fabrication of the present gages differs from the procedure used at Calspan. The film is sputtered onto the surface of the substrate and the gage is subjected to a lower temperature. For the present method of fabrication, the change in substrate thermal properties from bulk values may be much smaller than that observed in the Calspan study.

Correction Factor Accounting for Variation in Substrate Properties With Temperature

Noting that the diffusivity α was only slightly temperature dependent for $\Delta T_s < 150$ K, Hartunian and Varwig (ref. 11) obtained an approximate correction factor for heat-transfer rate that accounts for variation in thermal properties for Pyrex 7740 and quartz substrates. This correction has the form

$$\frac{(\dot{q})_{\beta_s(T)}}{(\dot{q})_{\beta_{s,o}}} = 1 + b\left[\left(1 + \frac{T_w}{T_o - 273}\right)\left(\frac{T_o - 273}{T_w}\right)\log_{10}\left(1 + \frac{T_w}{T_o - 273}\right) - 0.434\right] \qquad \text{(A4)}$$

where T_o and T_w are given in K, $b = 4.73$ for Pyrex, and $b = 1.75$ for quartz.

This correction factor is shown in figure 27 for Pyrex and quartz, where the ratio of heat-transfer rate for variable substrate properties to heat-transfer rate for constant properties $(\dot{q})_{\beta_s(T)}/(\dot{q})_{\beta_{s,o}}$ is plotted as a function of change in surface temperature ΔT_w. The results of figure 27 show that the correction factor required for a quartz substrate is less than that for Pyrex. The correction factor for Pyrex is significant (greater than 5 percent) for temperature changes in excess of 15 K, compared with 45 K for quartz. This is one of the primary reasons quartz is frequently selected over Pyrex as the substrate material for heat-transfer gages. Another reason is that the thermal properties for quartz are well documented, and discrepancies between experimentally observed values of the thermal product and theoretical values are less for quartz, as will be discussed subsequently.

Cook (refs. 22 and 23) performed a theoretical study of the effect of variable thermal properties on the heat-transfer rate deduced from surface-temperature measurements. Values of the heating rate were computed rigorously for Pyrex 7740; the thermal properties of Pyrex 7740 were obtained from the measurements of Hartunian and Varwig (ref. 11). The thermal conductivity k_s was assumed to vary linearly with temperature (ref. 16); that is, a linear curve fit was applied to the data of reference 11. Computations were performed for two boundary conditions, corresponding to a step change in temperature (ϕ = Constant), as observed on the wall of a shock

tube for laminar boundary layer, and to a constant heat-transfer rate for which the surface-temperature changes as $\sqrt{t}$ ($\phi \propto \sqrt{t}$). The results of these computations were plotted in references 22 and 23 in terms of $(\dot{q})_{\beta_s(T)}/(\dot{q})_{\beta_{s,o}}$ against surface temperature, and these curves are also shown in figure 27. Correction factors computed by Cook for Pyrex are 6 to 7 percent less than those estimated by Hartunian and Varwig (ref. 11) between values of ΔT_w of 100 K and 150 K. As discussed in reference 2, no straightforward technique exists for correcting for variable thermal properties except for the cases where $\dot{q}(t)$ = Constant and $\dot{q}(t) \propto t^{-1/2}$; and even in these simple cases large discrepancies exist between the corrections recommended.

As observed in figure 27, values of $(\dot{q})_{\beta_s(T)}/(\dot{q})_{\beta_{s,o}}$ computed by Cook (refs. 22 and 23) for Pyrex vary linearly with change in surface temperature. This variation for the boundary condition corresponding to a constant heating rate ($\phi \propto \sqrt{t}$) is given by the relation

$$(\dot{q})_{\beta_s(T)}(t)/(\dot{q})_{\beta_{s,o}}(t) = 1 + 0.00233\ \Delta T_w(t) \tag{A5}$$

By assuming that this ratio of heating rates also varies linearly with $\Delta T_w(t)$ for quartz for a value of ΔT_w less than 200 K, then

$$s_{quartz} = \frac{1}{\Delta T_w}\left[(1 + 0.00233\ \Delta T_w)\frac{(\beta_s/\beta_{s,o})_{quartz}}{(\beta_s/\beta_{s,o})_{Pyrex}}\right] \tag{A6}$$

where $\beta_s/\beta_{s,o}$ is a function of ΔT_w. The values of $\beta_s/\beta_{s,o}$ required to determine the slope s for quartz in equation (A6) were determined from equations (A1) and (A2). Although the slope s for quartz determined from equation (A6) is a function of ΔT_w, the maximum error in the correction factor for ΔT_w from 100 K to 200 K is less than 2 percent for a constant value of s equal to 0.0012. Thus, the ratio of heating rates for quartz is given by the relation

$$(\dot{q})_{\beta_s(T)}(t)/(\dot{q})_{\beta_{s,o}}(t) = 1 + 0.0012\ \Delta T_w(t) \tag{A7}$$

An independent estimate of the slope for quartz of 0.001 was obtained from William J. Cook via private communication (author of refs. 22 and 23). At ΔT_w = 150 K, the ratio of heating rates or correction factor corresponding to this slope of 0.001 is within 2.6 percent of that from equation (A7).

From figure 27, the correction factor for quartz inferred from Cook's correction factor for Pyrex (eq. (A7)) is observed to be in close agreement (within 2.2 percent for the range of ΔT_w in fig. 27) with that derived by Hartunian and Varwig (ref. 11). Equation (A7) was used to correct the value of heating rate calculated from equation (7) with β constant for thin-film gages having quartz substrates in the present study.

APPENDIX A

The present study provided an opportunity to compare values of heat-transfer rate obtained by using quartz and MACOR substrates for a given model geometry and flow condition. By assuming that the value of $\beta_{s,o}$ and the ratio $(\dot{q})_{\beta(T)}/(\dot{q})_{\beta_{s,o}}$ are well known for quartz, this comparison should provide an insight to the correct values for MACOR. A similar study was performed in the Langley Expansion Tube when thin-film gages on a MACOR substrate were tested on the center line of a sharp-leading-edge flat plate. Thin-film gages located fore and aft of the MACOR substrate were deposited on quartz substrates. For the 200-μsec test period, the surface-temperature increase was less than approximately 5 K. By using the values of $\beta_{s,o}$ from equations (A2) for quartz and from equations (A3) for MACOR, a relatively smooth, monotonic decrease in heat-transfer rate with distance from the leading edge was observed for the three substrates. Thus, it was concluded that equations (A3) provided a reasonably accurate value of $\beta_{s,o}$ for MACOR.

Data obtained in this study with the MACOR thin-film hemispheres were initially reduced by using the value of thermal conductivity given in equation (A3a) and correction factors ($(\dot{q})_{\beta(T)}/(\dot{q})_{\beta_{s,o}}$) derived in the same manner as those for quartz (that is, eq. (A6), where quartz is replaced by MACOR). This method resulted in such a small value of the slope that the correction factor was within 1 percent of unity for temperature changes ΔT_w up to 200 K. After the initial analysis of the present data for the MACOR hemispheres, the thermal conductivity of MACOR was given a temperature dependence (eq. (26)). Also, the procedure for obtaining the correction factors was revised, since the variation of β_s with ΔT_w for MACOR relative to that for Pyrex 7740 differs from the variation of quartz. (See fig. 28.) Thus,

$$s_{MACOR} = \frac{s^2_{quartz}}{s_{Pyrex}} \left[\frac{\overline{(\beta_s/\beta_{s,o})^2_{quartz}}}{(\beta_s/\beta_{s,o})_{MACOR}(\beta_s/\beta_{s,o})_{Pyrex}} \right] \tag{A8}$$

where $s_{Pyrex} = 0.0023$ per K, $s_{quartz} = 0.0012$ per K, and the mean value of the quantity in the bracket for ΔT_w between 50 K and 150 K was used. The resulting relation for the correction factor for a MACOR substrate is

$$(\dot{q})_{\beta(T)}(t)/(\dot{q})_{\beta_{s,o}}(t) = 1 + 0.0006\ \Delta T_w(t) \tag{A9}$$

It must be emphasized that equation (A9) represents a crude method for correcting for the variation of thermal properties for MACOR. Additional study is required in this area if reliable values of $(\dot{q})_{\beta(T)}$ for MACOR substrates at $\Delta T_w > 50$ K are to be obtained.

APPENDIX B

CALIBRATION RESULTS FOR THIN-FILM GAGES BEFORE, DURING, AND AFTER TESTS IN THE CFHT

Calibration data, in terms of thin-film gage resistance as a function of temperature, are shown in figure 29 for the two MACOR hemispheres and for two quartz hemispheres. These calibrations were made before, during, and after the present tests and the gage current was 1 mA. In figure 29(a), the variation in gage resistance for a temperature change from 298 K to 353 K is shown for MACOR hemispheres nos. 1 and 2. Calibration data obtained prior to any testing in the CFHT are represented by the circles, and the square symbols represent data obtained midway through the test series. (At the midpoint, MACOR hemisphere no. 1 had been tested four times and MACOR hemisphere no. 2 six times.) Other symbols denote calibration data obtained after the tests were completed in the CFHT. The results of figure 29(a) show that MACOR hemisphere no. 1 experienced a 45-percent change in slope dR/dT and a 6.3-percent change in α_R after four tests; MACOR hemisphere no. 2 changed 28 percent in dR/dT and 3.3 percent in α_R. Calibrations performed after the test series revealed that both MACOR hemispheres experienced an 8-percent change in dR/dT and a 2.3- to 3.2-percent change in α_R between the midtest calibration and this post-test calibration. The calibration results of figure 29(a) demonstrate that the palladium films were annealed by exposure to the high-temperature flow of the CFHT. (Annealing metal films generally results in a lowering of the resistance.)

Thin-film resistance measured prior to each run in the CFHT and CF_4 Tunnel is presented in the following table for both MACOR hemispheres and the quartz hemisphere no. 4:

Tunnel	Run	$p_{t,1}$, MPa	T_o, K	Measured R_o, Ω, for hemisphere -		
				MACOR no. 1	MACOR no. 2	Quartz no. 4
CFHT	1	2.4	300.4		207	
CFHT	2	2.4	302.1		208	
CFHT	3	5.1	303.2	224	208	
CFHT	4	11.0	302.6	174	181	
CFHT	6	2.4	300.4	165	168	124
CFHT	7	5.1	301.5	165	168	139
CFHT	11	2.4	299.3		166	142
CFHT	12	2.5	298.2	164	166	145
CFHT	13	11.3	296.5	163	165	
CF_4	645	7.5	300.4	145	150	
CF_4	646	11.2	300.9	146	151	
CF_4	647	16.6	302.6	148	154	

The resistance R_o measured for MACOR hemisphere no. 2 remained unchanged after the first two tests in the CFHT at low-reservoir stagnation pressure $p_{t,1}$; however, R_o decreased approximately 15 percent after the test at $p_{t,1} = 5.2$ MPa and decreased 24 percent from the prerun 1 value after a test at the highest reservoir

pressure, $p_{t,1} = 11$ MPa. The resistance R_o remained relatively unchanged for the remaining CFHT tests and remained essentially constant for the three tests in the CF_4 Tunnel. MACOR hemisphere no. 1 experienced the same trend. The results of figure 29(a) and the values of R_o in the previously given table illustrate that the MACOR hemispheres were not conditioned properly for testing in the CFHT. However, for CFHT runs 11, 12, and 13, these results imply that the uncertainty in heat-transfer rate determined for MACOR hemispheres nos. 1 and 2 due to the uncertainty in α_R is less than 3 percent. (It should be noted that because of an incorrect setting on the differential amplifiers, heat-transfer rates to the hemispheres containing thin-film gages were measured successfully only for the last three runs (11, 12, and 13) of this series.)

Calibration results for quartz hemispheres nos. 2 and 4 are presented in figure 29(b). The quartz hemispheres used in this study were initially calibrated (series 1, of fig. 29(b)) between 297 K and 505 K. Quartz hemisphere no. 2 was calibrated twice before being tested and was destroyed during its initial test (run 11). Unlike quartz hemisphere no. 2, hemisphere no. 4 had survived two previous tests before being calibrated the second time (series 2, of fig. 29(b)). As shown in figure 8, hemisphere no. 4 suffered some damage during its initial test. From the initial calibration data presented in figure 29(b), a marked difference is observed between the ascending and descending (denoted by flagged symbols) values of resistance R for a given temperature T, indicative of annealing. The variation of R with T becomes nonlinear for $T > 422$ K during the ascent phase of the calibration, but it is nearly linear for the descent phase over the temperature range from 505 K to 297 K. The results for the second calibration performed on quartz hemisphere no. 2 for a temperature range from 297 K to 353 K are in good agreement with the descending phase of the first calibration. Thus, a conditioning of this hemisphere occurred during the first calibration to a relatively high temperature, and the gage resistance at a temperature of 297 K remained essentially constant between the two calibrations. Quartz hemisphere no. 4 experienced the same trend as hemisphere no. 2 during the initial, high-temperature calibration, although the variation in resistance for a given temperature was not as pronounced. The results of figure 29(b) again demonstrate that the thin-film gage must be annealed at high temperatures prior to calibration and testing.

The increase in resistance for a given temperature between the two calibrations for quartz hemisphere no. 4, as shown in figure 29(b) and in the previous table, is attributed primarily to the erosion of the palladium leads between the serpentine pattern and the silver leads during the first test. This erosion results in the lead resistance no longer being small compared with the resistance of the serpentine pattern, thereby increasing the resistance between the silver leads.

Following the last test in the CFHT, MACOR hemispheres nos. 1 and 2 were calibrated between 297 K and 380 K to obtain a value of α_R to compare with the value obtained in previous calibrations, and then they were calibrated twice from 297 K to 505 K. The results of these post-test calibrations are shown in figures 29(c) and 29(d) for MACOR hemispheres nos. 1 and 2, respectively. The ascending and descending results for MACOR hemisphere no. 2 (fig. 29(d)) are in close agreement, however, the resistance for hemisphere no. 1 is less during the descending phase of the first high-temperature calibration (fig. 29(c)), but it is in good agreement during the second high-temperature calibration. The data of figures 29(c) and 29(d) illustrate that hemisphere no. 2 was conditioned during the nine tests in the CFHT, whereas the conditioning received by hemisphere no. 1 during six tests (including two at the highest reservoir pressure) was not as complete.

APPENDIX B

Comparison of the post CFHT calibrations with the post CF_4 Tunnel calibrations showed that neither MACOR thin-film hemisphere experienced an appreciable change in gage properties due to the three CF_4 tests. The MACOR hemispheres were calibrated twice after the CF_4 tests, the first with an oil bath and the second with an air oven. These two methods of heating the gages were used to determine if ohmic effects might possibly be revealed by the different thermal conductivity of the oil, compared to air, and to compare the data scatter associated with each method. For both hemispheres, the resistance measured during the descending phase of the calibration in the oil bath was within 0.7 percent of that measured during the ascending phase of the calibration in the oven for a given temperature.

For the present tests, the excitation current was maintained below 1 mA. The reason for such low excitation currents was to minimize ohmic (I^2R) heating of the thin film and the corresponding temperature gradient in the substrate. To illustrate this point, calibration data are shown in figures 30(a) and 30(b) for two quartz flat-faced cylinders having a thin-film gage deposited at the center of the face. These gages (nos. 50 and 51) were selected from a batch of 70 such gages to be subjected to a range of current I_o from 0.7 to 20 mA. From figure 30(a), the value of α_R for gage no. 51 remains essentially constant (within 0.2 percent) as the current is increased from 0.7 to 5 mA; however, a pronounced increase in α_R occurs as the current is increased to 10 mA, indicating an effect of ohmic heating. For gage no. 50 (fig. 30(b)), α_R varies approximately 2.5 percent as the current is increased from 0.7 to 5 mA. The quality of the calibration data for gage no. 50 deteriorates rapidly as the current is increased above 5 mA. These and similar calibration data lead to the establishment of the maximum allowable current being 2 mA.

After completion of the present tests in the CFHT, MACOR hemisphere nos. 1 and 2 were examined for ohmic heating effects (figs. 30(c) and 30(d), respectively). Although the resistance at a given temperature increased for values of the current greater than 10 mA, corresponding values of α_R varied less than 1.3 percent over the range of I_o from 1 to 20 mA for both hemispheres. Values of stagnation-point heat-transfer rate inferred from the hemisphere thin-film gages correspond to excitation currents less than 0.8 mA, and the current used during the test with the flat-plate model was less than 0.8 mA. The results of figure 30 demonstrate that for such low levels of current, ohmic heating effects or α_R are negligible.

APPENDIX C

FACTORS CONTRIBUTING TO UNCERTAINTY IN HEAT-TRANSFER RATE INFERRED FROM THIN-FILM RESISTANCE GAGES AND THIN-SKIN CALORIMETRY GAGES

As in most experimental studies, a number of factors may contribute to the uncertainty associated with the measurement. The purpose of this appendix is to list and briefly discuss factors that may contribute to the differences observed between the thin-film hemispheres, thin-skin hemispheres, and prediction. (A detailed study of each factor is beyond the scope of this report. However, several factors were discussed in some detail in a previous section entitled "Data-Reduction Procedure for Heat-Transfer Gages.")

The primary uncertainties contributing to errors in heat-transfer rate inferred from the thin-film hemispheres are given as follows: (1) the value of β_s, (2) the value of α_R, (3) the measured voltage output of ΔE of the circuit, (4) the correction for current I variation during the test, (5) the correction required to account for the variation in substrate thermal properties with temperature, (6) the loss of infinite slab behavior for the substrate, (7) the fact that a serpentine thin-film element measures a resistance change corresponding to a stagnation region and not a point, and (8) the fact that the resistance of the palladium leads is not negligible compared with the resistance of the sensing elements. The primary uncertainties contributing to errors in values of C_h inferred from the thin-skin hemispheres are given as follows: (1) measured skin thickness, (2) value of $\rho_m c_m$, (3) method used to determine the slope dT_i/dt, (4) selection of T_w for determining $\dot{q}_{t,2}/(T_{t,2} - T_w)$, (5) conduction effects, (6) nose geometry, (7) the geometric correction to determine the effective skin thickness, and (8) for the hemisphere with an insert, the effect of a surface-temperature discontinuity due to the different thermal properties of the insert and the MACOR hemispheres.

Thin-Film Gages

The maximum uncertainty in α_R is believed to be less than 3 percent, since these gages were calibrated before and after the first series. Because the thin-film resistance was small compared with the ballast resistance in the electrical circuit, the current was essentially constant during the test. (The correction applied to $\dot{q}_{t,2}$ for variation in current was less than 2.2 percent.) Ohmic heating effects are negligible for the present low levels of current through the film. The differential amplifiers were calibrated prior to the present tests, and the voltage output from the circuit was of a sufficient level to assure a high degree of accuracy with the recording system; thus, the overall uncertainty in the measured millivolt output is believed to be within approximately 1 percent. As discussed previously, the hemispherical substrate is believed to appear as a semi-infinite slab to the thin-film gage.

Comparisons of the value of heat-transfer rate for MACOR and quartz hemispheres in figure 13(a) lend a degree of creditability to the correction factor (eq. (A9)) used for MACOR. In figures 14 and 15, the heat-transfer coefficient for MACOR hemispheres was essentially constant with time, which also indicates that the method used to account for variation in substrate thermal properties is reasonably accurate. (As noted in appendix A, values of $\beta_{s,o}$ for MACOR measured at Calspan are 1.14 times

the values used herein; hence, this area needs additional study.) Because the serpentine pattern lies within 8° of the stagnation point, the heat-transfer rate over this area should be within approximately 1 percent of the heat transfer at the stagnation point. This is shown in figure 31, where heat-transfer distributions measured on a 10.16-cm-diameter, continuous thin-skin sphere model in the CF_4 Tunnel and in the 20-Inch Mach 6 Tunnel are compared with a predicted distribution (ref. 47).

Ideally, the resistance of the leads from the thin-film sensing element should be negligible compared with the resistance of the element. If the assumption is made that the thickness of the serpentine sensing elements and of the palladium leads for the present thin-film gages are equal, the resistance of the leads represents 4 percent of the total resistance of the gage. During calibration of the thin-film hemispheres in an oil bath, the sensing element and leads experience the same temperature. The corresponding change in resistance is given as

$$\Delta R = \Delta R_{\text{sensing element}} + \Delta R_{\text{palladium leads}} \tag{C1}$$

where the resistance of the thick silver leads is assumed negligible. During a test, the surface temperature decreases with distance from the stagnation point, resulting in a smaller variation in $\Delta R_{\text{palladium leads}}$ than that observed in the calibration for the same temperature at the sensing element. Thus, the inferred stagnation-point heating rate will be less than the actual value, and since the heating rate is proportional to ΔR, the maximum uncertainty in the inferred value of heating rate is 4 percent. It should be noted that the tip of the hemisphere was roughly normal to the palladium target during the sputtering process, and the leads are believed to be somewhat thinner than the sensing element. This will result in the leads representing a larger percentage of the total gage resistance. Because the contribution of the leads to the gage resistance is not accurately known, no correction accounting for this effect was applied to the present thin-film data.

The primary contributors to the uncertainty in the heat-transfer rate inferred from the MACOR thin-film hemispheres are believed to be, in the order of their magnitude, (1) the fact that the lead resistance was not negligible compared with the resistance of the sensing element, (2) the correction factor accounting for variation in substrate properties with temperature, and (3) the value of β_s.

Thin-Skin Hemispheres

Turning to the thin-skin hemispheres, the skin or insert thickness was carefully measured prior to the thermocouple installation. Some degree of creditability of the measured thickness τ_m is derived from the fact that good agreement between the calculated density of the stainless-steel insert for the MACOR hemisphere and the book value of density was obtained. It should be noted, however, that an error in τ_m of only 0.025 mm corresponds to an uncertainty of 2.5 percent in heat-transfer rate. The calorimeter skin thickness was assumed constant in the derivation of equation (2). This assumption may be examined by considering the definition of the coefficient of linear expansion η in

$$\tau_m(t) = \tau_{m,o}(1 + \eta\,\Delta T) \tag{C2}$$

where η for type 347 stainless steel is 1.67×10^{-5} per K over the temperature range from 273 K to 373 K. This equation shows that for the maximum change in the inner surface temperature of 110 K for a 1-sec period in the present study, the variation in skin thickness is negligible. The relation used to determine the specific heat c_m (eq. (4)) represents a curve fit to three sources of data for type 347 stainless steel over a range of temperature. For the present range of thin-skin temperature, the value of c_m is believed accurate to within 2 percent.

The quantity dT_i/dt was obtained by differentiating a second-order least-squares curve fit to the temperature time history. The time in equation (3) was selected early in the time interval for which the slope was determined. This value of dT_i/dt was compared with the value corresponding to selection of a time midway through the time interval, which is equivalent to a first-order fit. The second-order fit evaluated at an earlier time yields a larger slope dT_i/dt than the second-order fit evaluated at the midpoint of the time interval (generally, by a few percent for the time interval where conduction effects are negligible).

The value of T_w used to compute the heat-transfer coefficient for the thin-skin hemispheres corresponds to the temperature on the inside surface at a time $t' = 0$ sec. Now, a finite time is required for the time rate of change of the temperature on the inside surface to become the same (within 1 percent) as the time rate of change of the average temperature in the calorimeter. For air as the backing material, this finite time (referred to as the response time) is approximately equal to $\tau_m^2/2\alpha_m$. For the present thin-skin hemispheres, the response time is about 0.11 sec. Thus, dT_i/dt is equal to dT_{av}/dt for the time at which $\dot{q}$ is determined herein. The limiting temperature difference between the front and rear or inside surfaces can be evaluated from the approximation (ref. 2)

$$T_w - T_i \approx \frac{\tau_m^2}{2\alpha_m} \frac{\Delta T_i}{\Delta t'} \tag{C3}$$

For the heating rates shown in figure 24, the slope $\Delta T_i/\Delta t'$ was evaluated over a time interval $\Delta t'$ close to the value of response time; hence,

$$(T_w)_{t'=-0.125} \approx (T_i)_{t'=-0.125} + (\Delta T)_{t'=-0.125 \text{ to } 0} = (T_i)_{t'=0} \tag{C4}$$

and the quantities $\dot{q}$ and T_w used to compute C_h correspond to $t' = -0.125$ sec. (The maximum decrease in C_h resulting from using T_w at $t = -0.125$ sec is 3 percent.)

For the thin-skin hemispheres in the CFHT, $C_h\tau_m/k_m$ varies from 0.033 to 0.063, where k_m for type 347 stainless steel is 16.1 W/m-K. As noted in reference 48, the criterion $C_h\tau_m/k_m \ll 1$ implies that the temperature difference across the thin skin required to conduct the heat-transfer rate characterized by C_h is small compared with the driving temperature; that is, the temperature within the thin skin is approximately uniform. For this case, the value of C_h inferred from the temperature of the inside surface will be the same as the existing value of C_h.

The heat-transfer rate inferred from the thin-skin hemispheres should be relatively free of conduction effects for the present time interval

(-0.125 sec $< t' < 0$ sec). Now, the fact that the continuous thin-skin hemispheres have a slightly flattened nose will result in a decrease in the stagnation-region velocity gradient, hence, heat-transfer coefficient. Also, the geometric correction factor ω applied to the measured skin thickness τ_m of the continuous thin-skin hemisphere to obtain an effective skin thickness τ_{eff} will be in error. The factor ω used differs substantially from unity ($\tau_{eff} \approx 0.75\tau_m$) and is based on the assumption that the outer and inner surfaces are spherical. However, the outer surface at the stagnation region of the continuous thin-skin hemispheres is flattened, as well may be the case for the inner surface. Hence, the surface element in the vicinity of the thermocouple may be more like a disk, resulting in a larger value of τ_{eff}. ($\tau_{eff} = \tau_m$ for a disk.) This larger τ_{eff} would result in a higher heat-transfer rate. The uncertainty associated with the determination of τ_{eff} for the present continuous thin-skin hemispheres and the change in the velocity gradient due to the nose being flattened are believed to be the primary reasons for the poor agreement between these models and the thin-film hemispheres, the MACOR hemisphere with an insert, and prediction. For the MACOR hemisphere with an insert, the stainless-steel insert will assume a lower temperature than the neighboring MACOR hemisphere. The resulting surface-temperature discontinuity is expected to have little effect on the boundary layer, hence, heat-transfer rate, for this model geometry and the flow conditions of the present study.

REFERENCES

1. Eckert, Ernst R. G.; and Goldstein, Richard J., eds.: Measurements in Heat Transfer, Second ed. Hemisphere Pub. Corp., c.1976.

2. Schultz, D. L.; and Jones, T. V.: Heat-Transfer Measurements in Short-Duration Hypersonic Facilities. AGARD-AG-165, Feb. 1973.

3. Baines, D. J.: A Comparative Theoretical Evaluation of Five Commonly Used Types of Unsteady Heat Flux Sensor. Rep. HSA 27, Weapons Res. Establ., Australian Def. Sci. Serv., Jan. 1970.

4. Dunavant, James C.; and Stone, Howard W.: Effect of Roughness on Heat Transfer to Hemisphere Cylinders at Mach Numbers 10.4 and 11.4. NASA TN D-3871, 1967.

5. Trimmer, L. L.; Matthews, R. K.; and Buchanan, T. D.: Measurement of Aerodynamic Heat Rates at the Von Karman Facility. ICIASF '73 Record, IEEE Publ. 73 CHO 784-9 AES, pp. 35-44.

6. Cary, Aubrey M., Jr.: Turbulent Boundary Layer Heat Transfer and Transition Measurements With Extreme Surface Cooling in Hypersonic Flow. M.A.E. Thesis, Univ. of Virginia, 1969.

7. Vidal, R. J.: Model Instrumentation Techniques for Heat Transfer and Force Measurements in a Hypersonic Shock Tunnel. WADC Tech. Note 56-315, AD-97238, U.S. Air Force, Feb. 1956.

8. Taylor, B. W.: Development of a Thin Film Heat-Transfer Gauge for Shock-Tube Flows. UTIA Tech. Note No. 27, Univ. of Toronto, June 1959.

9. Marrone, P. V.; and Hartunian, R. A.: The Performance of Thin-Film Thermometers in Partially Ionized Shock-Tube Flows. AFOSR TN 59-1046, AD-1118-A-5, U.S. Air Force, Nov. 1959.

10. Skinner, G. T.: Calibration of Thin Film Gage Backing Materials. ARS J., vol. 31, no. 5, May 1961, pp. 671-672.

11. Hartunian, R. A.; and Varwig, R. L.: On Thin-Film Heat-Transfer Measurements in Shock Tubes and Shock Tunnels. Phys. Fluids, vol. 5, no. 2, Feb. 1962, pp. 169-174.

12. Vidal, Robert J.: Transient Surface Temperature Measurements. CAL Rep. No. 114, Cornell Aeronaut. Lab., Inc., Mar. 1962.

13. Skinner, George T.: A New Method of Calibrating Thin Film Gauge Backing Materials. Rep. No. CAL-105, Cornell Aeronaut. Lab., Inc., June 1962.

14. Bogdan, Leonard: High-Temperature, Thin-Film Resistance Thermometers for Heat Transfer Measurements. NASA CR-26, 1964.

15. Bogdan, Leonard: Thermal and Electrical Properties of Thin-Film Resistance Gages Used for Heat Transfer Measurements. AIAA J., vol. 1, no. 9, Sept. 1963, pp. 2172-2173.

16. Walenta, Z. A.: Analogue Networks for High Heat-Transfer Rate Measurements. AFOSR 65-0261, U.S. Air Force, Nov. 1964.

17. Bogdan, Leonard: Measurement of the Thermal Parameter $(\rho ck)^{1/2}$ for Clear Fused Quartz. AIAA J., vol. 4, no. 8, Aug. 1966, p. 1477.

18. Knauss, D. T.: Techniques for Fabricating Fast Response Heat Transfer Gages. Tech. Note 1629, Ballistic Res. Lab., Aberdeen Proving Ground, Sept. 1966. (Available from DTIC as AD 648 041.)

19. Bowman, Robert M.: Improvements in Design of Thin-Film Heat Transfer Gages for a Low-Pressure Shock Tube. Phys. Fluids Suppl. I, vol. 12, no. 5, pt. II, May 1969, pp. I-147 - I-149.

20. Edney, B. E.: Temperature Measurements in a Hypersonic Gun Tunnel Using Heat-Transfer Methods. J. Fluid Mech., vol. 27, pt. 3, 1967, pp. 503-512.

21. Cook, W. J.; and Felderman, E. J.: Reduction of Data From Thin-Film Heat-Transfer Gages: A Concise Numerical Technique. AIAA J., vol. 4, no. 3, Mar. 1966, pp. 561-562.

22. Cook, William J.: Unsteady Heat Transfer to a Semi-Infinite Solid With Arbitrary Surface Temperature History and Variable Thermal Properties. ISU-ERI-AMES-67500, Iowa State Univ., Feb. 1970. (Available from NTIS as PB 190 040.)

23. Cook, W. J.: Determination of Heat-Transfer Rates From Transient Surface Temperature Measurements. AIAA J., vol. 8, no. 7, July 1970, pp. 1366-1368.

24. McCaa, David J.: Measurement of Film Thickness of Thin-Film Resistance Thermometers. AIAA J., vol. 6, no. 4, Apr. 1968, pp. 747-748.

25. Hanson, Ronald K.: Influence of Film Thickness on the Calibration of Thin-Film-Gage Backing Materials. AIAA J., vol. 9, no. 5, May 1971, pp. 975-977.

26. Willeke, Klaus; and Bershader, Daniel: An Improved Thin-Film Gauge for Shock-Tube Thermal Studies. Rev. Sci. Instrum., vol. 44, no. 1, Jan. 1973, pp. 22-25.

27. Cook, William J.; and Renaud, Merle A.: Analysis and Interpretation of the Response of Coated Thin-Film Heat Flux Gages. Paper MA2.3, Proceedings of the Fifth International Heat Transfer Conference, Volume V, Sci. Counc. of Japan, 1974, pp. 283-287.

28. Reddy, N. M.: Heating-Rate Measurements Over 30° and 40° (Half-Angle) Blunt Cones in Air and Helium in the Langley Expansion Tube Facility. NASA TM-80207, 1980.

29. Moore, John A.: Description and Initial Operating Performance of the Langley 6-Inch Expansion Tube Using Heated Helium Driver Gas. NASA TM X-3240, 1975.

30. Miller, Charles G.: Operational Experience in the Langley Expansion Tube With Various Test Gases. NASA TM-78637, 1977.

31. Henderson, A.; Rogallo, R. S.; Woods, W. C.; and Spitzer, C. R.: Exploratory Hypersonic Boundary-Layer Transition Studies. AIAA J., vol. 3, no. 7, July 1965, pp. 1363-1364.

32. Schaefer, William T., Jr.: Characteristics of Major Active Wind Tunnels at the Langley Research Center. NASA TM X-1130, 1965.

33. Midden, R. E.; and Miller, C. G.: Description and Preliminary Calibration Results for the Langley Hypersonic CF_4 Tunnel. NASA TM-78800, 1978.

34. Grossman, David G.: Machining a Machinable Glass-Ceramic. Vacuum, vol. 28, no. 2, Feb. 1978, pp. 55-61.

35. Cooper, Morton; and Mayo, Edward E.: Measurements of Local Heat Transfer and Pressure on Six 2-Inch-Diameter Blunt Bodies at a Mach Number of 4.95 and at Reynolds Numbers Per Foot Up to 81×10^6. NASA Memo 1-3-59L, 1959.

36. Conti, Raul J.: Approximate Temperature Distributions and Streamwise Heat Conduction Effects in the Transient Aerodynamic Heating of Thin-Skinned Bodies. NASA TN D-895, 1961.

37. Erickson, Wayne D.; and Creekmore, Helen S.: A Study of Equilibrium Real-Gas Effects in Hypersonic Air Nozzles, Including Charts of Thermodynamic Properties for Equilibrium Air. NASA TN D-231, 1960.

38. Ames Research Staff: Equations, Tables, and Charts for Compressible Flow. NACA Rep. 1135, 1953. (Supersedes NACA TN 1428.)

39. Properties and Applications of the "Freon" Fluorocarbons. Tech. Bull. X-88F, E. I. Du Pont De Nemours & Co., Sept. 3, 1968. (Revised Feb. 3, 1969.)

40. Fay, J. A.; and Riddell, F. R.: Theory of Stagnation Point Heat Transfer in Dissociated Air. J. Aeronaut. Sci., vol. 25, no. 2, Feb. 1958, pp. 73-85, 121.

41. Brahinsky, Herbert S.; and Neel, Charles A.: Tables of Equilibrium Thermodynamic Properties of Air. Volume III. Constant Entropy. AEDC-TR-69-89, Vol. III, U.S. Air Force, Apr. 1969. (Available from DTIC as AD 687 092.)

42. Kays, W. M.: Convective Heat and Mass Transfer. McGraw-Hill Book Co., Inc., c.1966.

43. Erickson, Wayne D.: Vibrational-Nonequilibrium Flow of Nitrogen in Hypersonic Nozzles. NASA TN D-1810, 1963.

44. Jones, Robert A.; and Hunt, James L. (appendix A by James L. Hunt, Kathryn A. Smith, and Robert B. Reynolds, and appendix B by James L. Hunt and Lillian R. Boney): Use of Tetrafluoromethane To Simulate Real-Gas Effects on the Hypersonic Aerodynamics of Blunt Vehicles. NASA TR R-312, 1969.

45. Touloukian, Y. S., ed.: Thermophysical Properties of High Temperature Solid Materials. Volume 4 - Oxides and Their Solutions and Mixtures. Macmillan Co., c.1967.

46. Creel, Theodore R., Jr.: A Device for Rapid Determination of Thermophysical Properties of Phase-Change Wind-Tunnel Models. NASA TM X-3421, 1976.

47. Lees, Lester: Laminar Heat Transfer Over Blunt-Nosed Bodies at Hypersonic Flight Speeds. Jet Propul., vol. 26, no. 4, Apr. 1956, pp. 259-269, 274.

48. George, A. R.; and Reinecke, W. G.: Conduction in Thin-Skinned Heat Transfer and Recovery Temperature Models. AIAA J., vol. 1, no. 8, Aug. 1963, pp. 1956-1958.

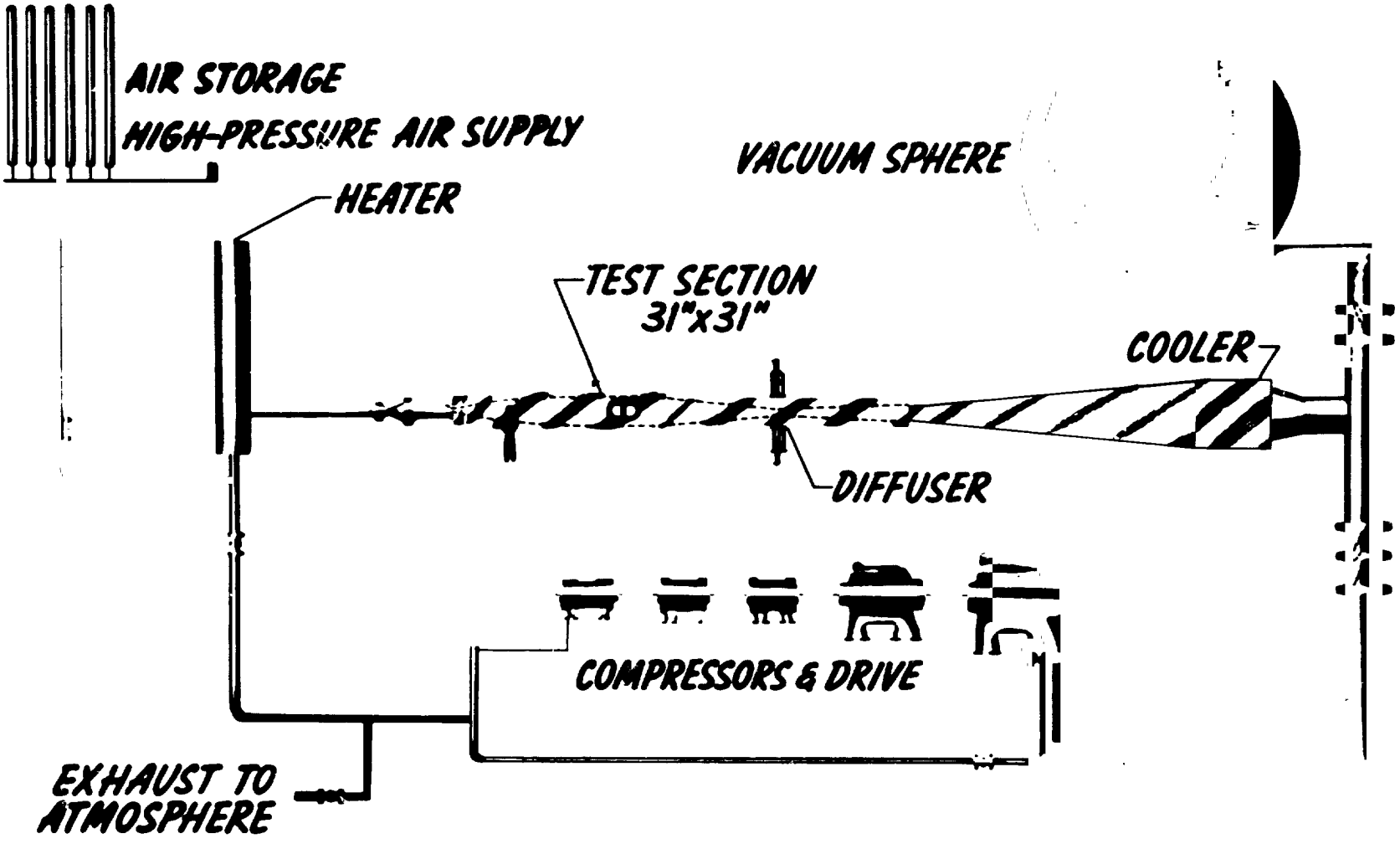

Figure 1.- Schematic drawing of Langley Continuous-Flow Hypersonic Tunnel.

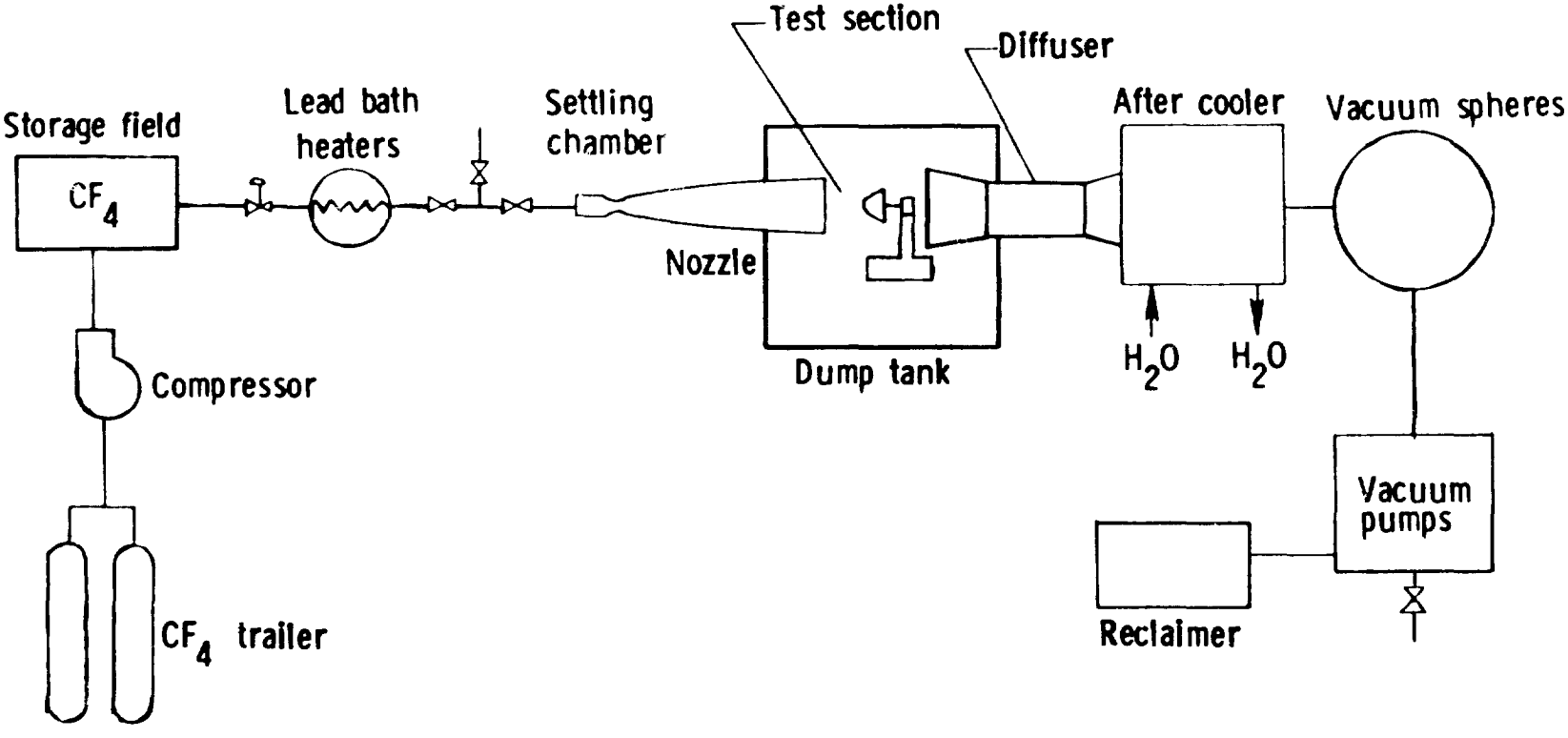

Figure 2.- Schematic drawing of Langley Hypersonic CF_4 Tunnel.

(a) Thin-skin hemisphere with τ_m = 1.135 mm.

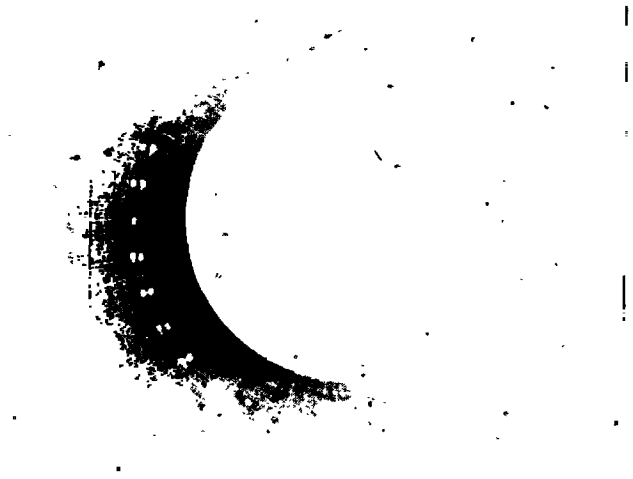

(b) MACOR hemisphere with thin-skin insert.

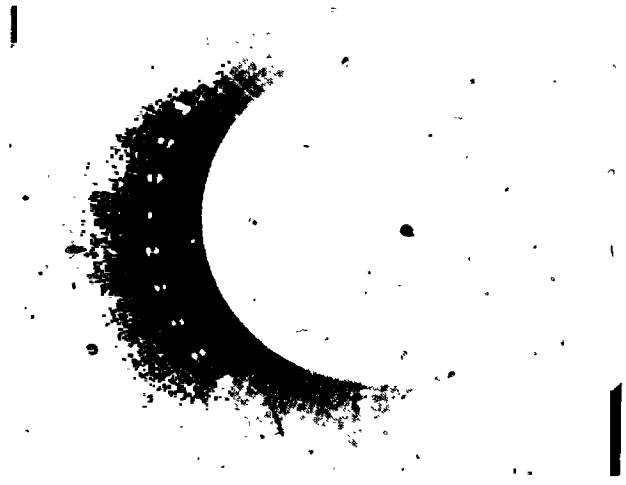

(c) MACOR thin-film hemisphere no. 2.

L-81-233

Figure 3.- Photographs of hemisphere heat-transfer gages taken on an optical comparator with a magnification of 20 times full scale.

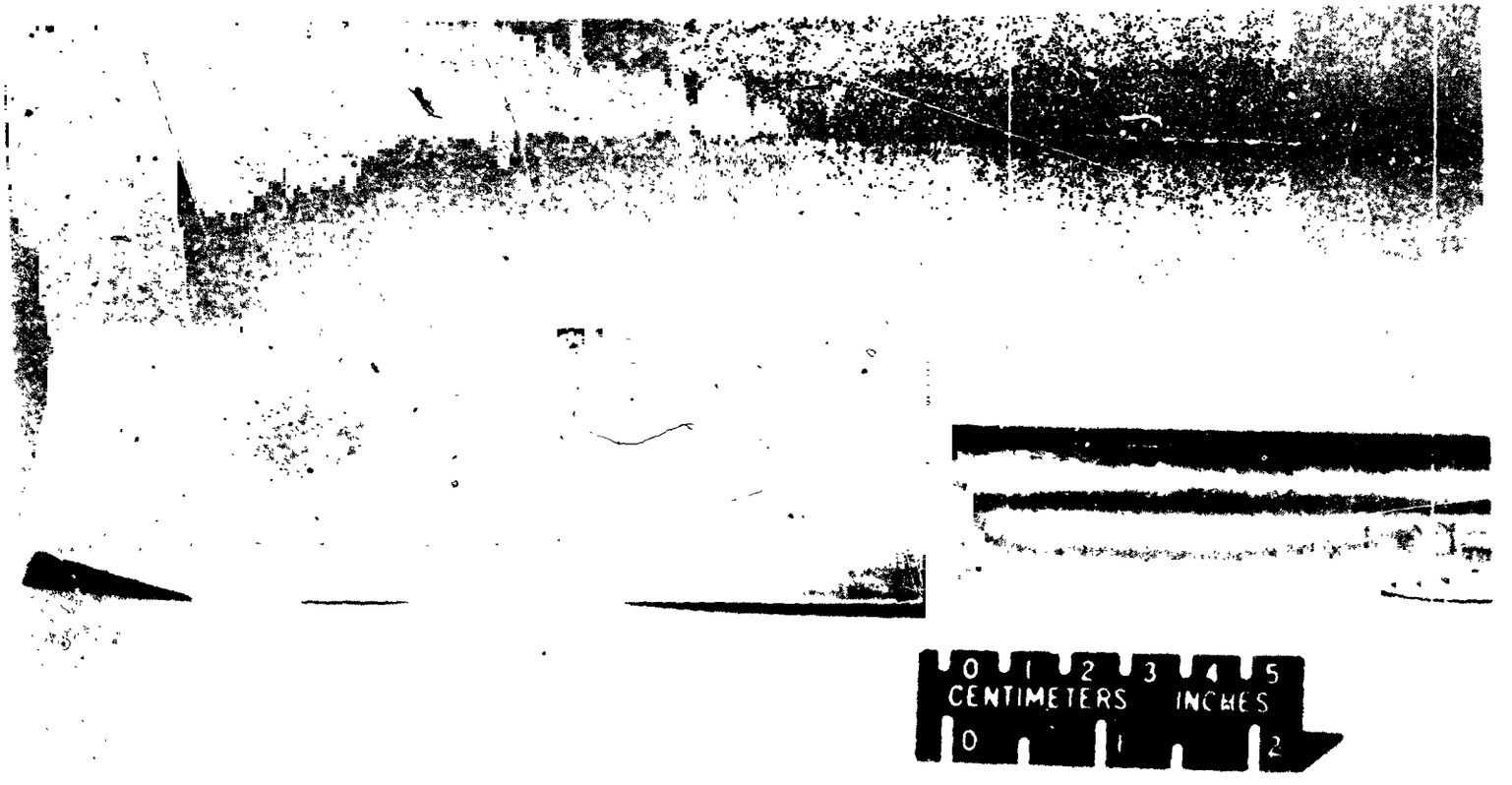

ORIGINAL PAGE IS
OF POOR QUALITY

L-80-7859

(a) Photograph of flat plate.

Figure 4.- Sharp-leading-edge flat-plate model with thin-film gages mounted flush with the surface.

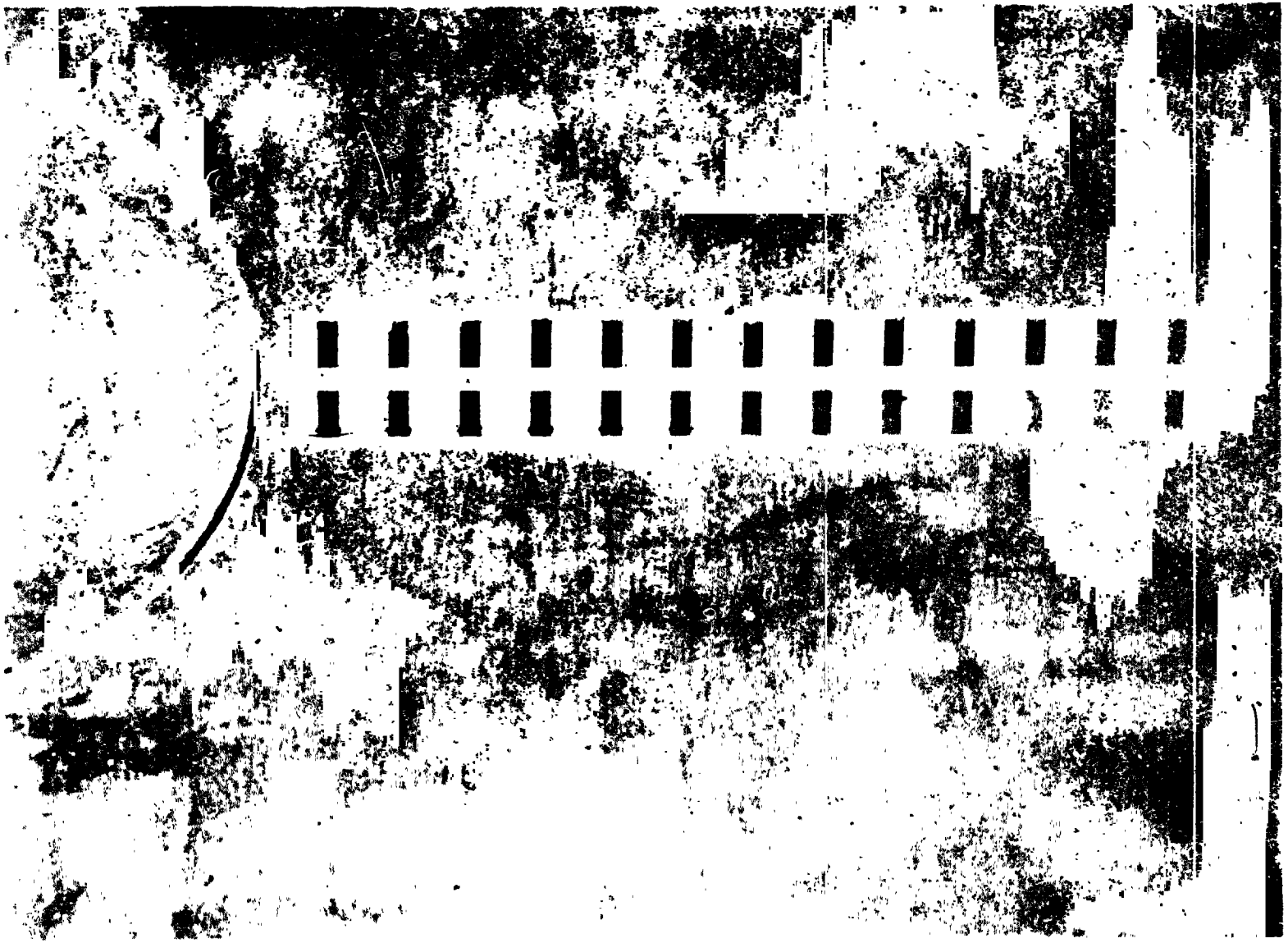

L-80-7858

(b) Quartz substrate with palladium thin-film sensors (serpentine pattern).

Figure 4.- Concluded.

(a) Disks and holders.

Figure 5.- Photograph of MACOR disks having thin-film gages deposited at the center of the front and rear surfaces.

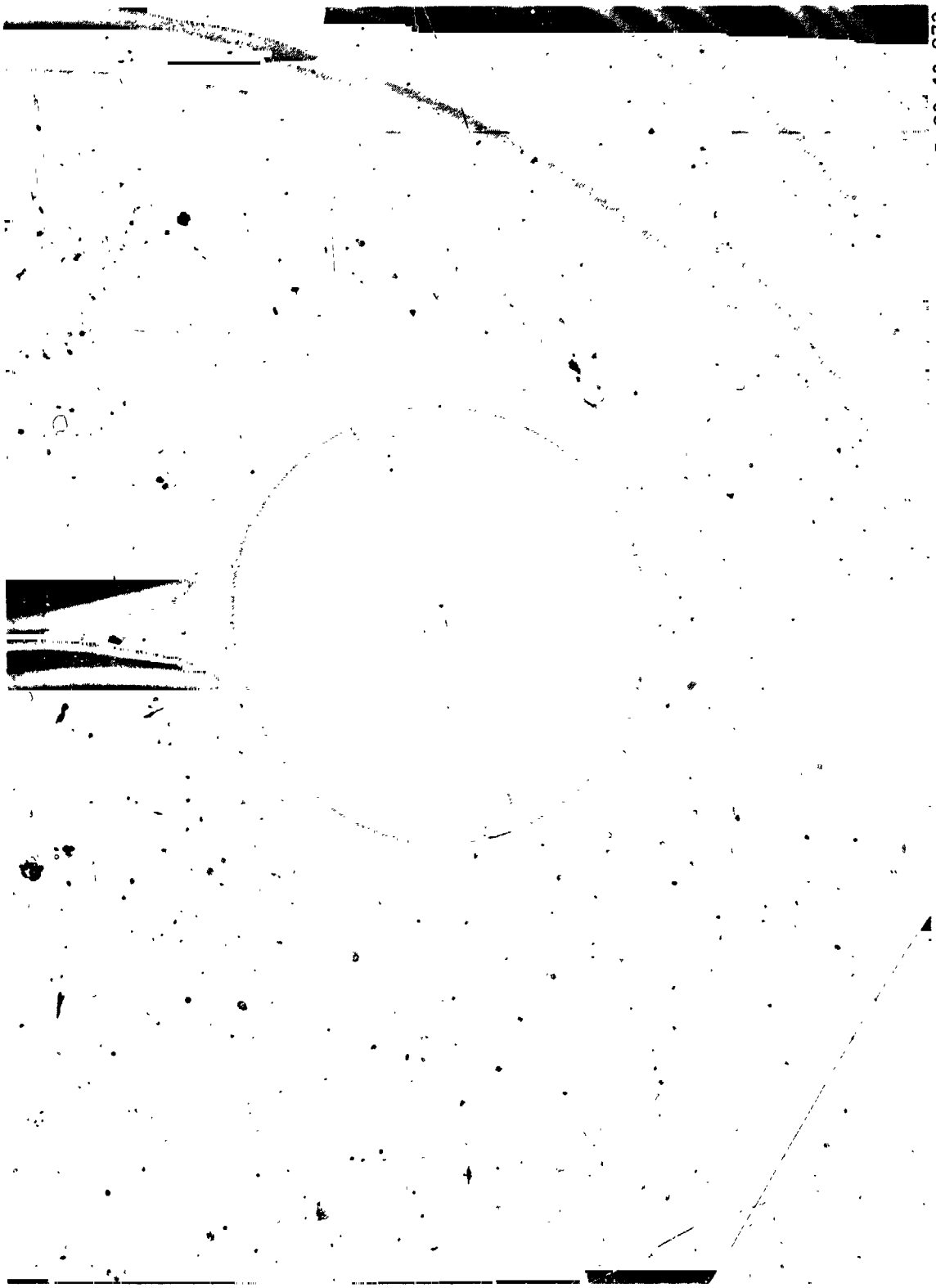

L-80-10,972

(b) Palladium thin-film sensor on front surface.

Figure 5.- Concluded.

L-80-7142

Figure 6.- Photograph of quartz hemisphere with thin-film gage deposited at the stagnation region.

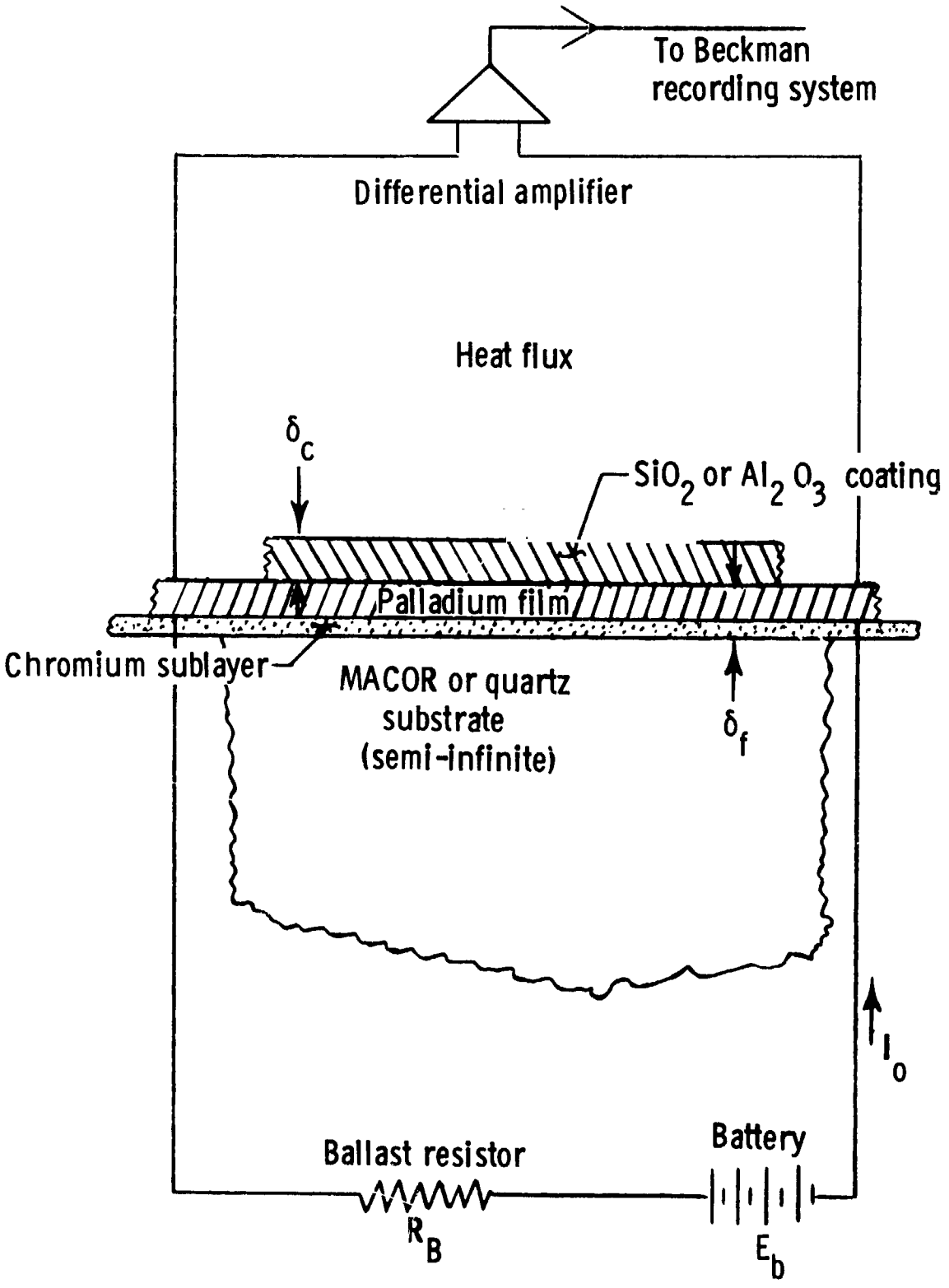

Figure 7.- Schematic diagram of a thin-film resistance gage and associated electrical circuit.

(a) Quartz hemisphere no. 4.

Figure 8.- Photographs of quartz hemisphere no. 4 illustrating damage incurred after four runs in the CFHT and of MACOR hemisphere no. 1 after six tests in the CFHT and three tests in the CF_4 Tunnel.

(b) MACOR hemisphere no. 1.

Figure 8.- Concluded.

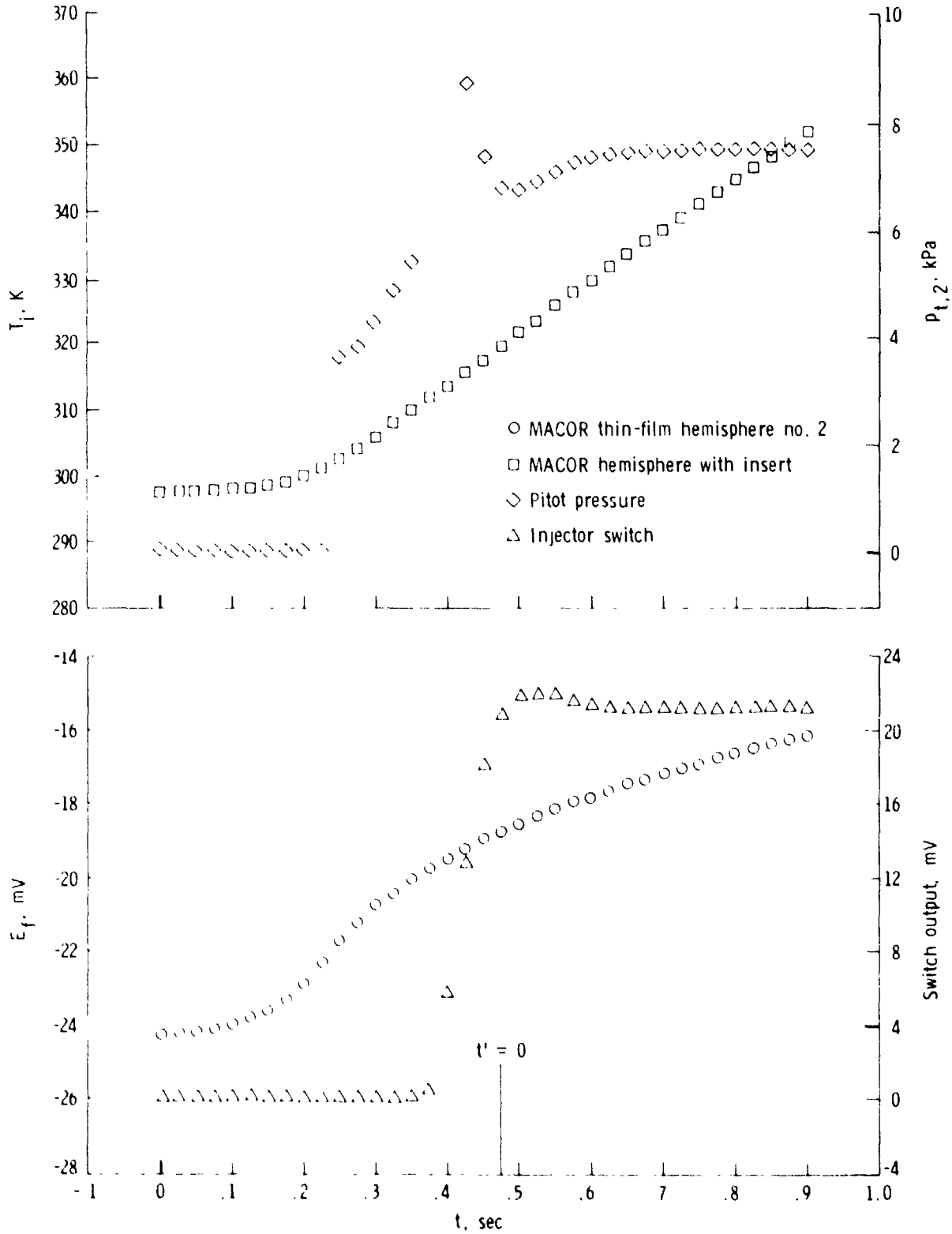

Figure 9.- Time histories of pitot pressure, injector-switch output, temperature on inner surface of thin-skin insert in the MACOR hemisphere, and thin-film gage output for run 11 in the CFHT. $p_{t,1}$ = 2.4 MPa.

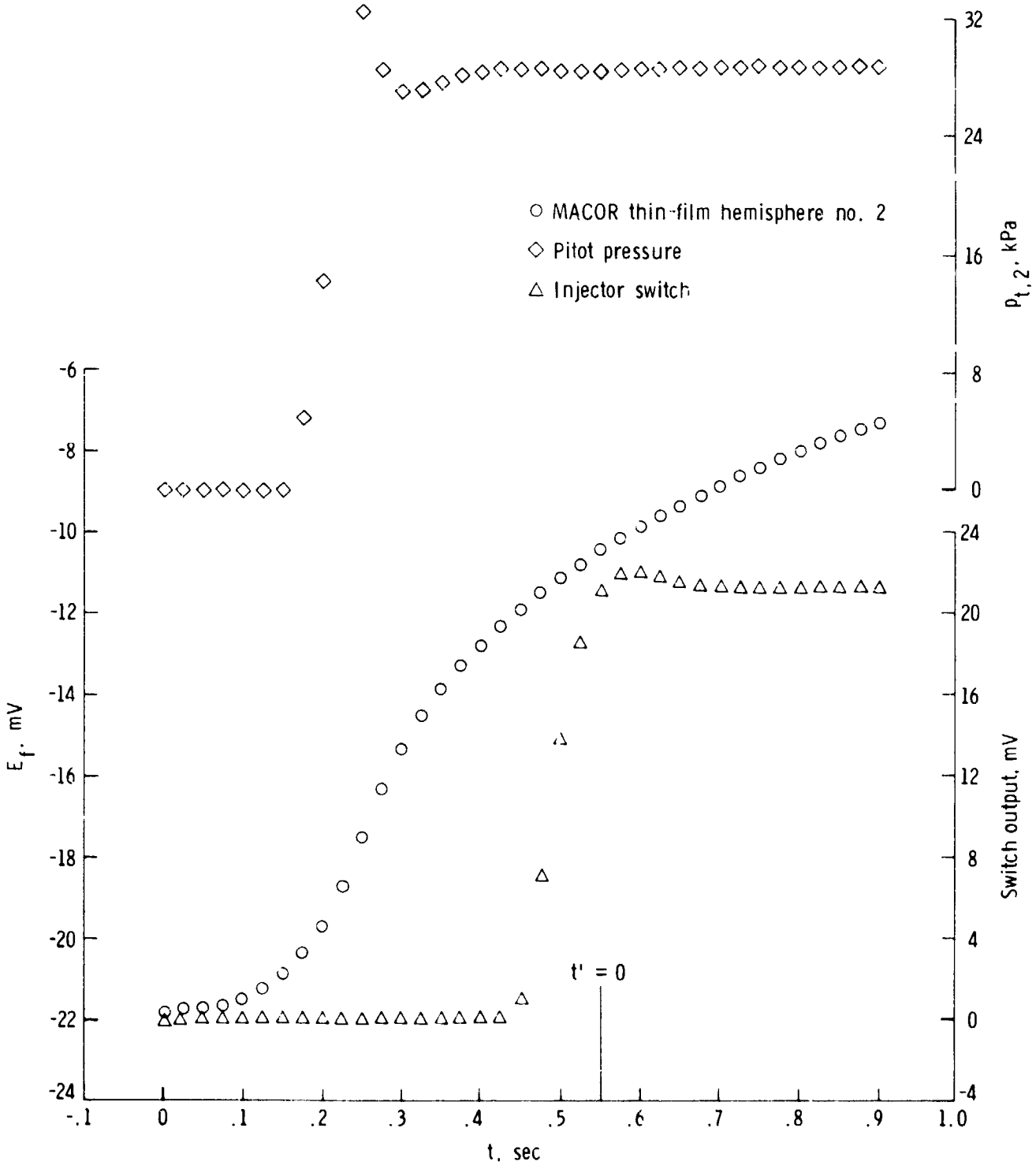

Figure 10.- Pitot pressure, injector switch output, and MACOR thin-film-hemisphere no. 2 output as a function of time for run 13 in the CFHT. $p_{t,1}$ = 11.3 MPa.

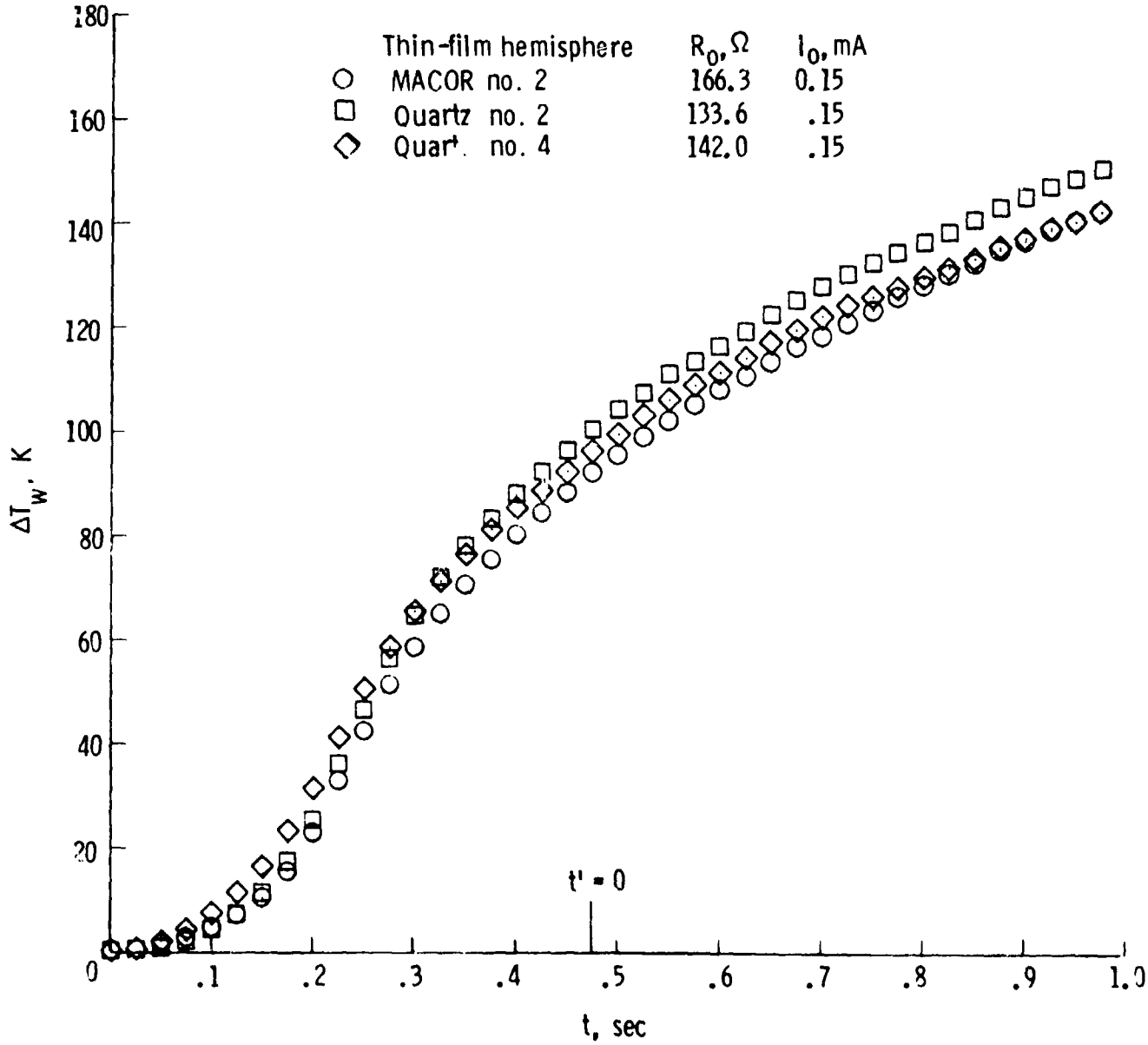

(a) $p_{t,1}$ = 2.4 MPa. Run 11.

Figure 11.- Time histories of thin-film-hemisphere surface-temperature change for two reservoir pressures in the CFHT.

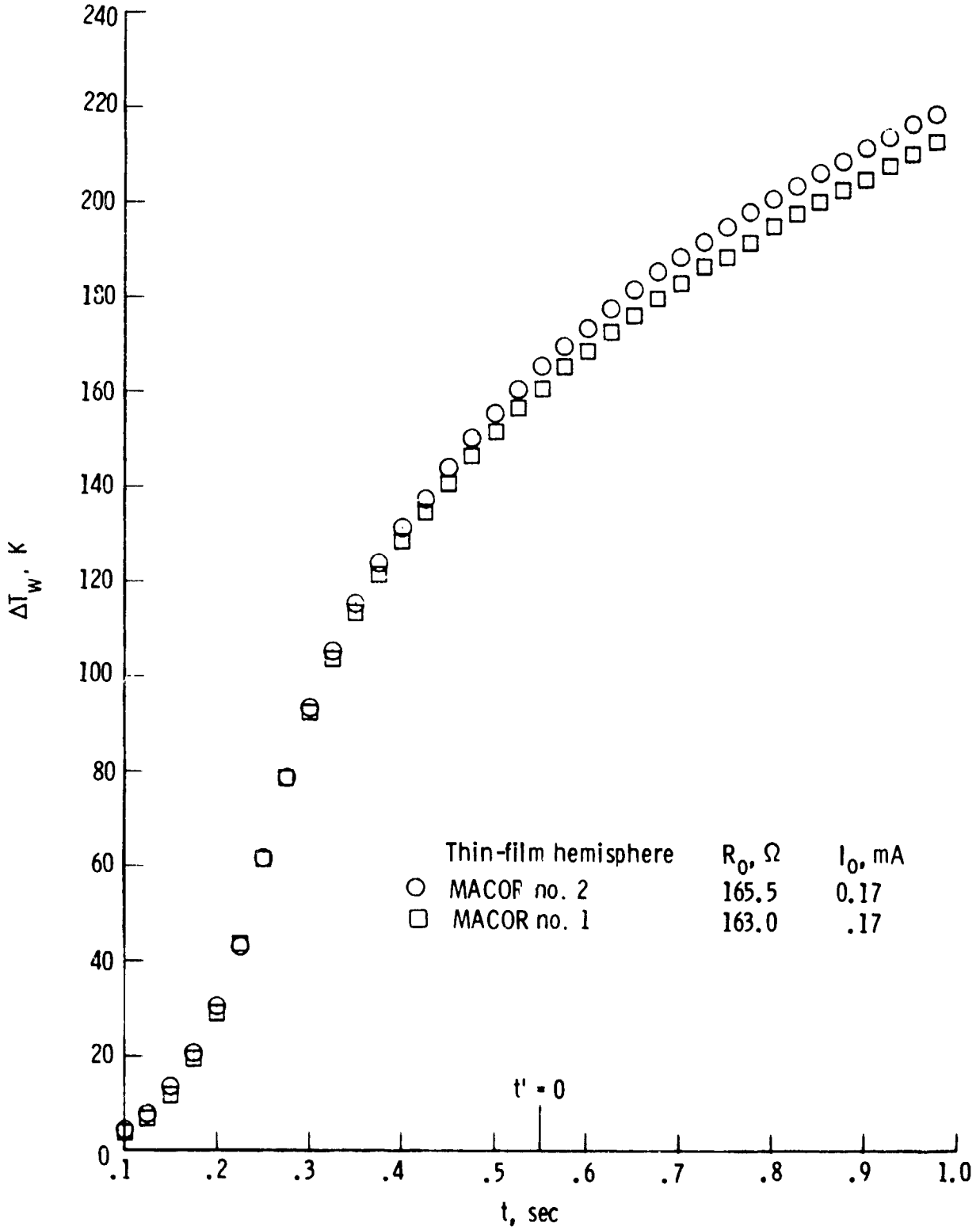

(b) $p_{t,1}$ = 11.3 MPa. Run 13.

Figure 11 - Concluded.

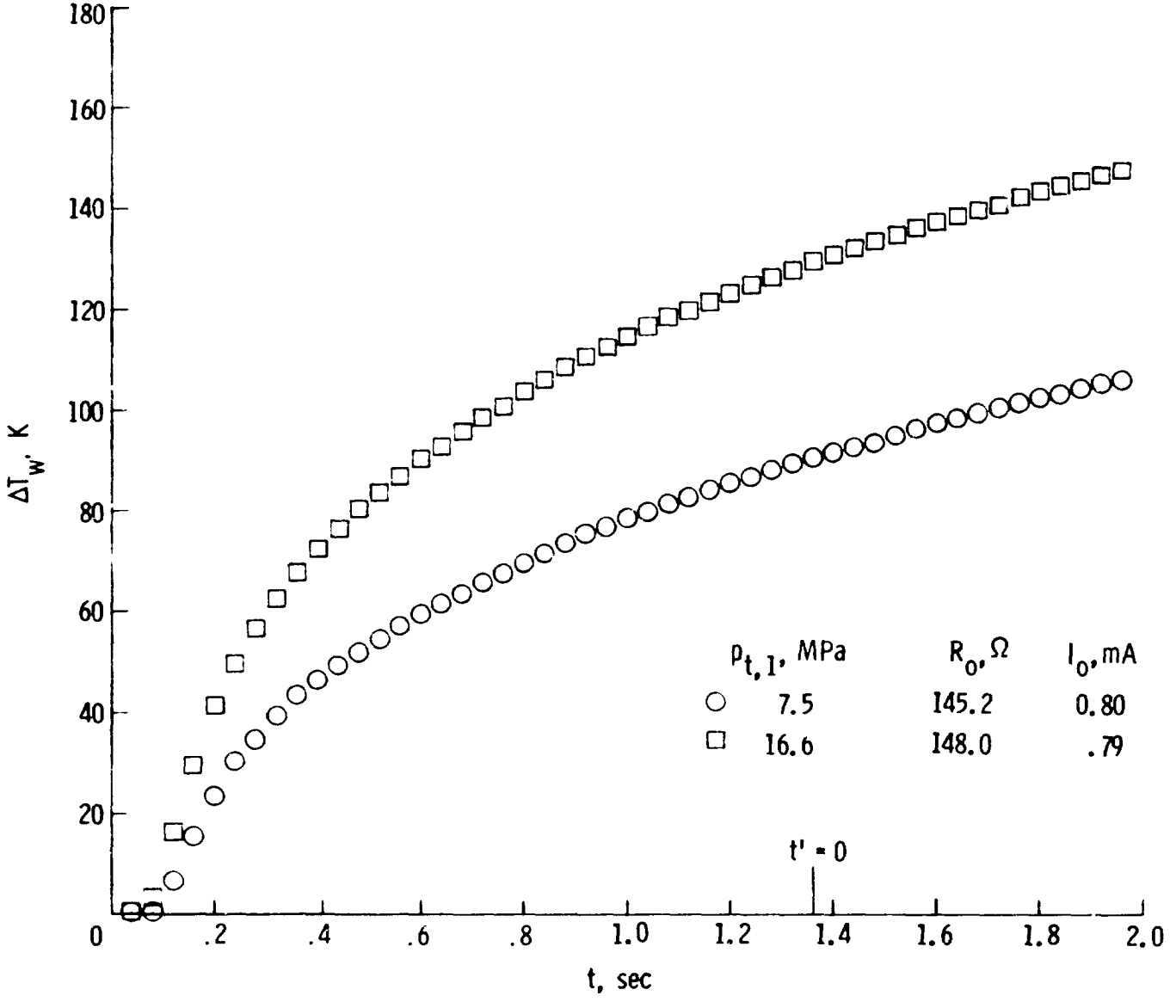

Figure 12.- Surface-temperature change as a function of time for MACOR thin-film hemisphere no. 1 in the CF_4 Tunnel.

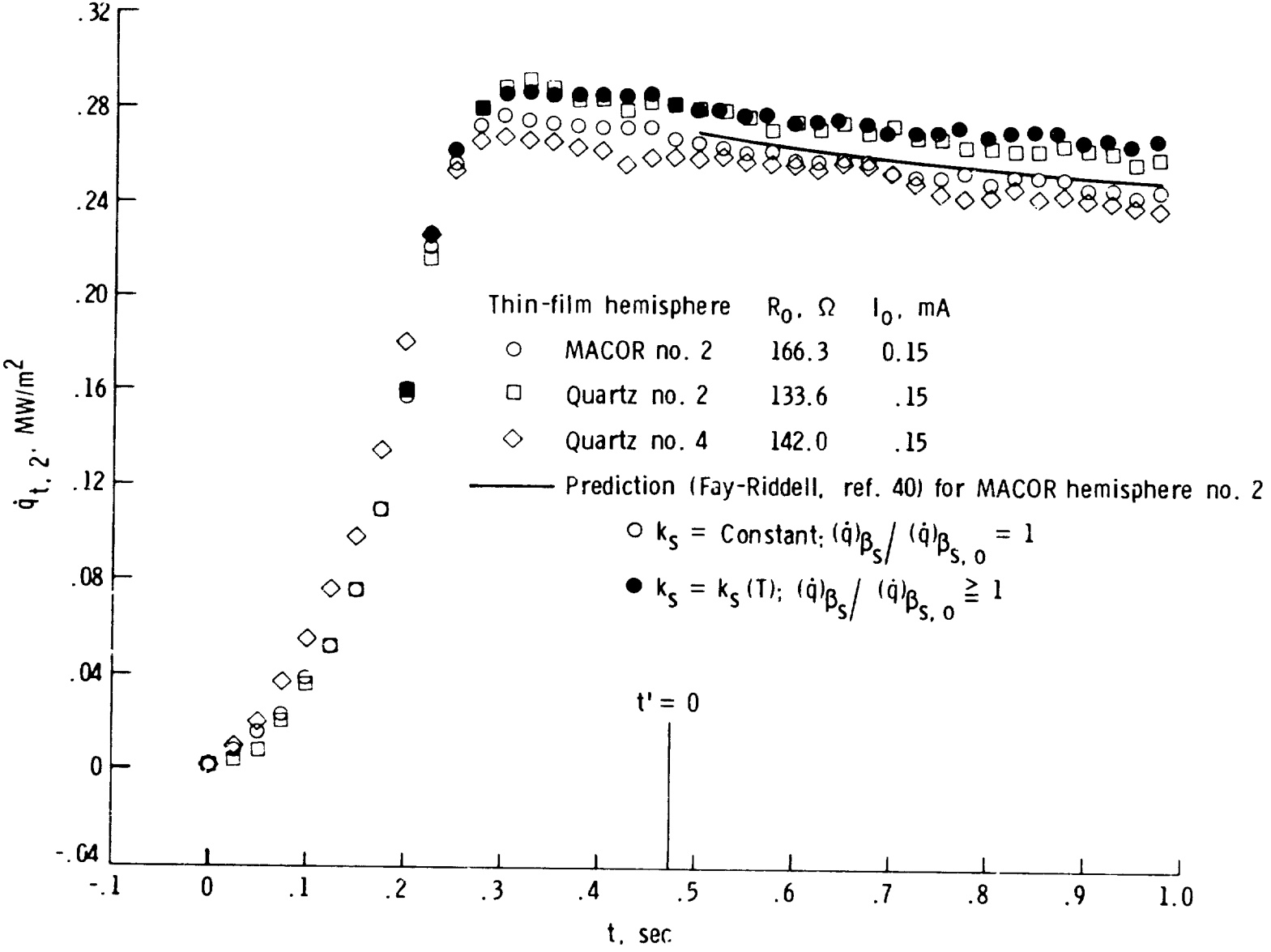

(a) $p_{t,1}$ = 2.4 MPa. Run 11.

Figure 13.- Stagnation-point heat-transfer rate as a function of time for two reservoir pressures in the CFHT.

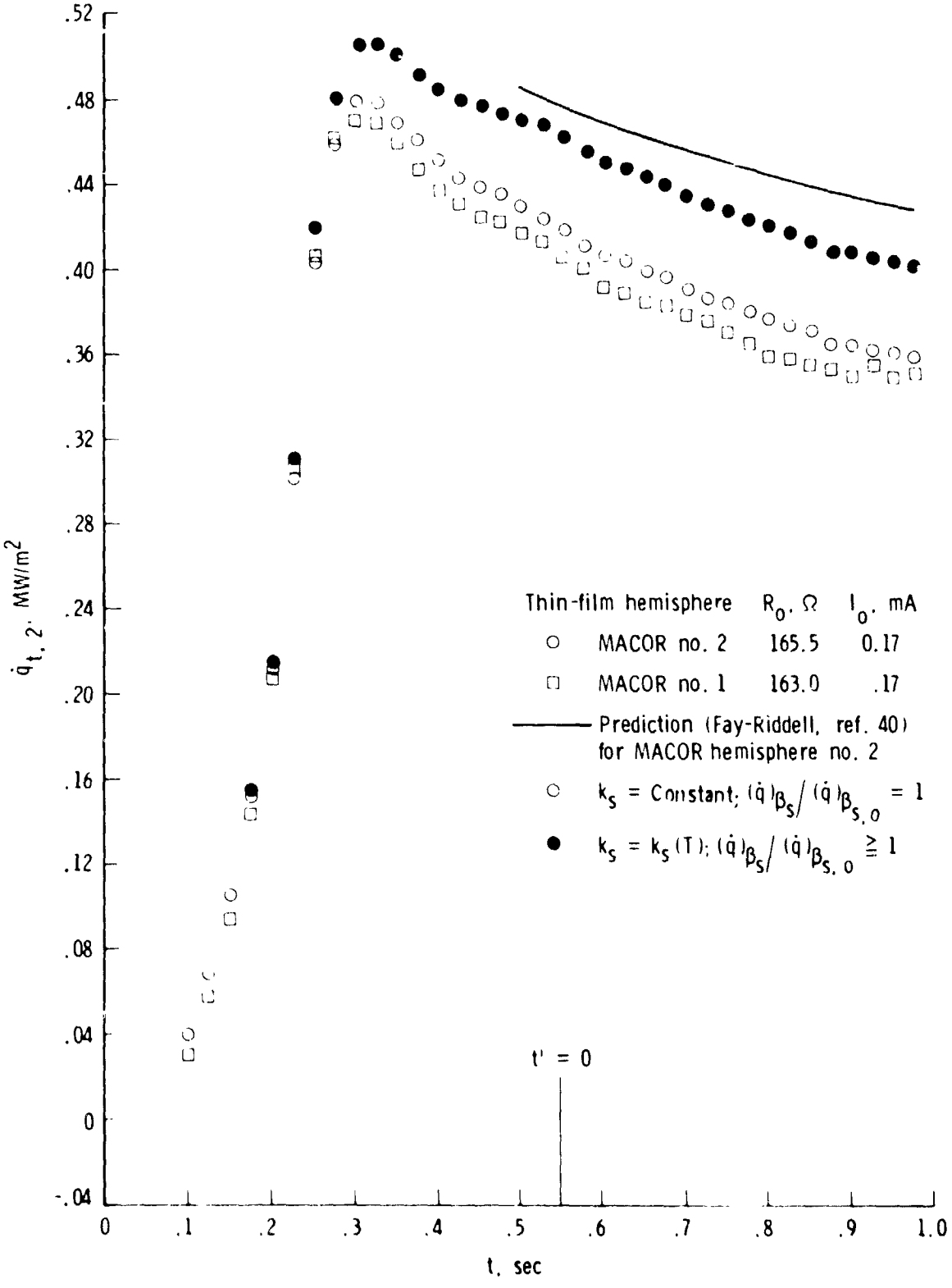

(b) $p_{t,1}$ = 11.3 MPa. Run 13.

Figure 13.- Concluded.

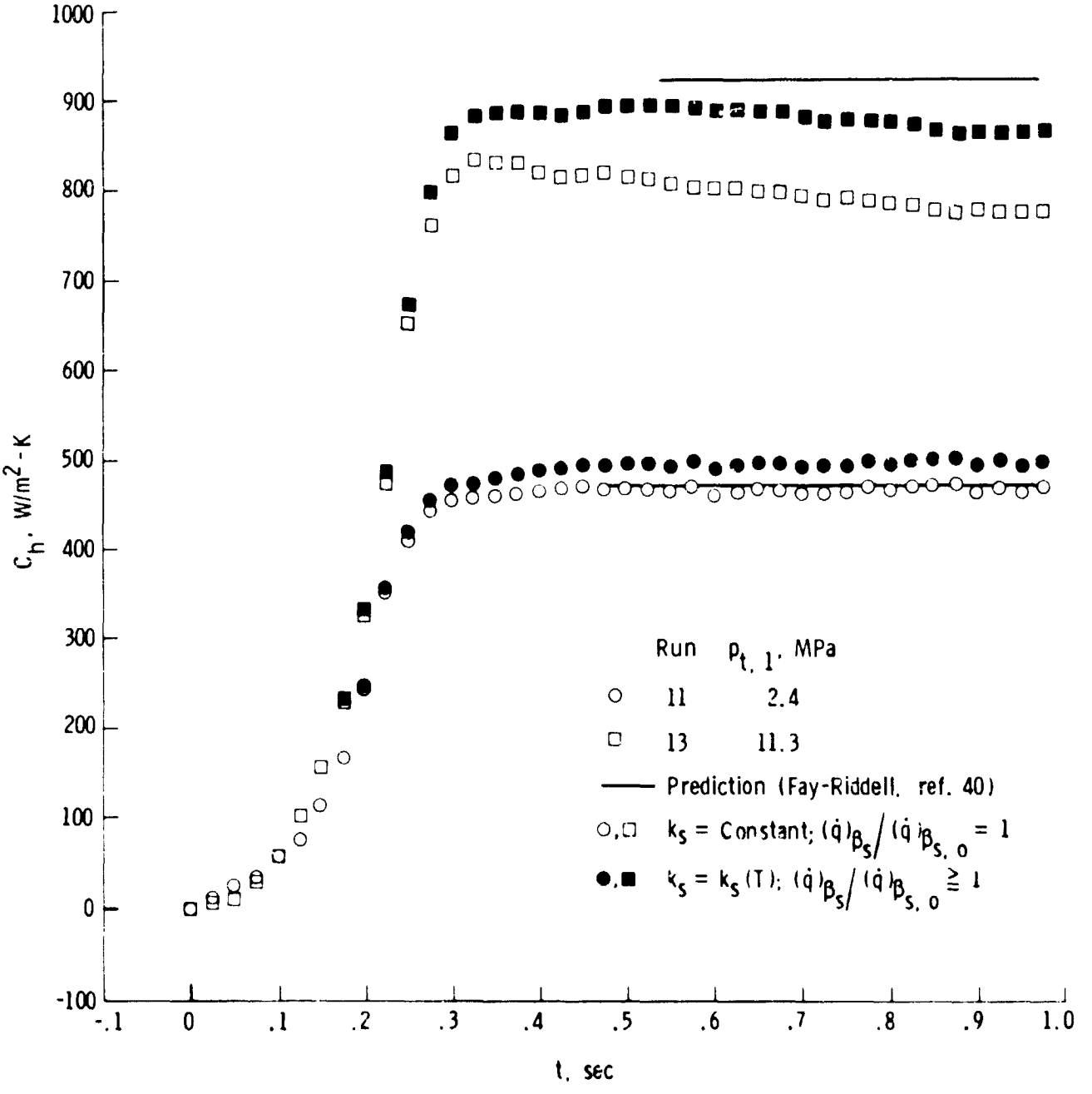

Figure 14.- Stagnation-point heat-transfer coefficient as a function of time for MACOR thin-film hemisphere no. 2 at the minimum and maximum values of reservoir pressure tested in the CFHT.

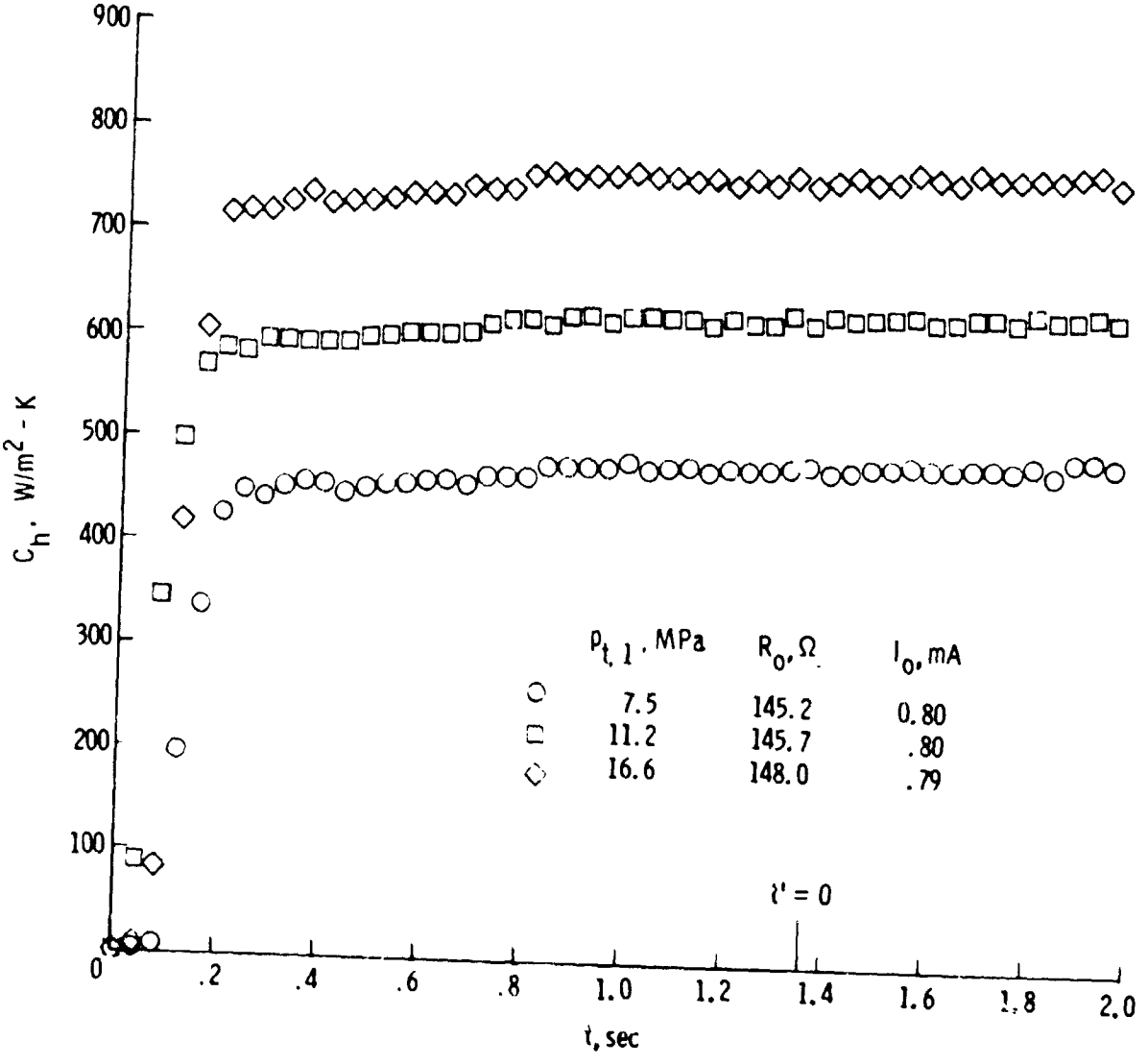

Figure 15.- Stagnation-point heat-transfer coefficient as a function of time for MACOR thin-film hemisphere no. 1 in the CF_4 Tunnel. Heat-transfer rate to MACOR hemisphere calculated by assuming $k_s = k_s(T)$ and $(\dot{q})_{\beta_s}/(\dot{q})_{\beta_{s,o}} > 1$

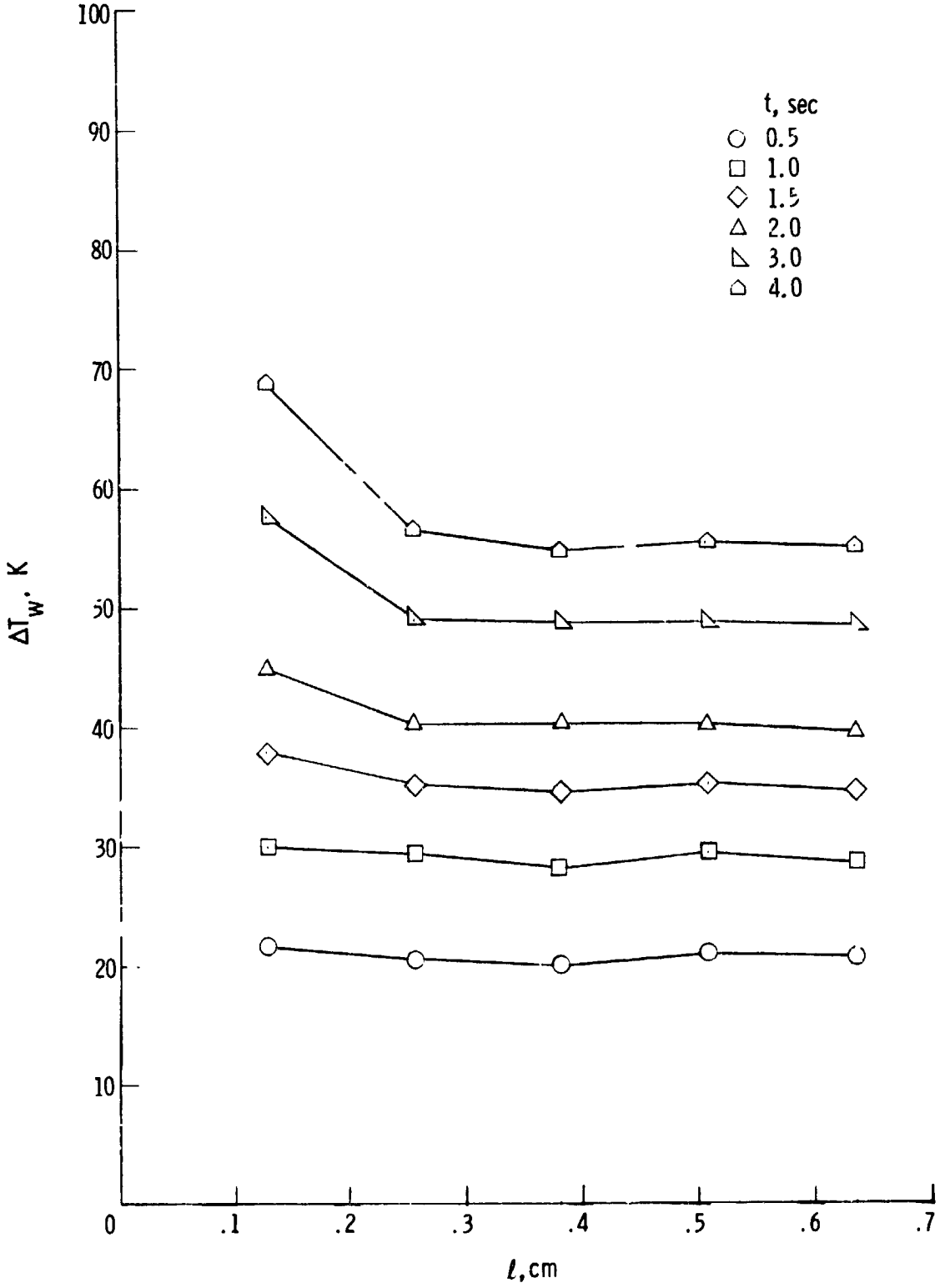

(a) $p_{t,1}$ = 7.65 MPa.

Figure 16.- Surface-temperature change at stagnation region of MACOR disks of different thickness for various times as measured in the CF_4 Tunnel.

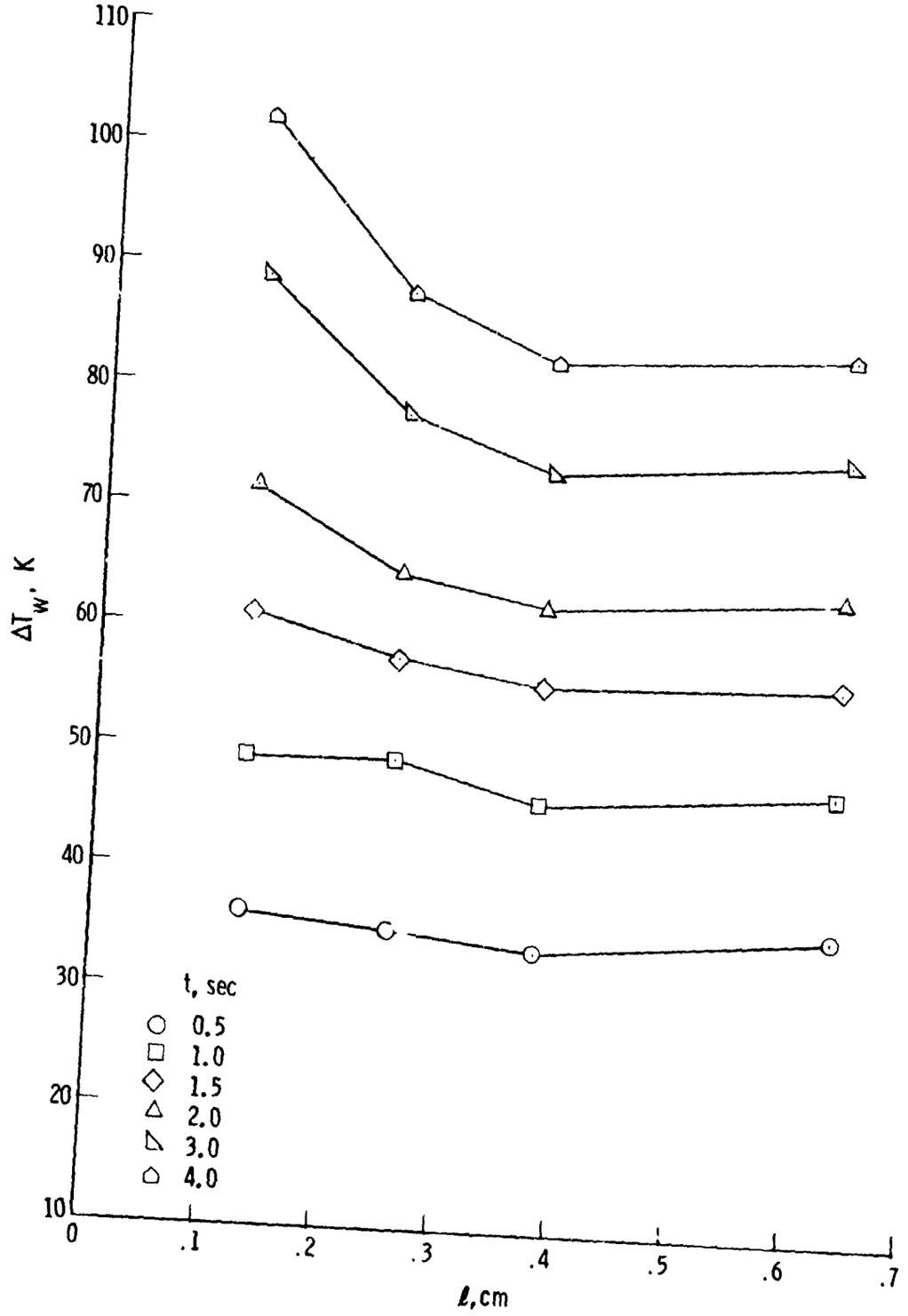

(b) $p_{t,1}$ = 17.2 MPa.

Figure 16.- Concluded.

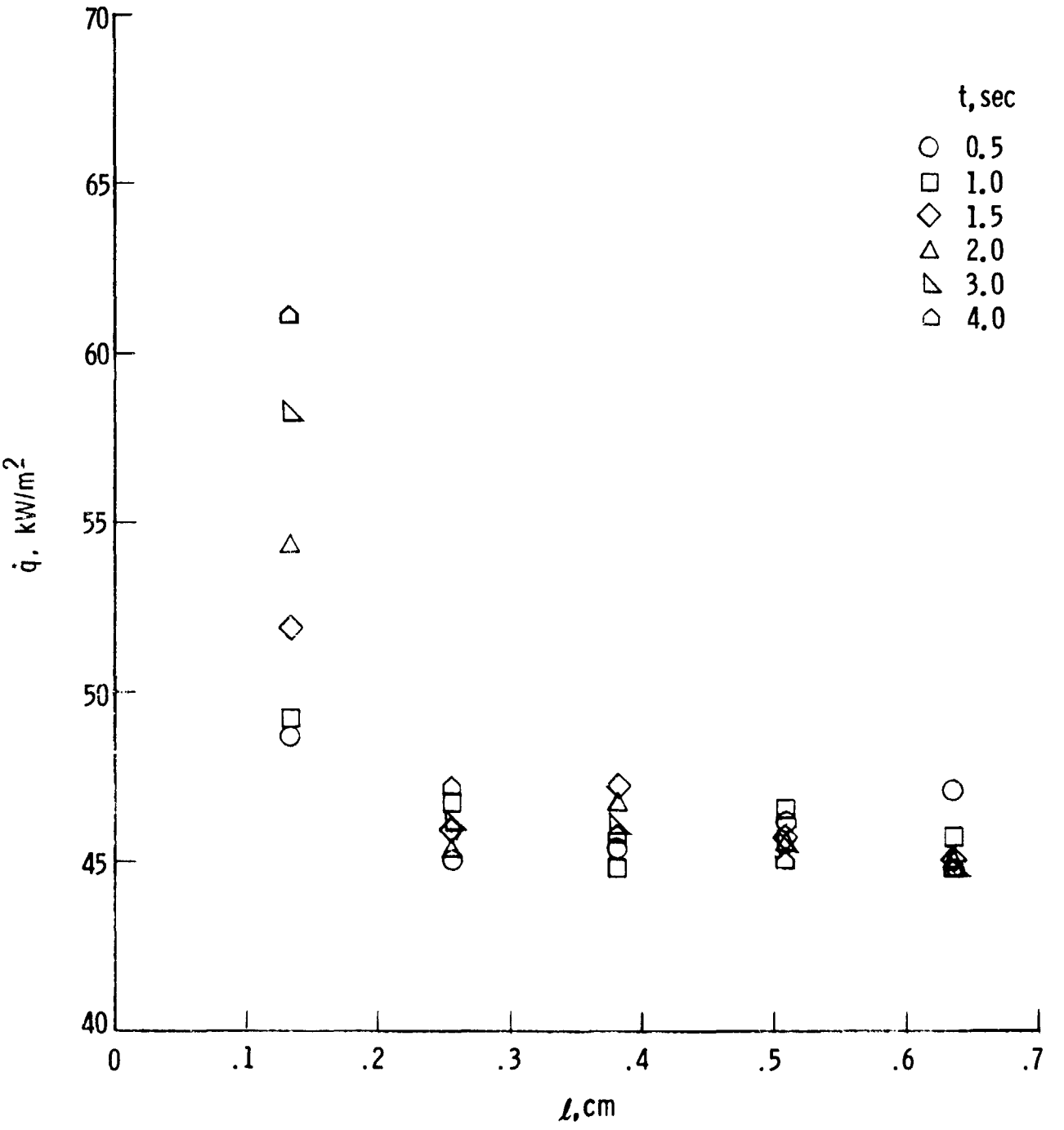

Figure 17.- Stagnation-region heat-transfer rate for MACOR disks of different thickness for various times. CF_4 Tunnel; $p_{t,1}$ = 7.65 MPa; $\dot{q}$ computed by using equations (7) and (A9).

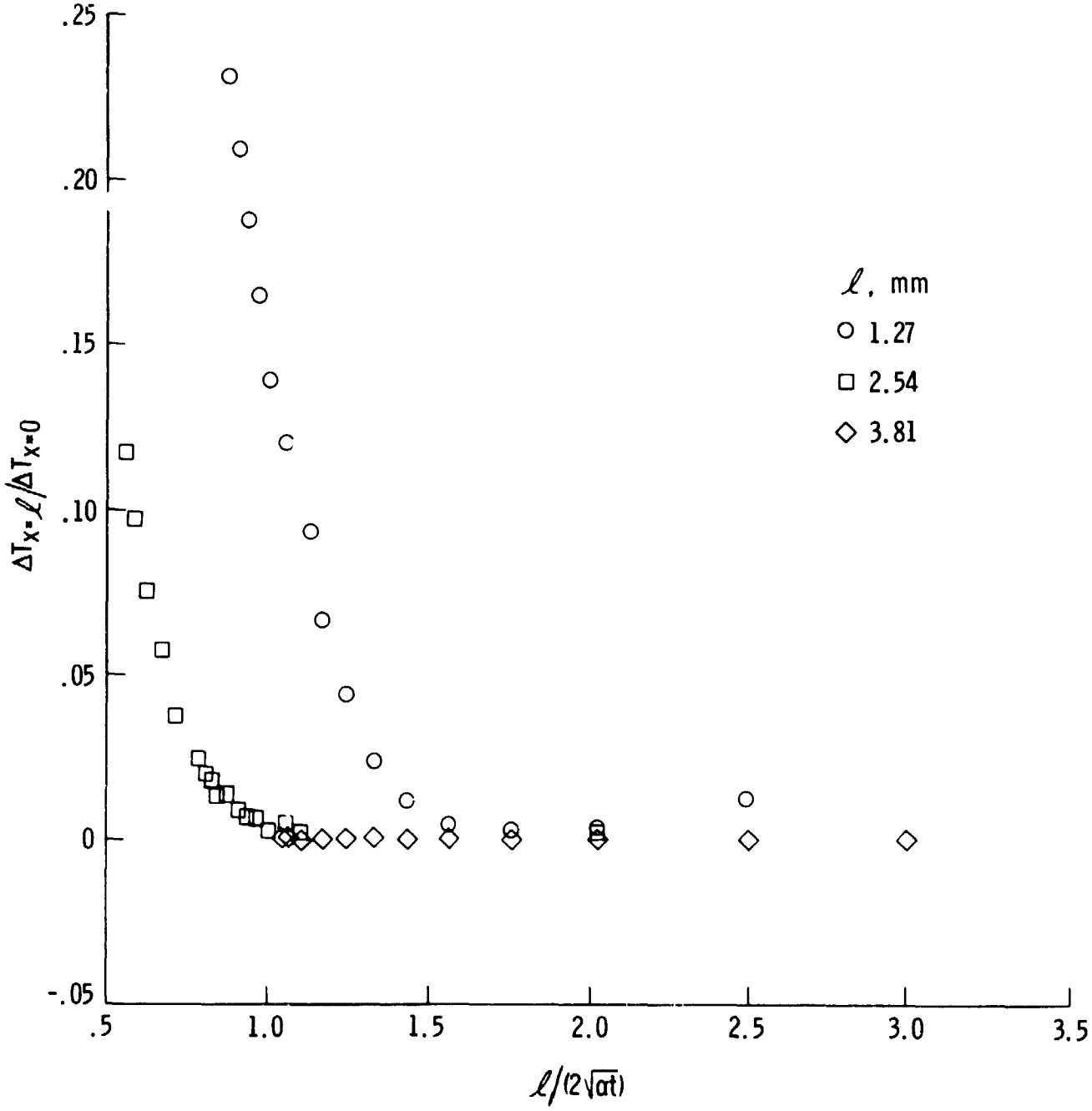

Figure 18.- Ratio of change of surface temperature on rear of MACOR disk to change in surface temperature on front of disk as a function of $\ell/(2\sqrt{\alpha t})$. CF_4 Tunnel; $p_{t,1}$ = 7.65 MPa.

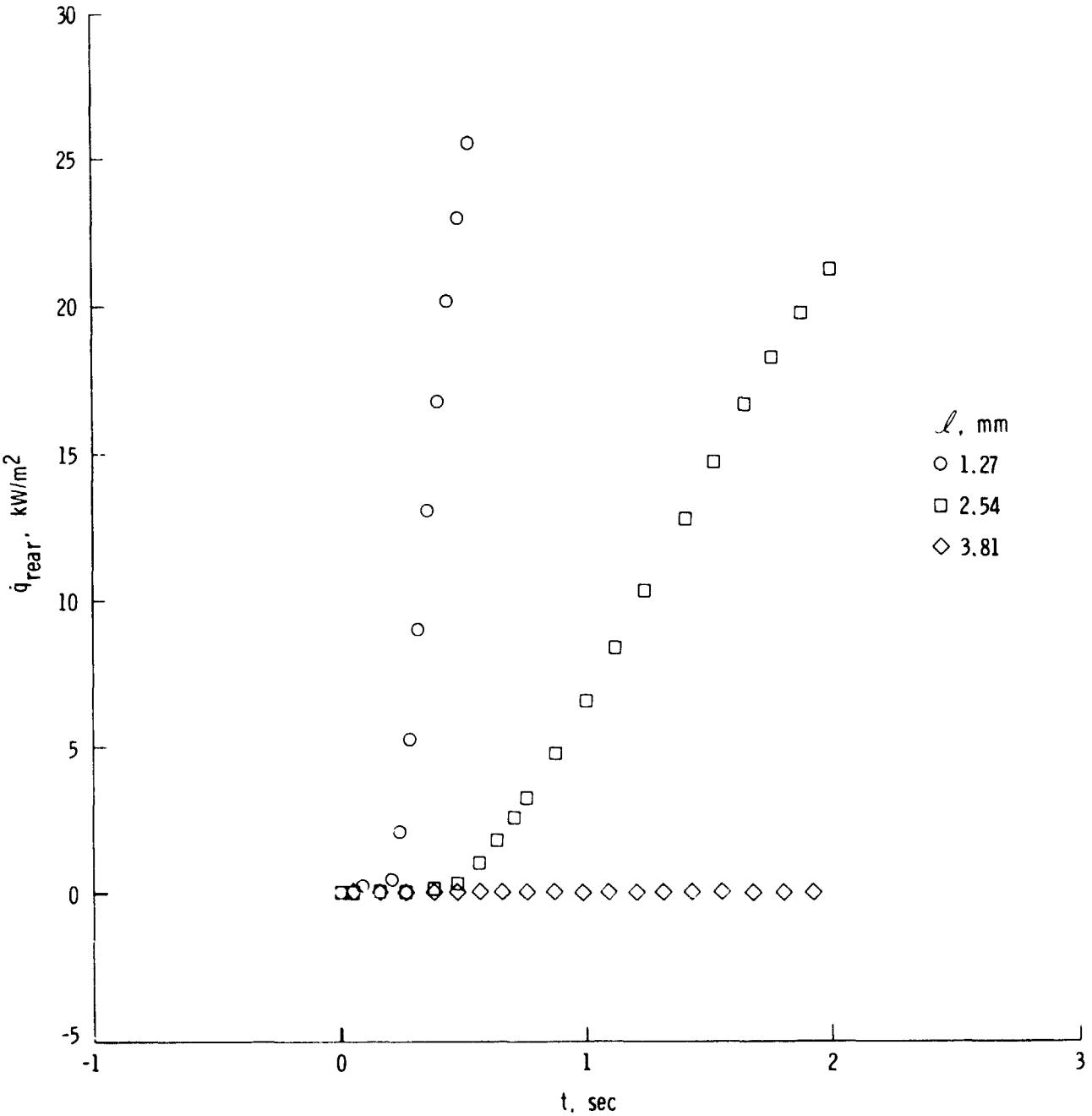

Figure 19.- Time history of heat-transfer rate inferred from surface-temperature change measured on rear of MACOR disks. CF_4 Tunnel; $p_{t,1}$ = 17.2 MPa; $\dot{q}_{rear}$ computed by using equations (7) and (A9).

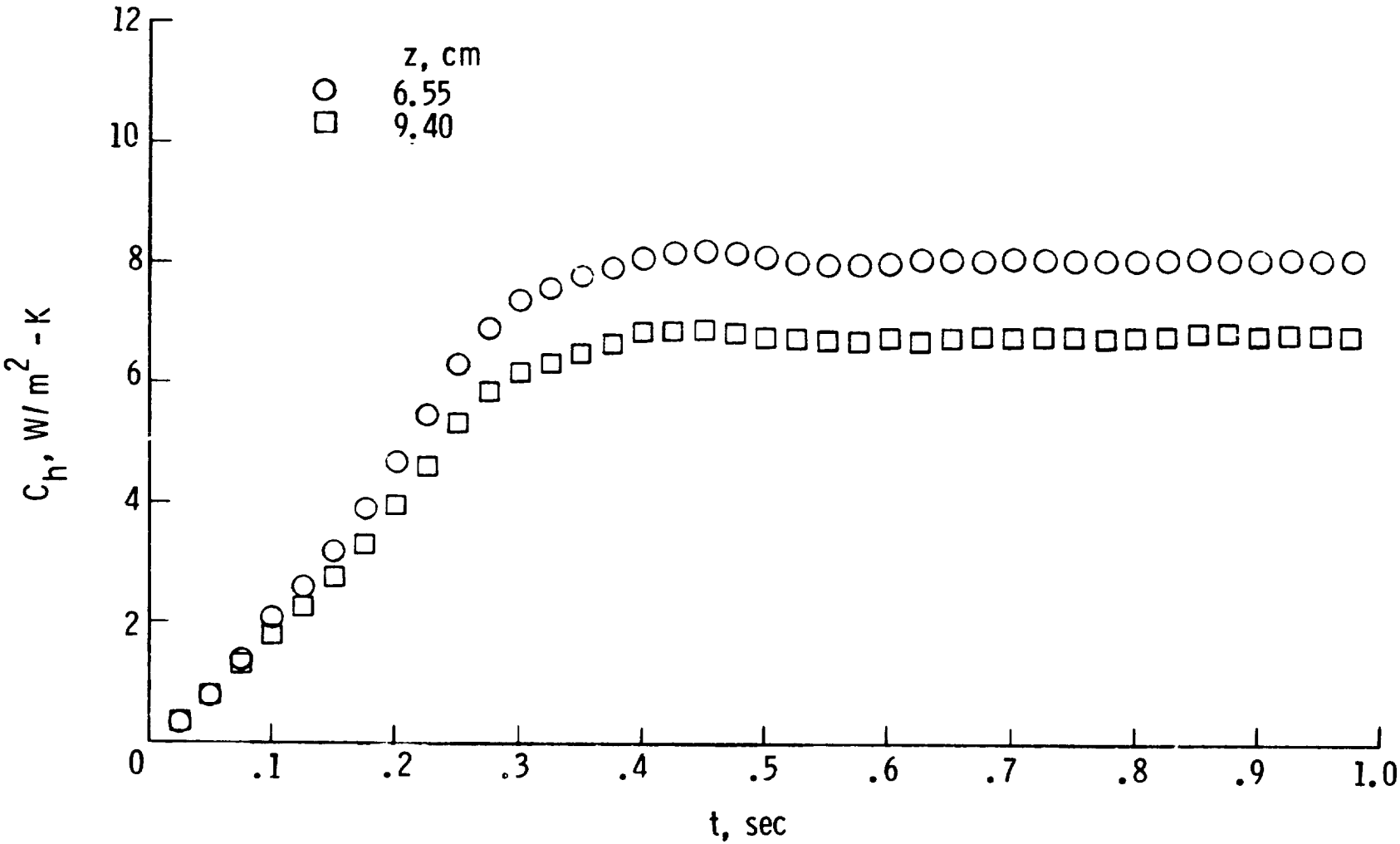

Figure 20.- Heat-transfer coefficient measured on surface of sharp-leading-edge flat plate with thin-film gages in the CFHT as a function of time.

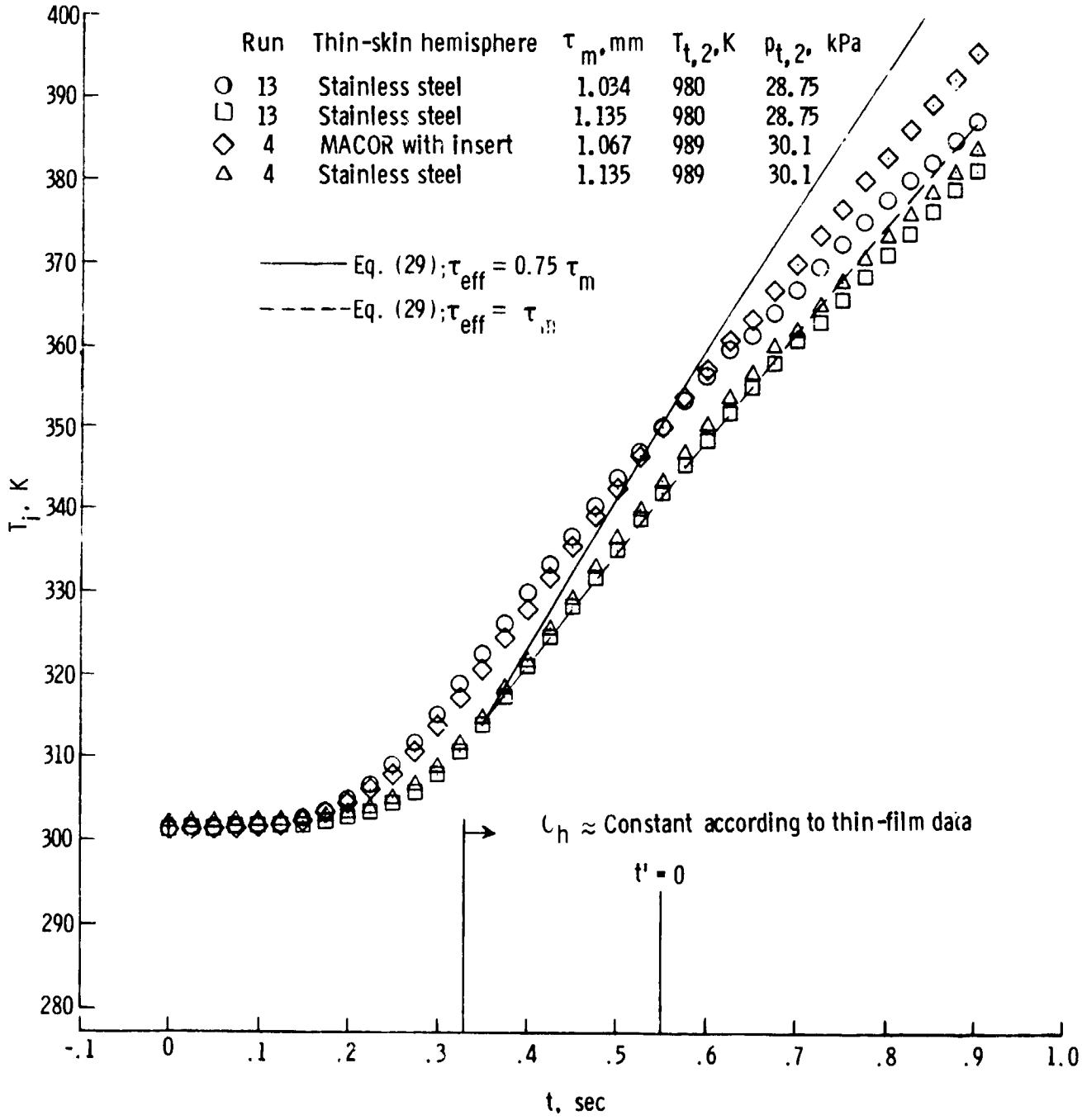

Figure 21.- Wall temperatures of thin-skin calorimetry hemispheres as a function of time t for $p_{t,1}$ = 11.3 MPa in the CFHT.

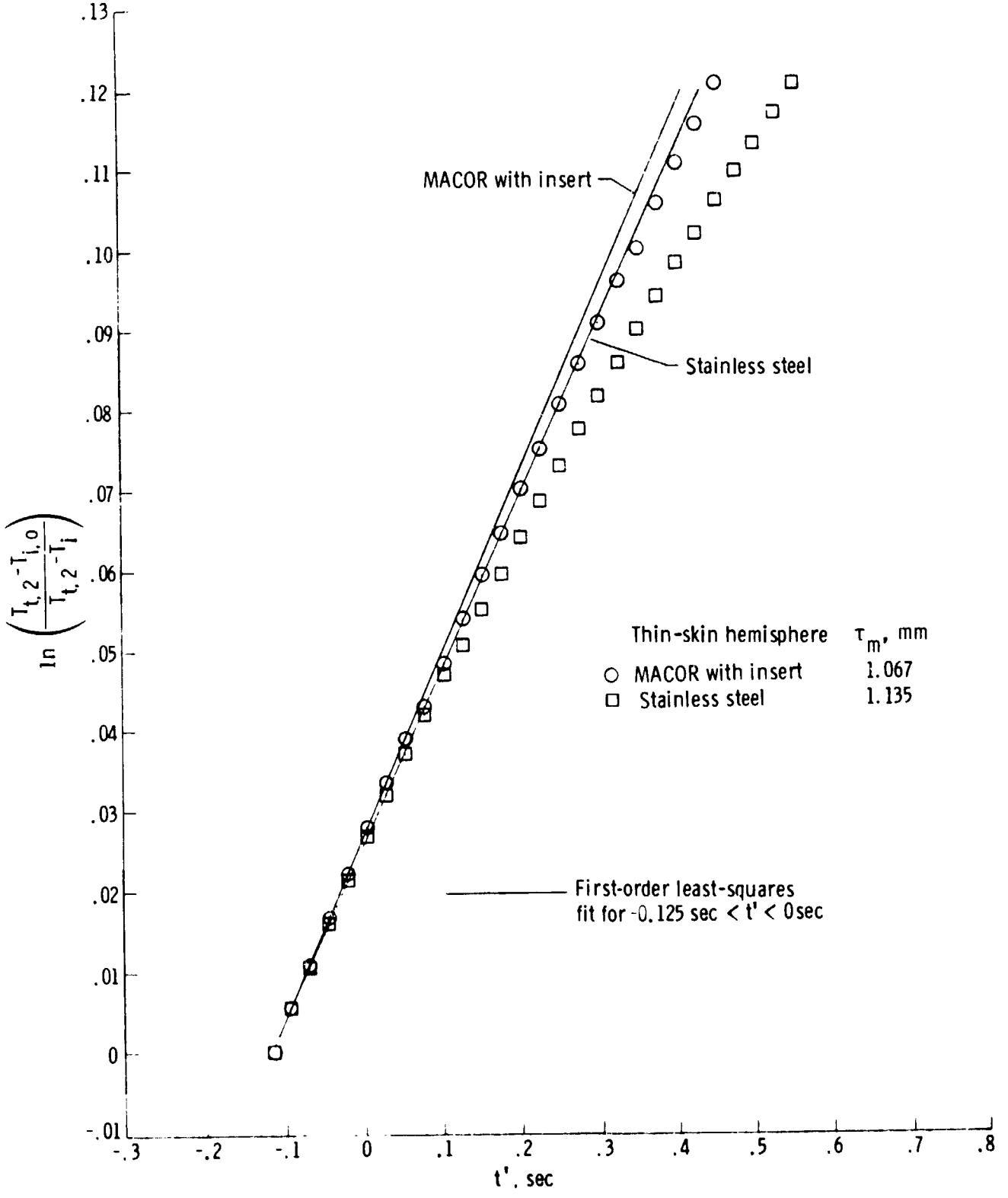

Figure 22.- Temperature parameter as a function of time t' for run 4 in the CFHT. $p_{t,1}$ = 11.3 MPa.

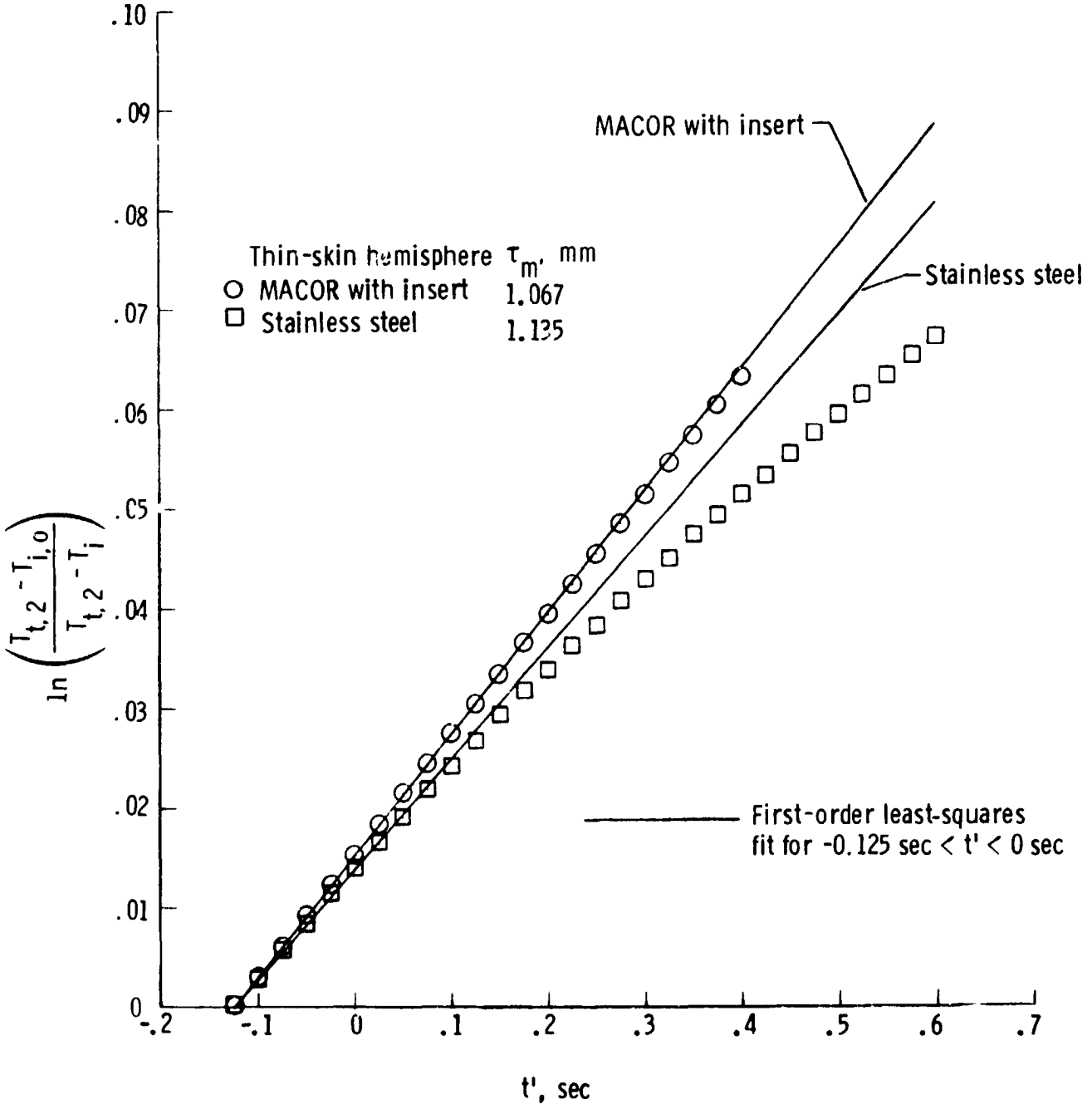

Figure 23.- Temperature parameter as a function of time t' for run 1 in the CFHT. $p_{t,1}$ = 2.4 MPa.

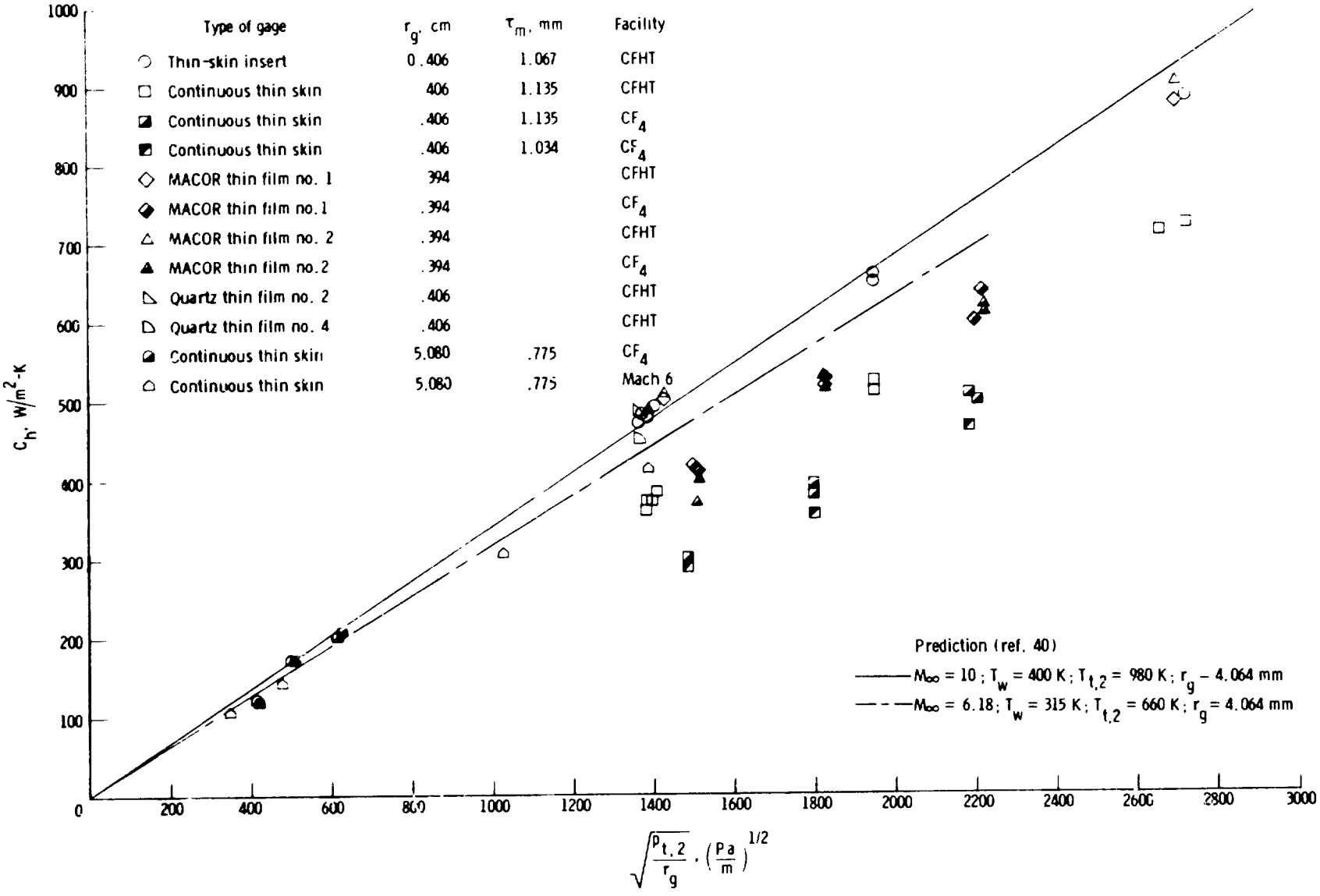

Figure 24.- Stagnation-point heat-transfer coefficient measured with thin-skin hemispheres and thin-film hemispheres as a function of pitot pressure.

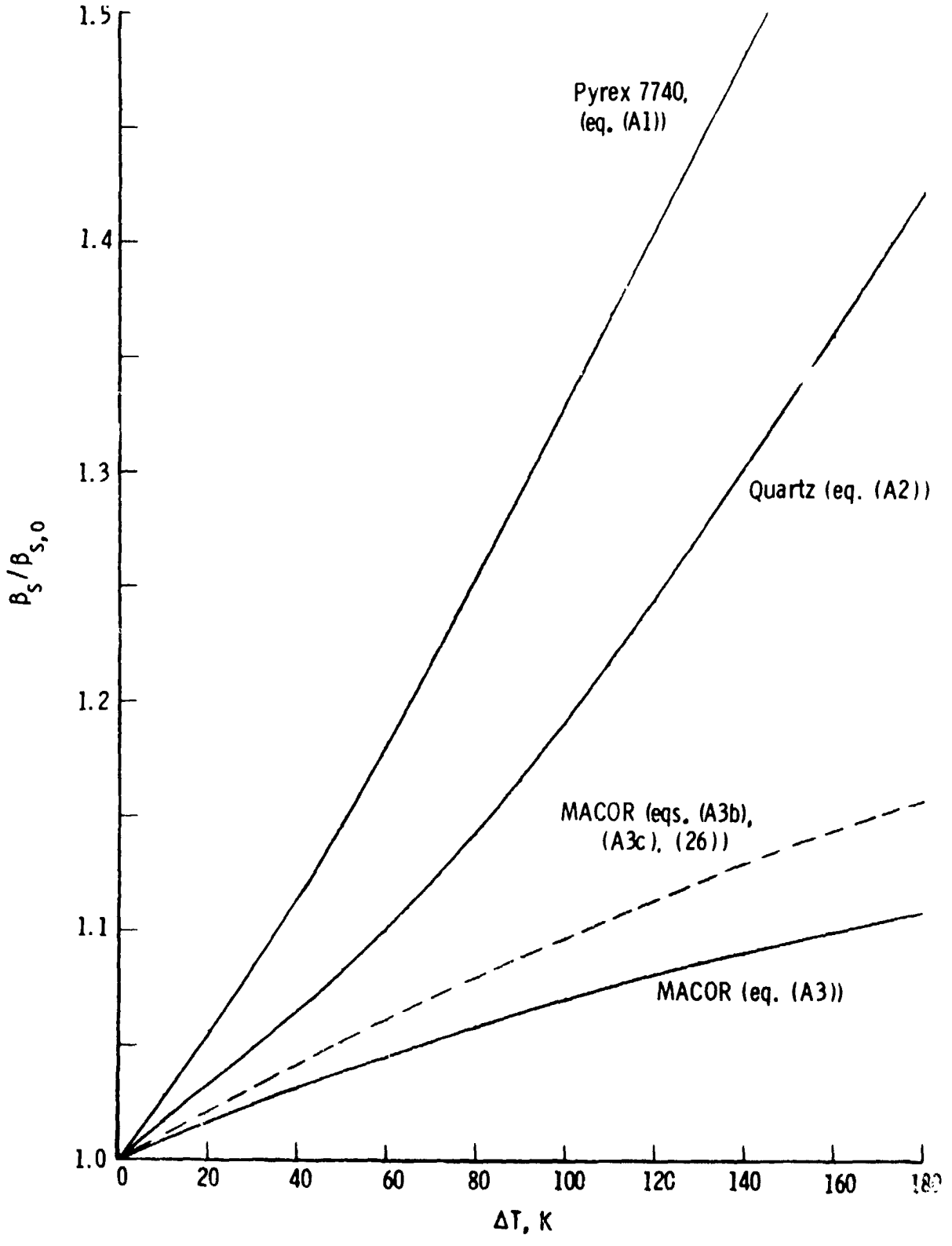

Figure 25.- Thermal product β as a function of change in temperature for Pyrex 7740, quartz, and MACOR substrates. T_o = 295 K.

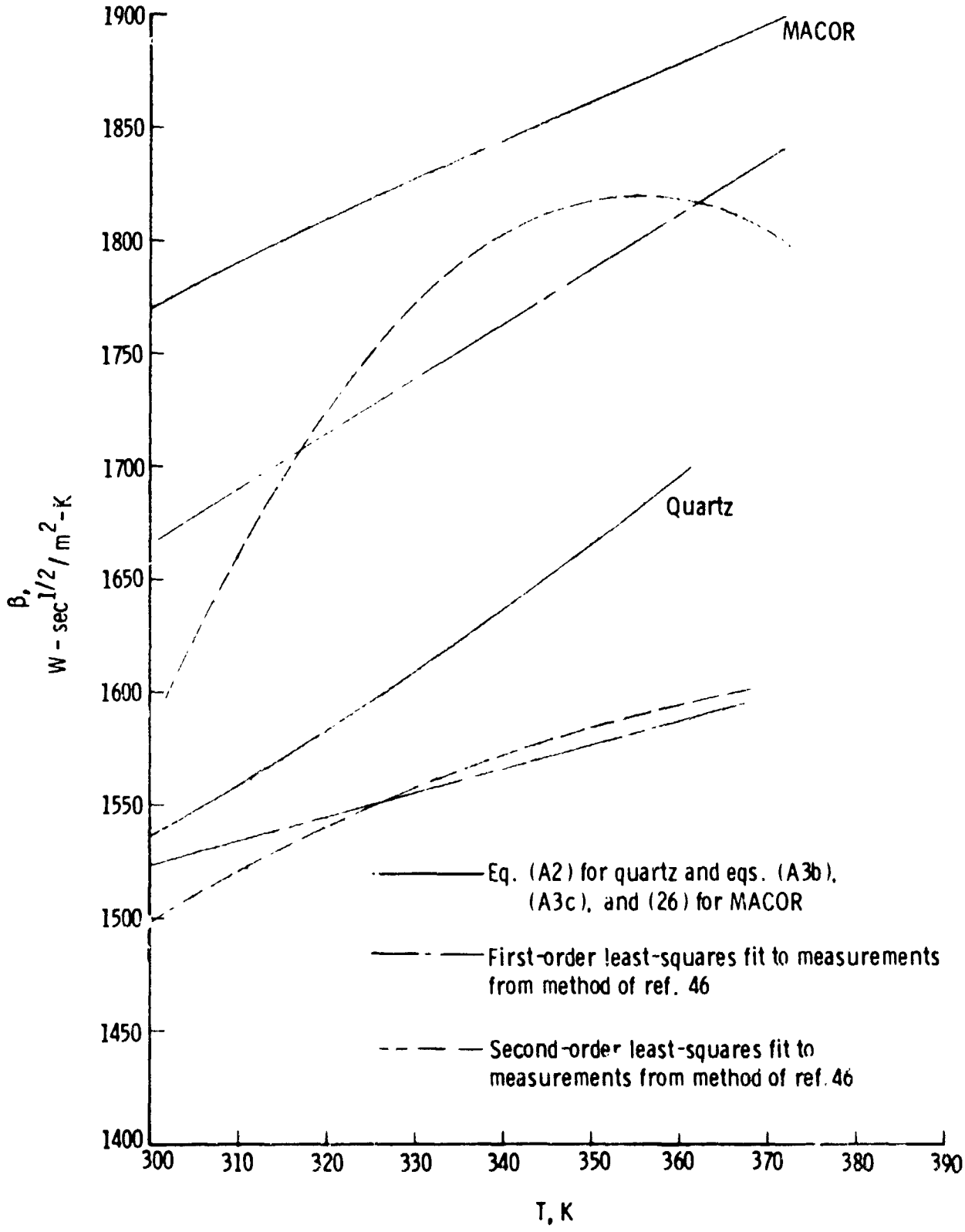

Figure 26.- Comparison of thermal product β measured by the method of reference 46 with values representing a curve fit to a collection of other data.

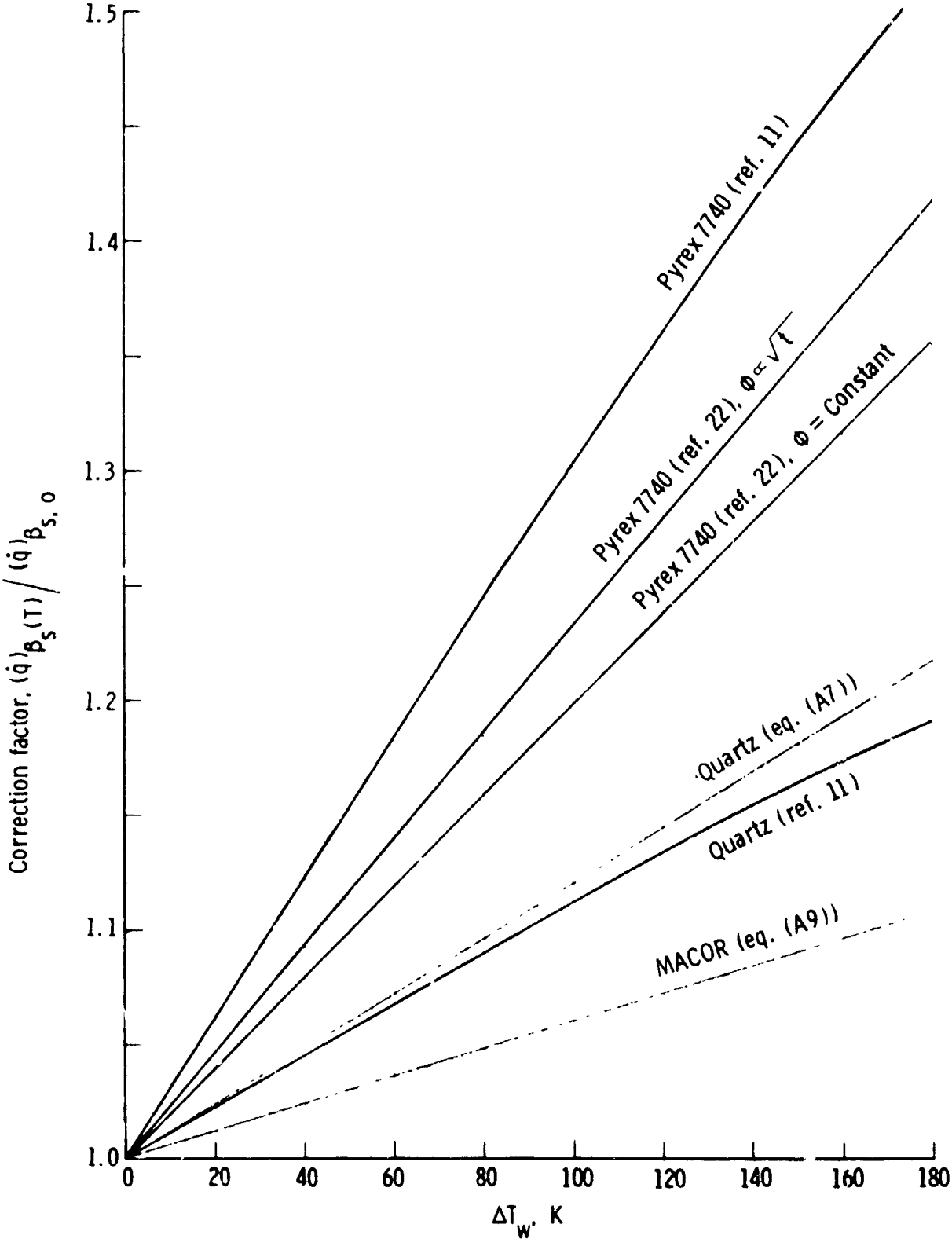

Figure 27.- Ratio of heat-transfer rate for variable substrate properties to heat-transfer rate for constant substrate properties as a function of temperature change for Pyrex 7740, quartz, and MACOR substrates. $T_{w,o}$ = 295 K.

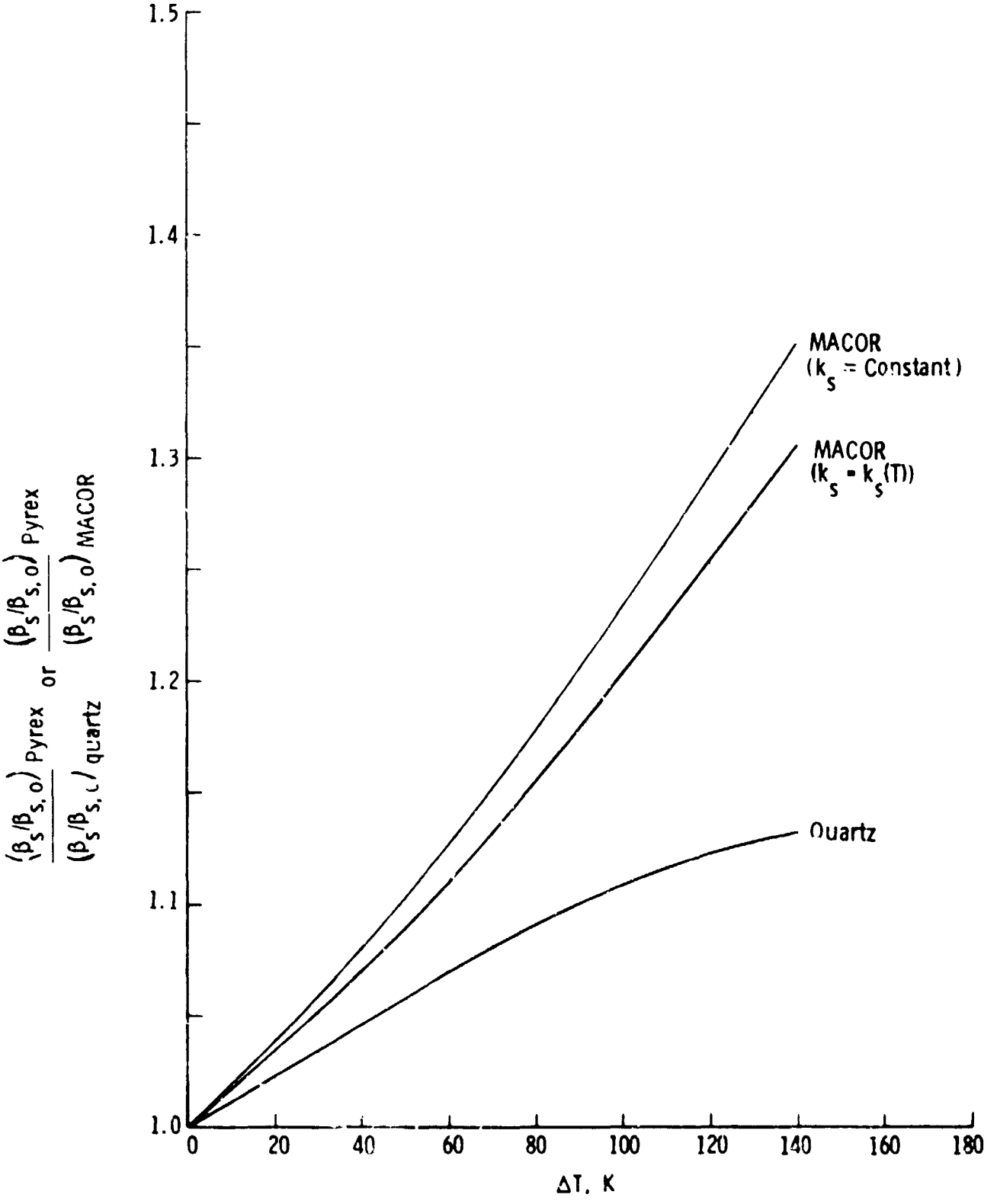

Figure 28.- Comparison of thermal product β for quartz and MACOR with that of Pyrex 7740. T_o = 295 K.

MACOR hemisphere number	Calibration series	First-order fit		Second-order fit	
		dR/dT, Ω/K	α_R per mK	dR/dT, Ω/K	α_R per mK
● 1	1	0.53379	2.4403	0.54542	2.4934
○ 2	1	.49693	2.4500	.50729	2.5011
■ 1	2	.36797	2.2914	.37683	2.3465
□ 2	2	.38673	2.3647	.39584	2.4203
◆ 1	3	.34072	2.2212	.34877	2.2738
◇ 2	3	.35536	2.3132	.36340	2.3656
▲ 1	4	.33399	2.1782	.35296	2.3018
△ 2	4	.34985	2.2777	.36574	2.3814

Series 1 performed prior to testing in CFHT.

Series 2 performed during testing (after six runs).

Series 3 performed after testing in CFHT.

Series 4 performed after testing, calibrating to 505 K, and varying I_o up to 20 mA.

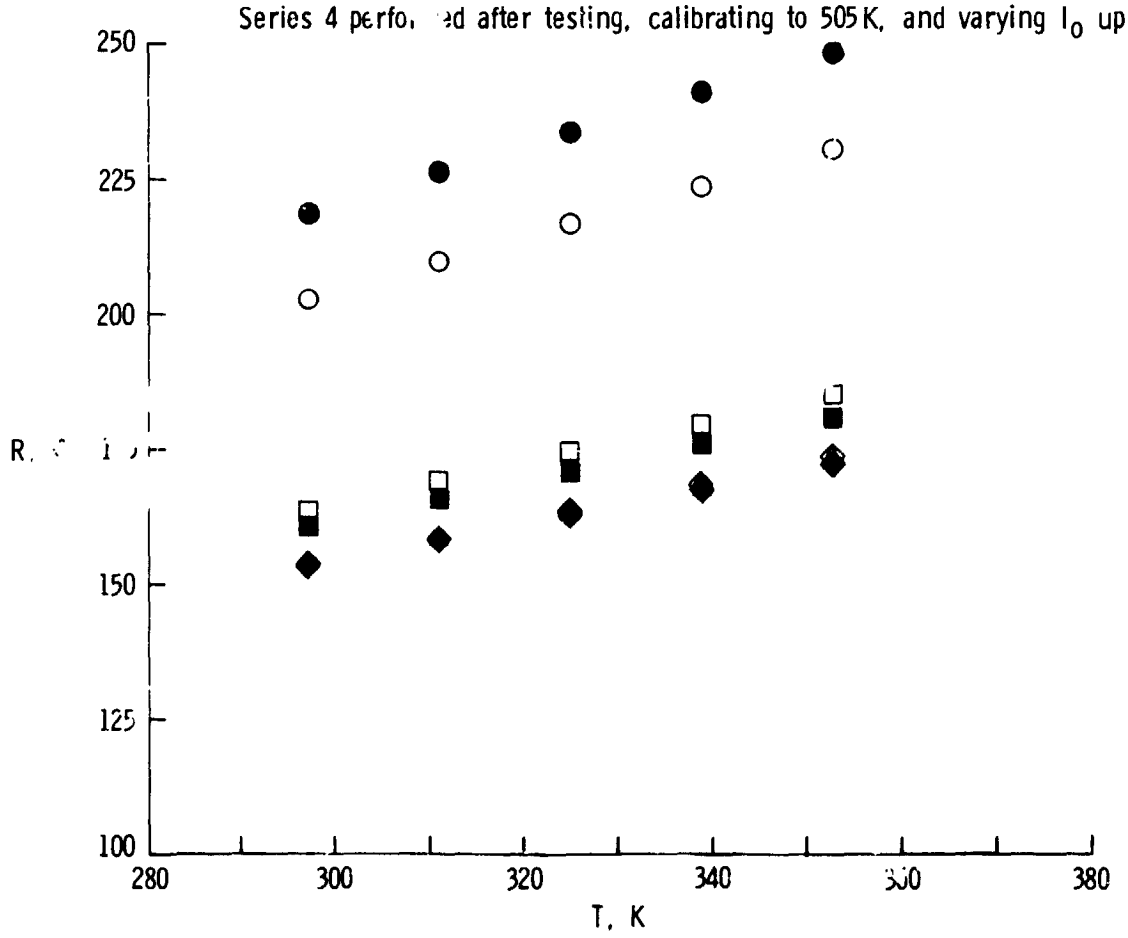

(a) MACOR hemisphere nos. 1 and 2; 297 K < T < 352.6 K.

Figure 29.- Resistance of thin-film gages as a function of temperature for MACOR and quartz hemispheres and two ranges of temperature. I_o = 1 mA; $\alpha_R = (dR/dT)/(R)_{at\ 297\ K}$.

Quartz hemisphere number	Series	First-order fit		Second-order fit	
		dR/dT, Ω/K	α_R per mK	dR/dT, Ω/K	α_R per mK
● 2	1	0.28456	2.1031	0.29970	2.2171
○ 4	1	.28345	2.3234	.29576	2.4244
■ 2	2	.27985	2.1395	.28604	2.1868
□ 4	2	.32015	2.3017	.33682	2.4215

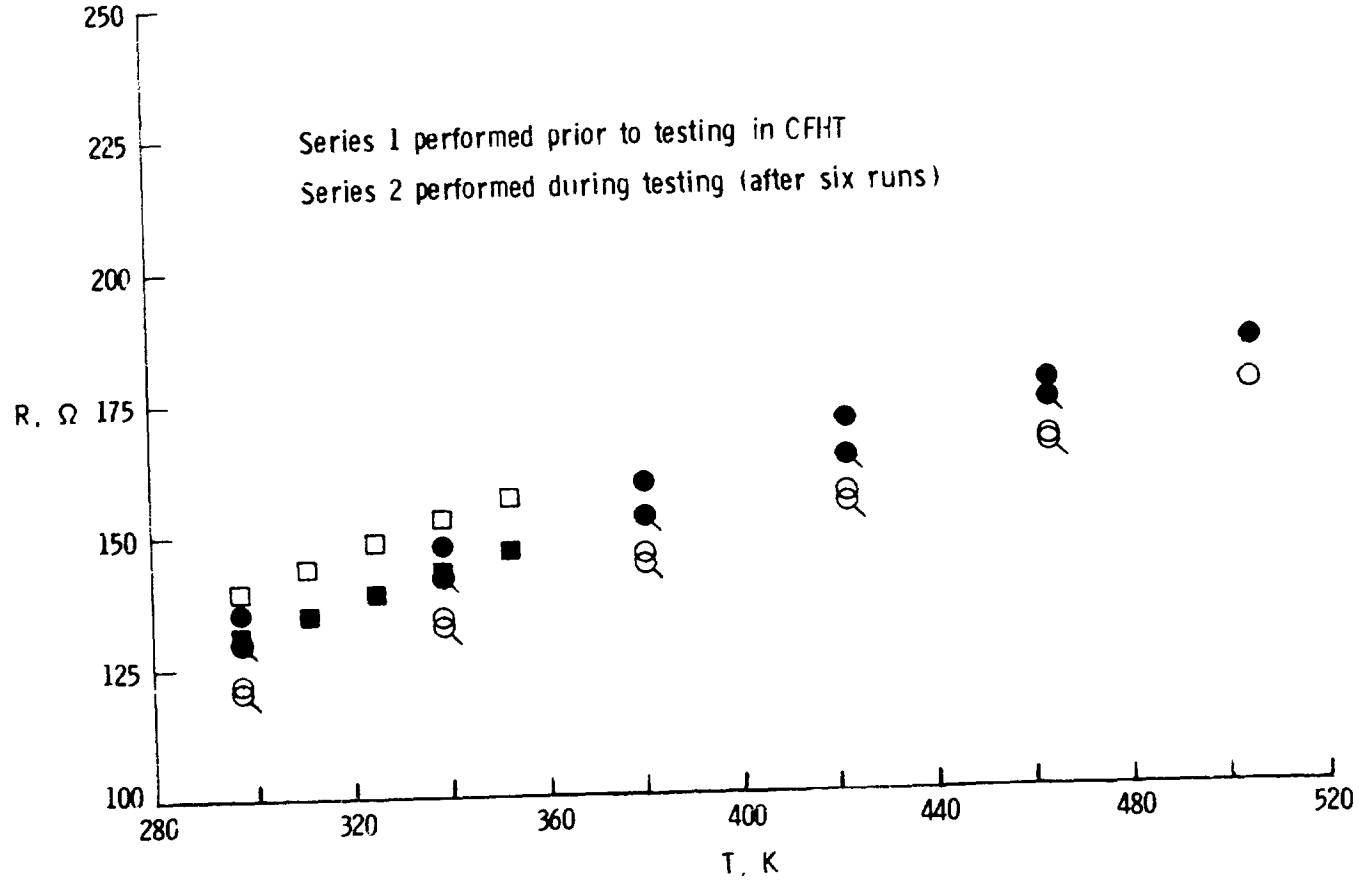

(b) Quartz hemispheres nos. 2 and 4. 297 K < T < 505.4 K. Flagged symbols denote descending temperature; curve fits to series 1 for 297 K < T < 380 K.

Figure 29.- Continued.

R_0, Ω, at T = 297 K	Range of T, K	First-order fit		Second-order fit	
		dR/dT, Ω/K	α_R per mK	dR/dT, Ω/K	α_R per mK
○ 153.34	297 to 380	0.33399	2.1782	0.35296	2.3019
□ 151.18	297 to 505	.31199	2.0637	.34621	2.2900
◇ 143.50	297 to 505	.32399	2.2578	.33545	2.3376
△ 144.62	297 to 408	.33116	2.2900	.34691	2.3988
▲ 143.64	297 to 408	32616	2.2707	.33356	2.3222

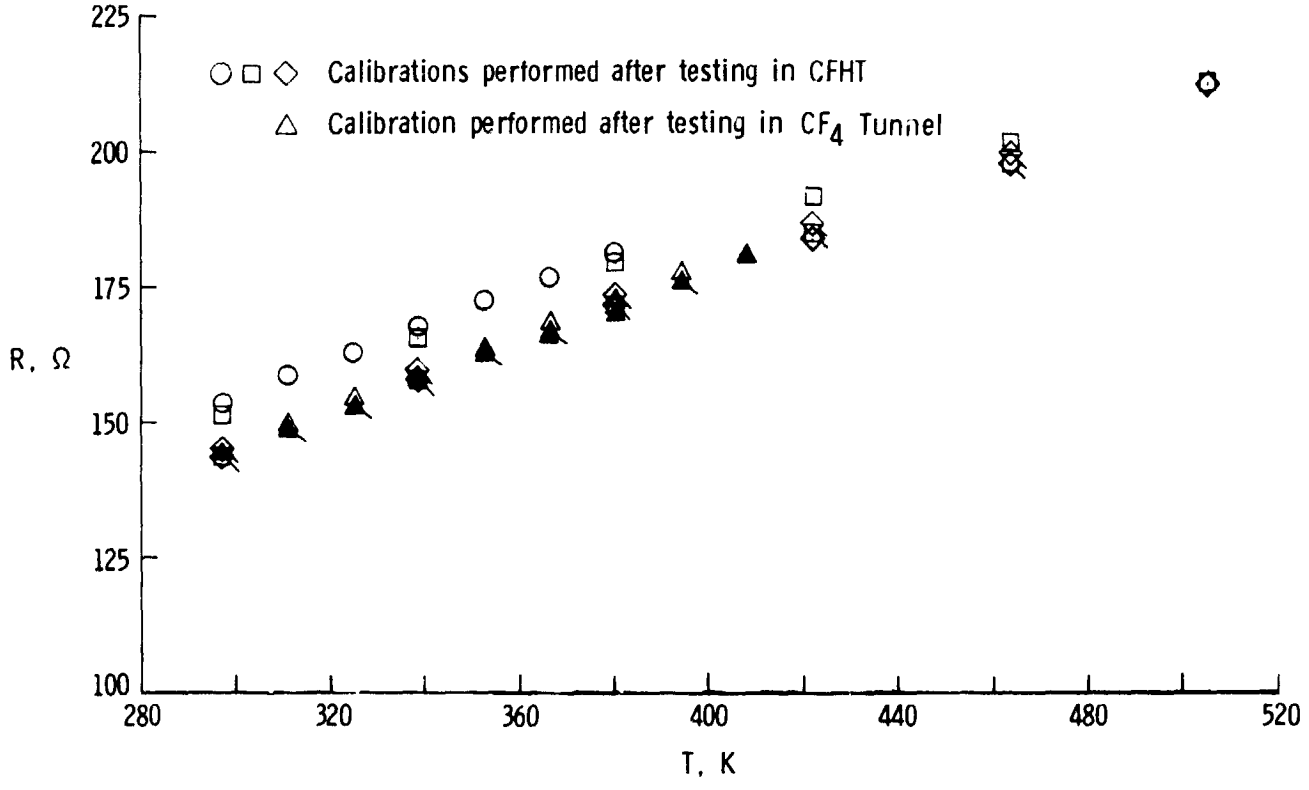

(c) MACOR hemisphere no. 1. 297 K < T < 505.4 K. Flagged symbols denote descending temperature; open symbols denote oil bath; closed symbols denote air oven.

Figure 29.- Continued.

R_0, Ω, at T = 297 K	Range of T, K	First-order fit		Second-order fit	
		dR/dT, Ω/K	α_R per mK	dR/dT, Ω/K	α_R per mK
○ 153.59	297 to 380	0.34985	2.2778	0.36574	2.3814
□ 152.58	297 to 505	.33093	2.1690	.36508	2.3928
◇ 149.19	297 to 505	.33934	2.2745	.34987	2.3450
△ 150.43	297 to 408	.34949	2.3233	.36238	2.4090
▲ 148.37	297 to 408	.34204	2.3053	.35019	2.3603

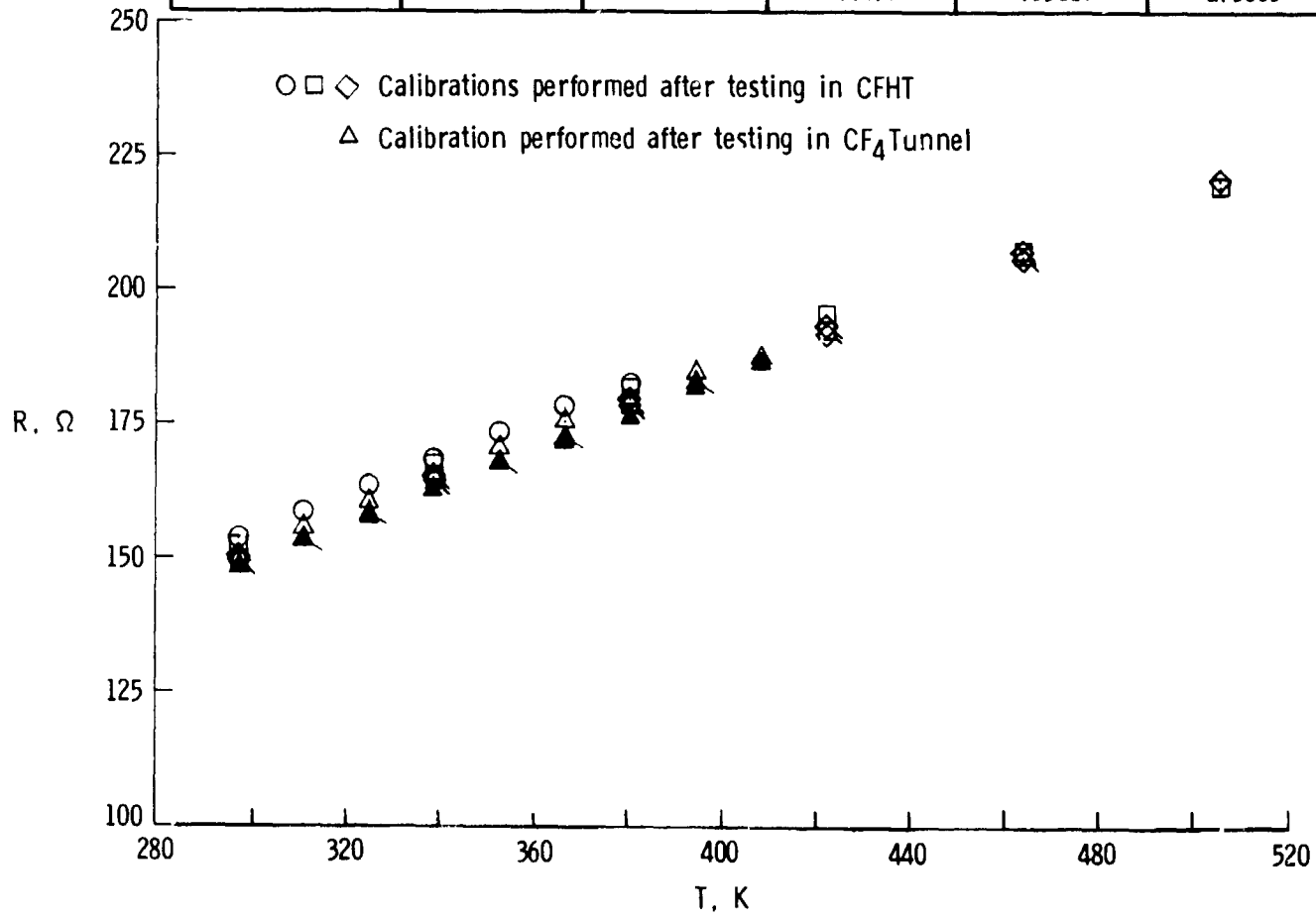

(d) MACOR hemisphere no. 2. 297 K < T < 505.4 K. Flagged symbols denote descending temperature; open symbols denote oil bath; closed symbols denote air oven.

Figure 29.- Concluded.

I_o, mA	First-order fit		Second-order fit	
	dR/dT, Ω/K	α_R per mK	dR/dT, Ω/K	α_R per mK
○ 0.7	0.16286	2.4977	0.16697	2.5605
□ 2.0	.16312	2.5009	.16666	2.5553
◇ 5.0	.16295	2.4970	.16672	2.55465
△ 10.0	.16054	2.4552	.17314	2.6478
▷ 15.0	.15410	2.3486	.17588	2.6809
▷ 20.0	.14918	2.2628	.16324	2.4302

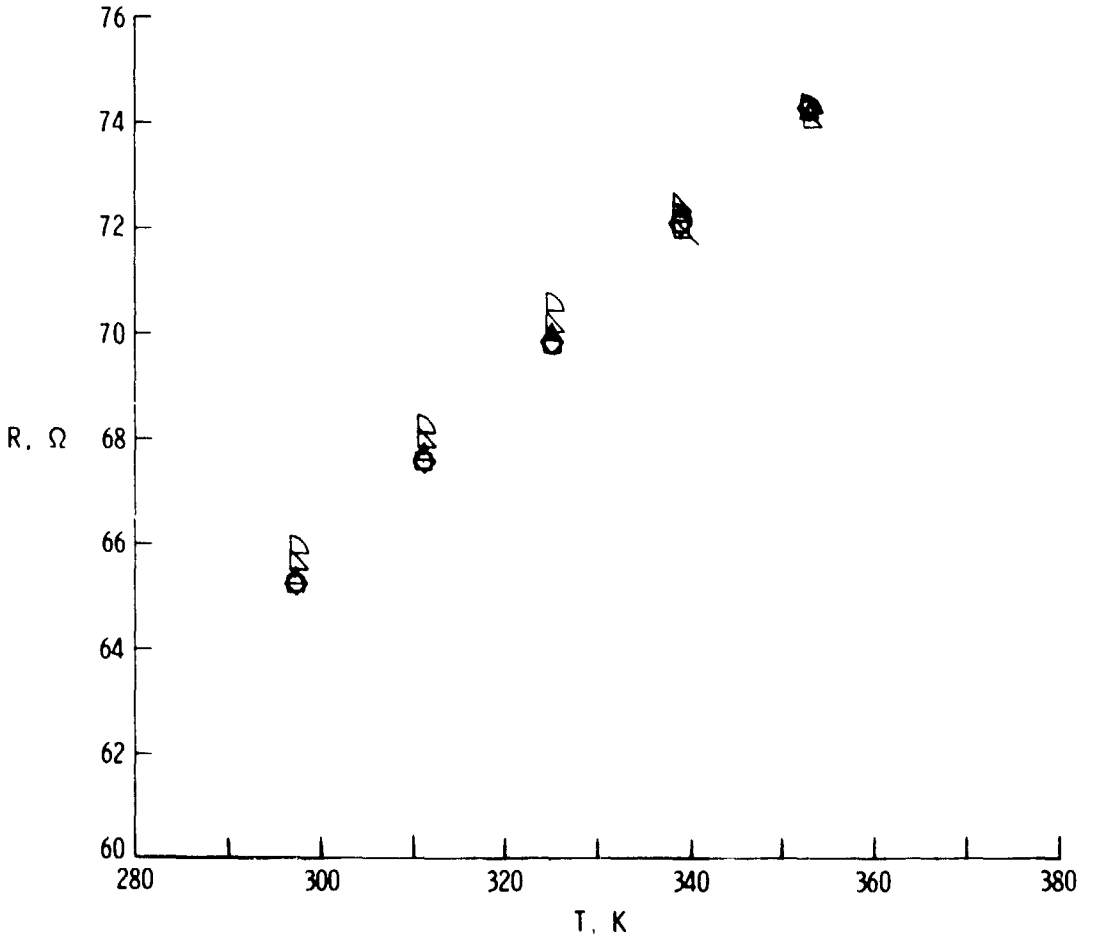

(a) Quartz flat-faced cylinder with gage no. 51. Flagged symbols denote descending temperature.

Figure 30.- Effect of thin-film current on measured resistance for quartz flat-faced cylinders and MACOR hemispheres nos. 1 and 2.

I_o, mA	First-order fit		Second-order fit	
	dR/dT, Ω/K	α_R per mK	dR/dT, Ω/K	α_R per mK
○ 0.7	0.13608	2.2259	0.14022	2.2925
□ 2.0	.13518	2.2037	.14058	2.2909
◇ 5.0	.13680	2.2354	.1368	2.2365
△ 10.0				
◺ 15.0				
◺ 20.0				

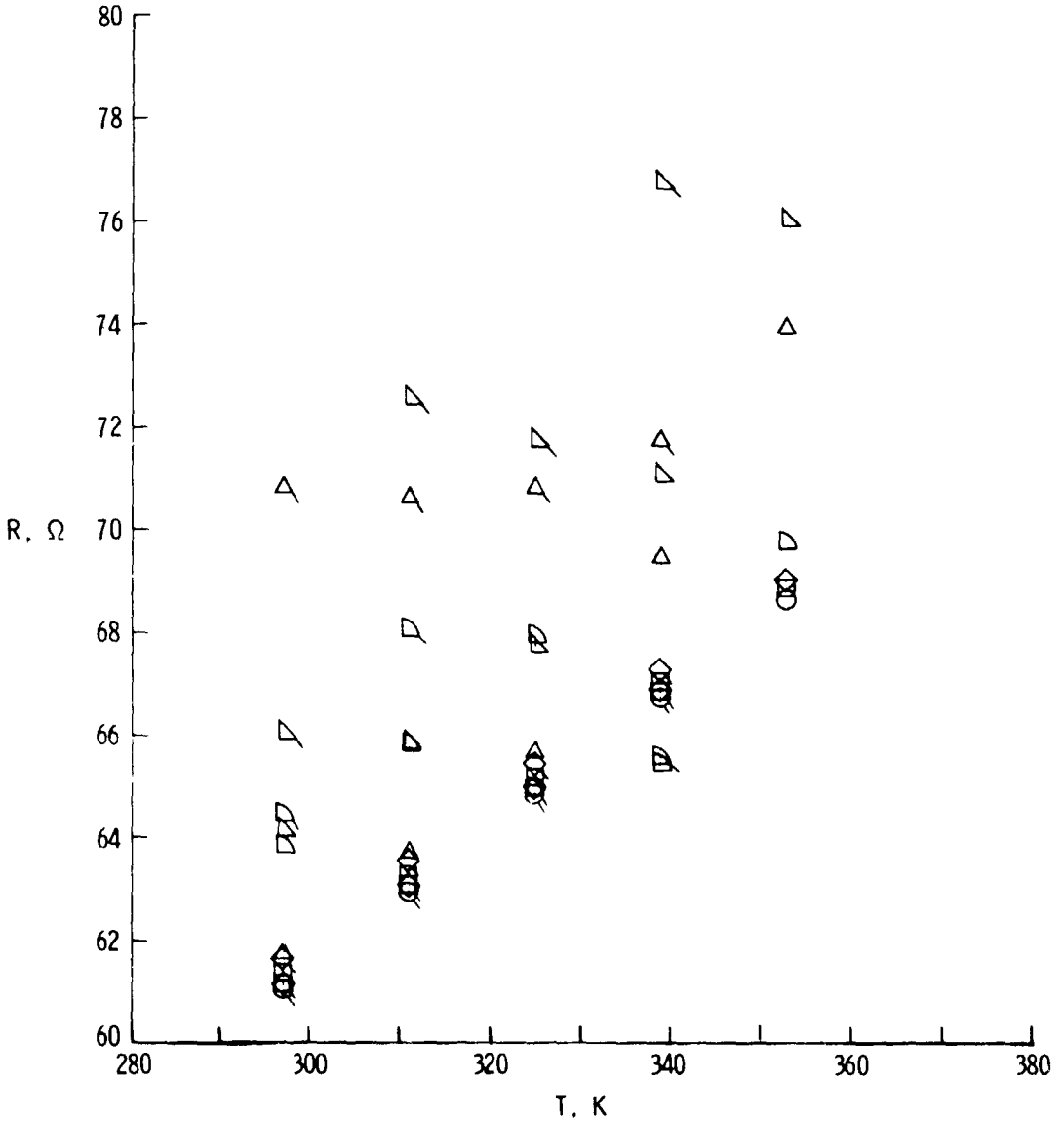

(b) Quartz flat-faced cylinder with gage no. 50. Flagged symbols denote descending temperature.

Figure 30.- Continued.

I_0, mA	R_0, Ω	First-order fit		Second-order fit	
		dR/dT, Ω/K	α_R per mK	dR/dT, Ω/K	α_R per mK
○ 1	153.34	0.33399	2.1782	0.35296	2.3019
□ 2	152.94	.33435	2.1862	.35136	2.2974
◇ 5	152.80	.33529	2.1943	.35053	2.2940
△ 10	152.92	.33642	2.1996	.35116	2.2963
◺ 15	153.87	.33574	2.1819	.34978	2.2731
◺ 20	155.17	.33820	2.1795	.35780	2.3059

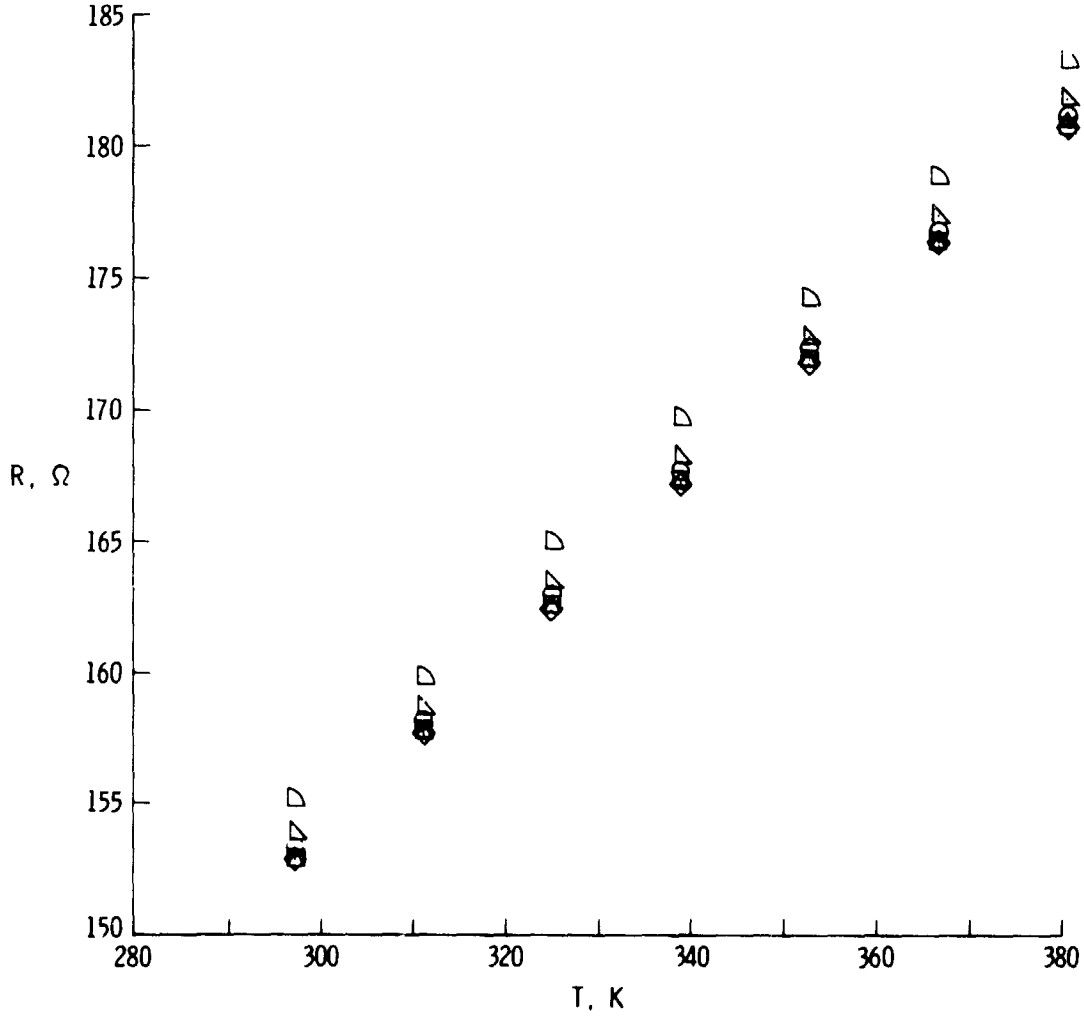

(c) MACOR hemisphere no. 1.

Figure 30.- Continued.

I_0, mA		R_0, Ω	First-order fit		Second-order fit	
			dR/dT, Ω/K	α_R per mK	dR/dT, Ω/K	α_R per mK
○	1	153.59	0.34985	2.2778	0.36574	2.3814
□	2	153.43	.34977	2.2796	.36410	2.3730
◇	5	153.445	.35019	2.2822	.36406	2.3727
△	10	153.818	.35060	2.2794	.36310	2.3606
◁	15	154.601	.35323	2.2848	.36954	2.3903
▷	20	155.874	.35383	2.2700	.37580	2.4109

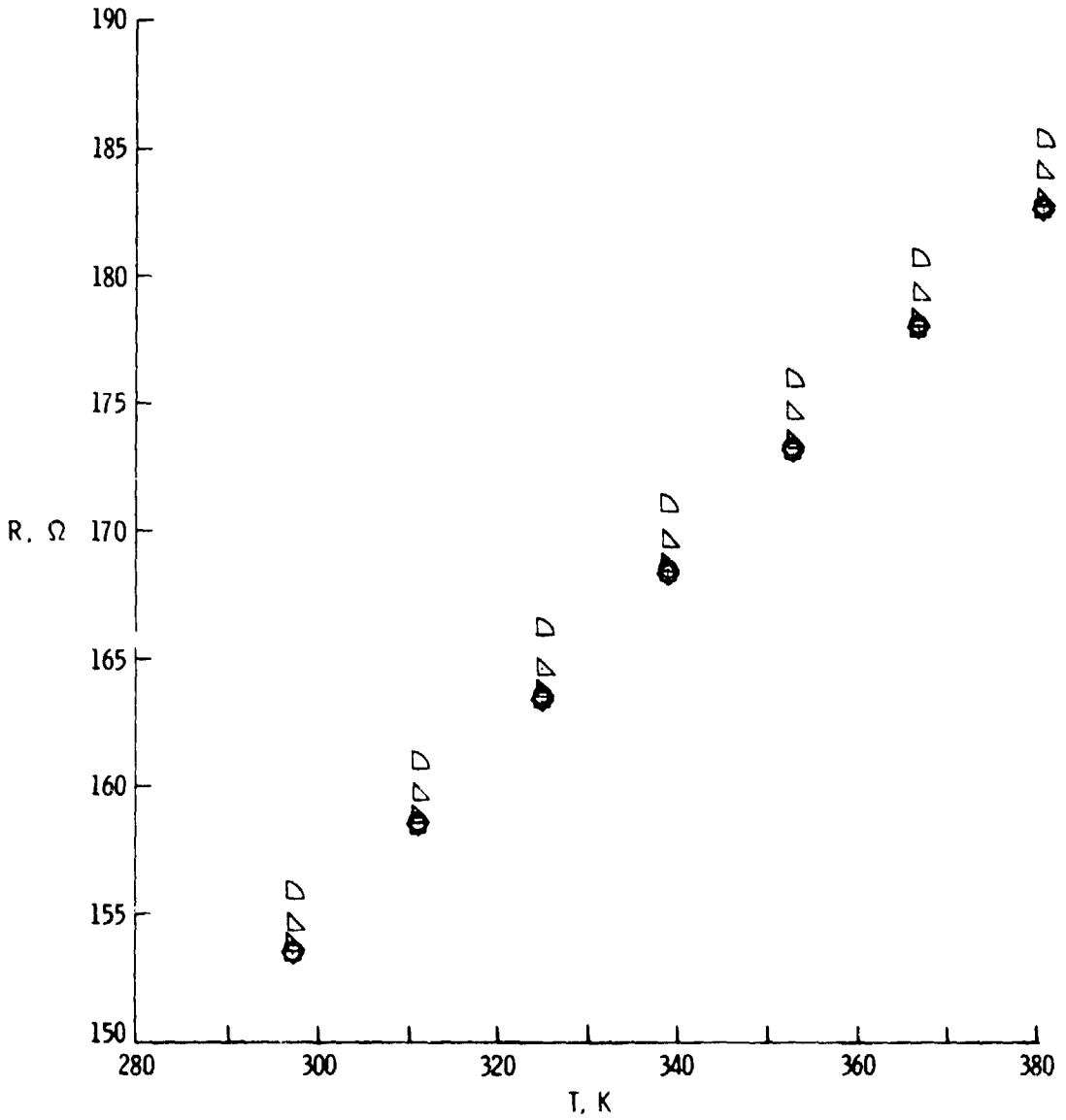

(d) MACOR hemisphere no. 2.

Figure 30.- Concluded.

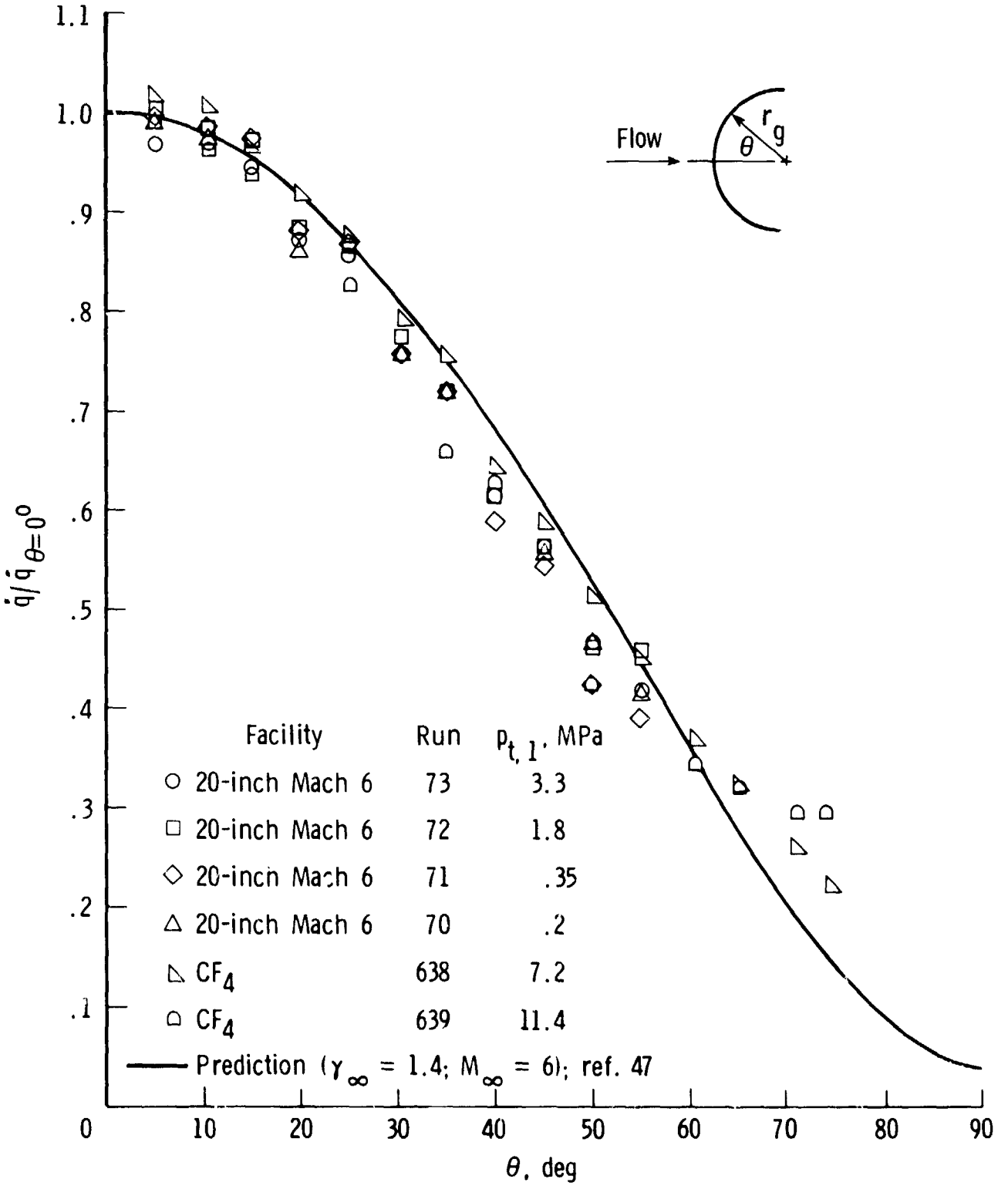

Figure 31.- Heat-transfer distribution about a 10.16-cm-diameter, continuous thin-skin-sphere model in the Langley 20-Inch Mach 6 Tunnel in air and in the Langley Hypersonic CF_4 Tunnel.